1994

Dry sliding wear of aluminum-silicon (A356) matrix composites with carbon fibre or graphite/silicon carbide reinforcement.

William. Ames
University of Windsor

NOTICE

The quality of this microform is heavily dependent upon the quality of the original thesis submitted for microfilming. Every effort has been made to ensure the highest quality of reproduction possible.

If pages are missing, contact the university which granted the degree.

Some pages may have indistinct print especially if the original pages were typed with a poor typewriter ribbon or if the university sent us an inferior photocopy.

Reproduction in full or in part of this microform is governed by the Canadian Copyright Act, R.S.C. 1970, c. C-30, and subsequent amendments.

AVIS

La qualité de cette microforme dépend grandement de la qualité de la thèse soumise au microfilmage. Nous avons tout fait pour assurer une qualité supérieure de reproduction.

S'il manque des pages, veuillez communiquer avec l'université qui a conféré le grade.

La qualité d'impression de certaines pages peut laisser à désirer, surtout si les pages originales ont été dactylographiées à l'aide d'un ruban usé ou si l'université nous a fait parvenir une photocopie de qualité inférieure.

La reproduction, même partielle, de cette microforme est soumise à la Loi canadienne sur le droit d'auteur, SRC 1970, c. C-30, et ses amendements subséquents.

Canada

DRY SLIDING WEAR OF ALUMINUM-SILICON (A356) MATRIX COMPOSITES WITH CARBON FIBRE OR GRAPHITE/SIC REINFORCEMENT

by

William Ames

A Thesis
Submitted to the Faculty of Graduate Studies
and Research Through the Engineering Materials Program
of the Department of Mechanical Engineering in Partial
Fulfilment of the Requirements for the
Degree of Master of Applied Science
at the University of Windsor

Windsor, Ontario, Canada

1994

ISBN 0-315-93252-X

Canada

Name William Ames

Dissertation Abstracts International is arranged by broad, general subject categories. Please select the one subject which most nearly describes the content of your dissertation. Enter the corresponding four-digit code in the spaces provided.

Material Science

SUBJECT TERM

0 7 7 7

SUBJECT CODE

UMI

Subject Categories

THE HUMANITIES AND SOCIAL SCIENCES

COMMUNICATIONS AND THE ARTS

- Architecture 0729
- Art History 0377
- Cinema 0900
- Dance 0378
- Fine Arts 0357
- Information Science 0723
- Journalism 0391
- Library Science 0399
- Mass Communications 0708
- Music 0413
- Speech Communication 0459
- Theater 0465

EDUCATION

- General 0515
- Administration 0514
- Adult and Continuing 0516
- Agricultural 0517
- Art 0273
- Bilingual and Multicultural 0282
- Business 0688
- Community College 0275
- Curriculum and Instruction 0727
- Early Childhood 0518
- Elementary 0524
- Finance 0277
- Guidance and Counseling 0519
- Health 0680
- Higher 0745
- History of 0520
- Home Economics 0278
- Industrial 0521
- Language and Literature 0279
- Mathematics 0280
- Music 0522
- Philosophy of 0998
- Physical 0523
- Psychology 0525
- Reading 0535
- Religious 0527
- Sciences 0714
- Secondary 0533
- Social Sciences 0534
- Sociology of 0340
- Special 0529
- Teacher Training 0530
- Technology 0710
- Tests and Measurements 0288
- Vocational 0747

LANGUAGE, LITERATURE AND LINGUISTICS

- Language
  - General 0679
  - Ancient 0289
  - Linguistics 0290
  - Modern 0291
- Literature
  - General 0401
  - Classical 0294
  - Comparative 0295
  - Medieval 0297
  - Modern 0298
  - African 0316
  - American 0591
  - Asian 0305
  - Canadian (English) 0352
  - Canadian (French) 0355
  - English 0593
  - Germanic 0311
  - Latin American 0312
  - Middle Eastern 0315
  - Romance 0313
  - Slavic and East European 0314

PHILOSOPHY, RELIGION AND THEOLOGY

- Philosophy 0422
- Religion
  - General 0318
  - Biblical Studies 0321
  - Clergy 0319
  - History of 0320
  - Philosophy of 0322
- Theology 0469

SOCIAL SCIENCES

- American Studies 0323
- Anthropology
  - Archaeology 0324
  - Cultural 0326
  - Physical 0327
- Business Administration
  - General 0310
  - Accounting 0272
  - Banking 0770
  - Management 0454
  - Marketing 0338
- Canadian Studies 0385
- Economics
  - General 0501
  - Agricultural 0503
  - Commerce-Business 0505
  - Finance 0508
  - History 0509
  - Labor 0510
  - Theory 0511
- Folklore 0358
- Geography 0366
- Gerontology 0351
- History
  - General 0578
  - Ancient 0579
  - Medieval 0581
  - Modern 0582
  - Black 0328
  - African 0331
  - Asia, Australia and Oceania 0332
  - Canadian 0334
  - European 0335
  - Latin American 0336
  - Middle Eastern 0333
  - United States 0337
- History of Science 0585
- Law 0398
- Political Science
  - General 0615
  - International Law and Relations 0616
  - Public Administration 0617
- Recreation 0814
- Social Work 0452
- Sociology
  - General 0626
  - Criminology and Penology 0627
  - Demography 0938
  - Ethnic and Racial Studies 0631
  - Individual and Family Studies 0628
  - Industrial and Labor Relations 0629
  - Public and Social Welfare 0630
  - Social Structure and Development 0700
  - Theory and Methods 0344
- Transportation 0709
- Urban and Regional Planning 0999
- Women's Studies 0453

THE SCIENCES AND ENGINEERING

BIOLOGICAL SCIENCES

- Agriculture
  - General 0473
  - Agronomy 0285
  - Animal Culture and Nutrition 0475
  - Animal Pathology 0476
  - Food Science and Technology 0359
  - Forestry and Wildlife 0478
  - Plant Culture 0479
  - Plant Pathology 0480
  - Plant Physiology 0817
  - Range Management 0777
  - Wood Technology 0746
- Biology
  - General 0306
  - Anatomy 0287
  - Biostatistics 0308
  - Botany 0309
  - Cell 0379
  - Ecology 0329
  - Entomology 0353
  - Genetics 0369
  - Limnology 0793
  - Microbiology 0410
  - Molecular 0307
  - Neuroscience 0317
  - Oceanography 0416
  - Physiology 0433
  - Radiation 0821
  - Veterinary Science 0778
  - Zoology 0472
- Biophysics
  - General 0786
  - Medical 0760

EARTH SCIENCES

- Biogeochemistry 0425
- Geochemistry 0996
- Geodesy 0370
- Geology 0372
- Geophysics 0373
- Hydrology 0388
- Mineralogy 0411
- Paleobotany 0345
- Paleoecology 0426
- Paleontology 0418
- Paleozoology 0985
- Palynology 0427
- Physical Geography 0368
- Physical Oceanography 0415

HEALTH AND ENVIRONMENTAL SCIENCES

- Environmental Sciences 0768
- Health Sciences
  - General 0566
  - Audiology 0300
  - Chemotherapy 0992
  - Dentistry 0567
  - Education 0350
  - Hospital Management 0769
  - Human Development 0758
  - Immunology 0982
  - Medicine and Surgery 0564
  - Mental Health 0347
  - Nursing 0569
  - Nutrition 0570
  - Obstetrics and Gynecology 0380
  - Occupational Health and Therapy 0354
  - Ophthalmology 0381
  - Pathology 0571
  - Pharmacology 0419
  - Pharmacy 0572
  - Physical Therapy 0382
  - Public Health 0573
  - Radiology 0574
  - Recreation 0575
  - Speech Pathology 0460
  - Toxicology 0383
- Home Economics 0386

PHYSICAL SCIENCES

Pure Sciences

- Chemistry
  - General 0485
  - Agricultural 0749
  - Analytical 0486
  - Biochemistry 0487
  - Inorganic 0488
  - Nuclear 0738
  - Organic 0490
  - Pharmaceutical 0491
  - Physical 0494
  - Polymer 0495
  - Radiation 0754
- Mathematics 0405
- Physics
  - General 0605
  - Acoustics 0986
  - Astronomy and Astrophysics 0606
  - Atmospheric Science 0608
  - Atomic 0748
  - Electronics and Electricity 0607
  - Elementary Particles and High Energy 0798
  - Fluid and Plasma 0759
  - Molecular 0609
  - Nuclear 0610
  - Optics 0752
  - Radiation 0756
  - Solid State 0611
- Statistics 0463

Applied Sciences

- Applied Mechanics 0346
- Computer Science 0984
- Engineering
  - General 0537
  - Aerospace 0538
  - Agricultural 0539
  - Automotive 0540
  - Biomedical 0541
  - Chemical 0542
  - Civil 0543
  - Electronics and Electrical 0544
  - Heat and Thermodynamics 0348
  - Hydraulic 0545
  - Industrial 0546
  - Marine 0547
  - Materials Science 0794
  - Mechanical 0548
  - Metallurgy 0743
  - Mining 0551
  - Nuclear 0552
  - Packaging 0549
  - Petroleum 0765
  - Sanitary and Municipal 0554
  - System Science 0790
- Geotechnology 0428
- Operations Research 0796
- Plastics Technology 0795
- Textile Technology 0994

PSYCHOLOGY

- General 0621
- Behavioral 0384
- Clinical 0622
- Developmental 0620
- Experimental 0623
- Industrial 0624
- Personality 0625
- Physiological 0989
- Psychobiology 0349
- Psychometrics 0632
- Social 0451

ABSTRACT

The unlubricated sliding wear of two reinforced A356 (Al-7%Si-0.3%Mg) metal matrix composites was studied using a block on ring wear machine with an AISI 52100 steel counterface (63 HRC). One composite was discontinuously reinforced with 4 ± 1 vol% non-graphitic carbon fibres coated with nickel. The composites were tested such that the fibres were either normal or parallel to the contact surface. The second composite was a hybrid composite with 20% SiC particulate and 3 or 10 vol% graphite particles. In the wear tests, the applied normal load varied from 5 to 441 N. Sliding speed ranged from 0.1 to 1 m/s with the majority of tests performed at 0.5 m/s.

The wear resistance of the A356-Carbon Fibre (CF) reinforced composites was superior to the unreinforced alloy over the entire load range tested. The improved wear resistance was related to an improvement in load carrying capability of the composites as a result of the carbon fibre addition and an interfacial reaction which produced a nickel aluminide intermetallic. These composites demonstrated regions of mild and severe wear. Mild wear was characterized by surface grooves, plastic deformation and loose debris in the form of particulates and flakes. The wear rate increased slowly with increasing load (n=0.3). At a critical load a transition from mild to severe wear was observed. Severe wear was characterized by deep longitudinal grooves on the worn surface and subsurface damage resulting

in a layered microstructure. The surface layer contained broken particles which hardened the surface of the composite and improved the wear resistance with respect to the unreinforced alloy. Above the critical load seizure always followed severe wear. The distance required for seizure to occur became shorter as the load increased.

The A356-Gr-SiC composites did not experience severe wear resulting in good wear resistance at high loads. This was due to a reduction in frictional heating and the formation of a tribolayer on the surface which consisted of iron, iron oxides, graphite, SiC and aluminum. Graphite addition resulted in a reduction in counterface wear. Higher graphite concentrations led to higher wear resistance at loads below 10 N. In the load range from 20 to 300 N the 10% graphite composite experienced wear rates 2 to 4 times that of the hybrid composite with only 3% graphite possibly due to a decrease in the load carrying ability due to higher graphite content.

To My Parents, Elmer and Ilene

ACKNOWLEDGEMENTS

I would like to express my sincere thanks to Dr. A.T. Alpas for his supervision, interest, encouragement and friendship. Mr. J. Zhang is acknowledged for his advice throughout my studies. The technical expertise of Mr. J.W. Robinson is much appreciated. I would like to thank Dr. D.L. Lloyd of Alcan and Drs T. Stephenson and J.A.E. Bell of INCO Ltd. for the fabrication of the composites and their continued interest in this work. Mr. A. Duft, of McMaster University, is recognized for his contribution to the AES investigation.

The financial support of NSERC and an Industrial Consortium of Alcan, INCO, Ontario Hydro, Sherrit-Gordon, Pratt and Whitney and ComDev is gratefully acknowledged. NSERC is further acknowledged for the awarding of a PGS 1 scholarship.

Finally, I would like to extend my appreciation to the professors, staff and students of the Engineering Materials Group for the useful discussions and guidance which contributed to this work.

TABLE OF CONTENTS

List of Tables

Table

LIST OF FIGURES

Figure

NOMENCLATURE

a	thermal diffusivity
A	nominal area of contact
A_p	parabolic rate constant for oxidation
A_R	real area of contact
C	intercept of the log-log plot of wear rate versus load
D	particle diameter
ε	strain
F	applied load
H	indentation hardness
k	Archard's wear coefficient
K	thermal conductivity
k_1	proportionality constant
L	load
Δm	oxygen uptake
n	slope of the log-log plot of wear rate versus load
P	load
p_m	flow pressure
Q	activation energy
r	radius of the pin in a pin on disk machine
R	universal gas constant

s	sliding distance
t	time
T	homologous temperature
T_i	interface temperature
T_s	heat sink temperature
μ	coefficient of friction
v	sliding speed
V_x	volume fraction of phase x
W	volume lost during wear
W_d	wear rate (mm^3/m)
Δx	distance from the interface to the heat sink

Chapter 1 : Introduction

Today composites are made with practically every type of engineering material known to humankind. Concrete has been reinforced with steel and wood with fibre glass. Polymer matrix composites have become a fixture of everyday life. Uses range from the auto body of your car to golf clubs and tennis racquets. Ceramic matrix composites have been produced with the intention of improving the poor damage tolerance traditionally associated with ceramics. Intermetallic matrices have been investigated for their elevated temperature properties. Metals, such as aluminum, titanium, copper, steel and magnesium, have been employed as the matrices with the intention of improving the stiffness, strength, fatigue resistance, creep resistance and wear resistance of the matrix alloy.

A metal matrix composite (MMC) may be defined as a material consisting of a metal phase into which a second phase, whose minimum dimension is 1 μm, is intentionally formed or placed. The second phase material is often a ceramic such as a metal carbide or oxide. The reinforcing phase may take the form of particles, whiskers, short fibres or continuous fibres.

The reinforcement of alloys by high modulus ceramic fibres, whiskers or particles results in composite materials which feature both high modulus and high

strength. The elevated temperature properties may be improved since the properties of the ceramics do not degrade as quickly as the metal with increasing temperature. Typically the ductility of the composite is lower than the ductility of the unreinforced alloy. In fact, the aerospace industry is concerned that the limited damage tolerance of MMCs may prevent wide usage of these new materials [1,2]. Today, some composites are specifically designed to address the problem of low damage tolerance [3]. Metal matrix composites have found applications in military aerospace structures, drive shafts, pistons, brake rotors and sporting goods such as mountain bikes. Applications which require sliding wear resistance include brake rotors and pistons.

The automotive industry has been very interested in reducing the weight of the automobile while improving efficiency. A significant weight savings may be made by replacing the cast iron engine block with an aluminum block. However, aluminum alloys have poor resistance to seizure and galling [4,5] necessitating the use of cast iron cylinder liners or hypereutectic Al-Si alloy blocks [6]. The cast iron liners provide good wear resistance due to their hardness and the presence of graphite nodules [7,8]. Linerless aluminum blocks are less wear resistant and tend to be more expensive to fabricate [6]. Metal matrix composites, with fibre, particle or whisker reinforcement, have been investigated as piston [9] and cylinder liner [10] materials. These materials have demonstrated a reduction in wear [9,10] and an improvement in engine efficiency [9].

The largest direct loss of mechanical energy in the automobile engine is due to the friction of the piston ring-cylinder wall interface accounting for 10^{17} J of energy lost to friction each year [11,12]. Using 1975 energy consumption data it was determined that 20% of the mechanical energy generated by the engine is lost to friction while one half of this is lost due to piston-cylinder friction [13]. The rest of the mechanical energy that is lost to friction is consumed by the other moving parts of the engine and the drive train. Obviously a reduction in energy losses would benefit engine efficiency.

Metal matrix composites may be fabricated which include solid lubricating materials [4]. These lubricants smear on to the wear surface and reduce intimate contact between the sliding partners resulting in a reduction in the coefficient of friction. Potentially, this fact could be used to reduce the frictional losses in the internal combustion engine leading to more efficient automobiles.

The purpose of this investigation was to examine the wear properties of a cast aluminum - 7% silicon - 0.3% magnesium alloy (A356 Al) with two different reinforcement strategies. Isotropic, non-graphitic carbon fibres were used to reinforce the matrix with the intention that the relatively inexpensive carbon fibres may act as load bearing constituents and may yield lubricating characteristics similar to graphite. In a second set of experiments, the matrix alloy was reinforced with both SiC and graphite particles representing a merging of two philosophies - hard

particle reinforcement and soft particle lubrication.

This thesis is divided in to four main chapters. Firstly the pertinent literature regarding sliding wear and materials for sliding wear applications is reviewed. This is followed by the experimental procedures, which apply to both materials, in Chapter 3. The experimental results and discussion are divided according to the materials studied. The A356 carbon fibre composites are dealt with in Chapter 4 and the A356-SiC-Graphite composites in Chapter 5. At the end of Chapter 5 the wear rates of the two composites are compared and discussed.

Chapter 2: Literature Survey

2.1: Sliding Wear

Tribology is the science and technology of friction, lubrication and wear. Wear may be defined as "damage to a solid surface, generally involving progressive loss of material, that is due to relative motion between that surface and a contacting substance or substances" [14]. The investigation of wear properties is a large part of the science of tribology. However, all aspects of tribology are related and it is difficult, or sometimes impossible, to isolate any one aspect of tribology. Tribologists have attempted to classify the various types of wear processes in to four or five categories.

Abrasive wear is the removal or displacement of material from one surface by loose hard particles or by the asperities of another surface [11]. The mechanism(s) may involve microcutting or plastic deformation accompanied by frictional heating [15].

Fatigue type processes can result in wear debris formation through the accumulation of damage in the subsurface due to the repeated application of stress on the surface of a component [11]. Other researchers have identified similar processes and refer to them as delamination wear [16].

Corrosion processes, including oxidational wear, involve the synergistic effect of mechanical wear and chemical reaction [11]. Quinn has published a review on the theory of oxidational wear [17,18]. Corrosion processes are found in many instances of wear under normal service conditions.

Adhesion involves the interaction of asperities on the sliding surface. Traditional thought states that the asperities meet and briefly weld together forming a junction which is subsequently fractured [11]. Debris formation occurs through repeated junction formation and fracture. Plastic deformation and surface heating result [15]. A critical review of the adhesive wear process can be found in reference [19].

There are other processes including fretting, erosion, polishing wear and impact wear. In the vast majority of wear cases many of these processes will occur simultaneously. In fact it would be very rare to observe only one of the forgoing mechanisms operating alone [11].

Sliding wear occurs when one solid surface slides across another solid surface [16]. This type of wear may involve aspects of abrasive wear, adhesive wear, corrosive or oxidational wear and delamination wear.

During sliding wear many materials may experience two forms of wear; mild

and severe. Drastic differences in the wear rate and the debris type exist between these two forms of wear [19]. In metals and alloys mild wear typically produces lower wear rates and fine debris. The debris is frequently oxidized. In severe wear the debris is metallic and larger. The difference in the mild wear and severe wear rates may be a factor of 10 to 10 000 [19]. In an attempt to understand mild and severe wear, models have been proposed to describe the wear processes which may be taking place.

One of the most commonly cited wear model is accredited to Archard [20-22]. Archard developed an expression that predicts that wear is proportional to the load and independent of the nominal contact area [20-22]. Archard's model takes the form of:

$$W = k_1 \cdot P \cdot s \qquad (2.1.1)$$

where W is the volume lost during wear, k_1 is a proportionality constant, P is the applied load, and s is the sliding distance. However, since it was postulated [20] that the true area of contact is proportional to the applied load, equation 2.1.1 may be rewritten to include the true contact area (given by $A_R=P/p_m$) [22]:

$$W = k \cdot P \cdot s/p_m \qquad (2.1.2)$$

where p_m is the flow pressure of the softer material. The coefficient, k, is termed the wear coefficient or Archard's wear coefficient. Archard considered the coefficient, k, to be indicative of the probability of forming a debris particle during an asperity interaction [22]. This provided an easy model to implement in the early applications of tribomaterials. For example, the value of k was used to differentiate between mild and severe wear. When k falls between 10^{-6} and 10^{-8} wear is considered to be mild [23]. Values of k greater than 10^{-4} imply severe wear [23]. Examples of wear coefficients for several materials sliding on tool steel at a load of 400 g, velocity 0.18 m/s, are listed in Table 2.1.1 [18].

The applicability of Archard's theory of wear is limited by the fact that wear volume is proportional to the load. Archard [22] noted this in experimental evidence where a direct proportionality between wear volume and applied load was rare [22]. Archard also observed both mild and severe wear but the equation does not indicate transitional behaviour [23]. Frequently the flow stress of the softer material, p_m, is assumed to be the indentation hardness [19]. Archard developed a starting point from which tribologists may base their studies.

Several attempts [24-37] have been made to explain the nucleation and coalescence of cracks and voids at a critical depth below the worn surface. In multiphase materials nucleation occurs at the boundary between the second phase and the matrix [26]. The applied stress is composed of the hydrostatic stress and the

Table 2.1.1: Wear rates, coefficients of friction and wear coefficients of several materials [18]

	Wear Rate (cm^3/cm)	μ	k
60/40 Leaded Brass	2.4×10^{-8}	0.24	6.0×10^{-4}
PTFE (Teflon)	2.0×10^{-9}	0.18	2.5×10^{-5}
Stellite	3.2×10^{-10}	0.60	5.5×10^{-5}
Ferritic Stainless Steel	2.7×10^{-10}	0.53	1.7×10^{-5}
Polythene	3.0×10^{-11}	0.65	1.3×10^{-7}

deviator stress. In order to achieve nucleation of a void the applied stress at the particle-matrix interface must exceed the adhesive strength of the interface. The magnitude and location of the maximum interfacial stress is a function of particle shape. A tensile hydrostatic stress will promote void nucleation while a compressive hydrostatic stress will retard void nucleation [26].

A necessary, but not sufficient, condition for void or crack nucleation is that the energy of the new surface created must be less than the elastic energy released by the formation of the crack. This energy criterion is particle size dependant. Very small particles will not nucleate a crack even if the stress criterion is satisfied. In metals the critical inclusion size is of the order of 25 nm [26]. Since most inclusions in metals are greater than 25 nm in size a crack will nucleate if the stress criterion is satisfied. Experimentally it has been shown that the crack will propagate until the delamination sheet is separated from the surface [24-27].

Initially Suh [24] proposed that dislocations in a very thin layer at the surface (of the order of 0.1 μm) were eliminated through migration to the surface. The driving force for this was the image force which arises due to the proximity of the stress free surface. It was also suggested that dislocation pile ups would form a certain distance below the surface due to forces which drive the dislocations in to the softer material. These forces are caused by the interaction of a hard slider against

a softer material and lead to strain hardening of the subsurface layer. Over a period of time voids would nucleate as a result of the high dislocation density. Second phase particles would provide a boundary upon which dislocations could pile up leading to enhanced void nucleation [24]. Heilman et al [28] suggested that subsurface cracks would develop parallel to the dislocation cell boundaries which form under large plastic strain.

Flemming and Suh [29], Kimura [30] and Ritchie [31] have proposed fatigue models which consider the cyclic nature of the asperity loading. Hearle and Johnson [32], Hills and Ashelby [33] and Rosenfield [34] used linear elastic fracture mechanics to investigate the phenomena of subsurface crack growth. Regretfully the subsurface of a ductile metal experiences plastic deformation. Linear elastic fracture mechanics assumes that plasticity occurs only at the crack tip. This contradiction erodes the basis upon which these theories are developed making realistic application questionable.

The deformation below the surface may be localized in to shear bands [35]. Alpas and Embury [35] indicated that strain localization in the subsurface of ductile metals led to crack nucleation and growth through the shear bands. Rosenfield [36] has proposed a shear instability model for sliding wear. In his theory a crack is nucleated and grown under Mode II loading. The depth of the crack is determined by two factors: 1) the local flow strength of the material and 2) the stress intensity

due to the crack. Since the flow strength decreases with increasing distance from the worn surface and the stress intensity has a maximum below the surface, there may be a point where the stress intensity may exceed the local flow stress leading to shear instability and continued crack propagation.

Zhang and Alpas [37] have developed a model which indicates a damage gradient below the worn surface. The damage gradient concept considers the competition between the subsurface plastic strain, which leads to crack nucleation at second phase particles, and the hydrostatic stress which opposes crack formation. Using an equation developed by Rice and Tracy [38] for void growth during ductile fracture the problem of subsurface plasticity, which limits linear elastic fracture mechanics approaches, was overcome. It was determined that an increase in hydrostatic stress results in an increase in crack depth but a reduction in the crack growth rate.

Other delamination wear models have been developed and are reviewed [39,40]. Oxidational wear theories are also relevant to dry sliding wear and will be discussed in section 2.5. Research in to the modelling of wear processes has not yielded design equations. Progress continues but is hampered by the fact that the laboratory test methods frequently do not represent reality adequately. Also there is a lack of fundamental micromechanistic and microstructural understanding. There also appears to be a lack of research effort in to the development of wear

models based on real physical processes.

The most significant practical development was based on the construction of wear mechanism maps, in analogy to deformation mechanism maps. This was suggested by Tabor [41] and since then developed by Lim and Ashby [40]. Basically, the normalised velocity and load are considered to be independent variables and form the abscissa and ordinate axis. The force is normalised by dividing the applied load (F) by the nominal area of contact at the start of the test (A) and the room temperature hardness of the pin (H). The velocity is normalised by dividing by the velocity by the radius of the pin (r) and the thermal diffusivity (a). Lines of constant wear rate are scribed on the map as well as boundaries between the dominant wear mechanisms. Consideration of specific testing or operating conditions would, ideally, indicate the operating wear mechanism and the effective wear rate. However, the data used to construct the maps presently available were compiled from the literature. Considerable variation in the testing methods used to achieve the data for the maps existed thus bring the validity of the maps in to question. A schematic example is shown in Figure 2.1 [40]. Wear mechanism maps are not presently used in design.

2.2: Environmental and Material Effects on Wear

Wear processes are complicated by many factors. Testing in air is very different than testing in vacuum [42]. In vacuum, the coefficient of friction is

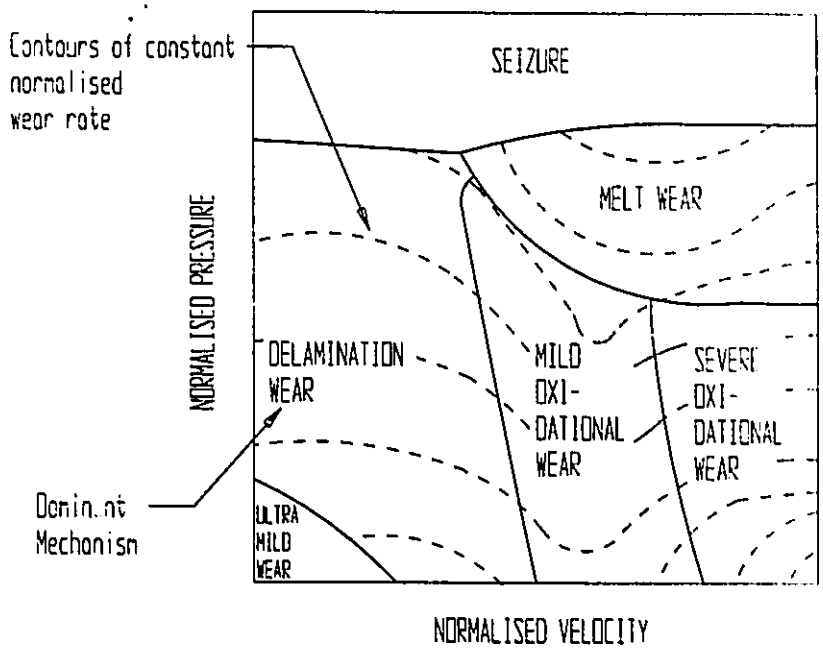

Figure 2.1: Schematic wear mechanism map (adapted from [40])

usually much higher than in air [26]. In air, the surface is contaminated with a layer of absorbed gases, hydrocarbons and moisture (Figure 2.2). Below this, in metals, is a reaction zone, typically oxides or sulfides, whose thickness is only of the order of 10 nm thick [16]. Below the reaction layer is a layer of deformed material due to the fabrication process. The thickness of this layer depends on the manufacturing process. Underlying this is the bulk material. When two surface are brought into contact, the surface contaminant layers can act as lubricants, preventing metal to metal contact at very low loads [11]. One of the factors affecting the properties of this film is the humidity. A critical review of the influence of environmental humidity on the friction, lubrication and wear of materials has been published by Lancaster [43].

Material variables must also be considered. Microstructural properties such as composition, grain size, number of phases, phase distribution, anisotropy as well as mechanical properties such as strength, hardness and ductility of both mating pairs affects the wear behaviour [11,23]. For instance, the presence of a second phase particle may lead to a reduction in the real area of contact, an increase in the load carrying ability or change the operating mechanism all together [39]. The distribution of the phases and any anisotropy in the material will affect the response of the material to the applied load. Studies on the effect of grain size has yielded contradictory results [39]. Many of the factors sited above are interrelated. A change in any one factor may result in a change in a related factor. For example,

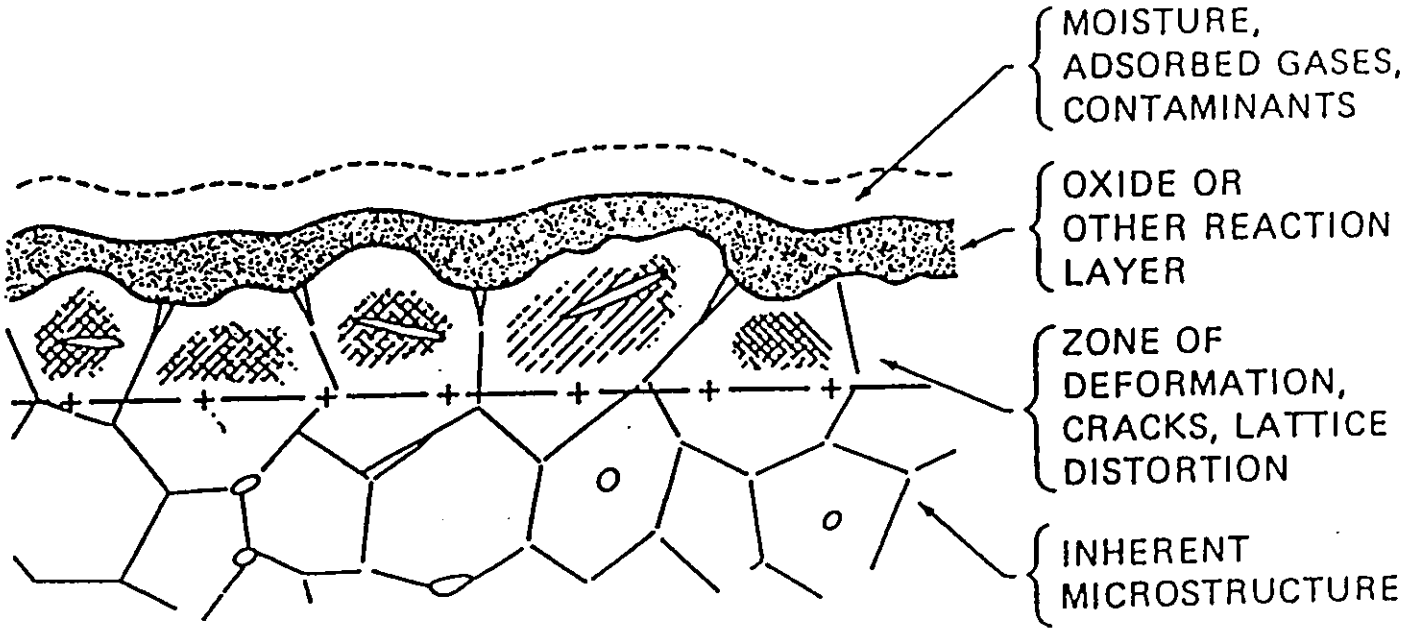

2.2: Schematic Condition of a metallic surface

decreasing the grain size increases the strength and hardness of a metal which suggests an increase in the wear [44-48] and seizure [49-50] resistance. An increase in ductility, possibly through increasing the grain size, should also increase the wear resistance [39]. Hence appropriate reporting of the microstructural and mechanical properties is important. All of this is further complicated by the large number of variables introduced through different testing methods.

2.3: Testing Methods for Dry Sliding Wear

There are three main testing methods used for evaluating dry sliding wear of metals. These are the pin-on-disk test (ASTM G-99), the crossed cylinder test (ASTM G-83) and the block-on-ring test (ASTM G-77).

A typical pin-on-disk system is shown in Figure 2.3. It uses a spherical-end pin which is slid against a rotating disk counterface. The wear volume is determined from examination of the wear scar [51]. Alternatively, the displacement of the pin may be measured to yield the wear rate continuously during the test. The pin-on-disk system is the most widely used for non-lubricated, non-abrasive wear testing [51]. Variations of this apparatus have been designed for special applications such as in-situ wear observation [52].

Crossed cylinder machines (Figure 2.4) are frequently used when the sample

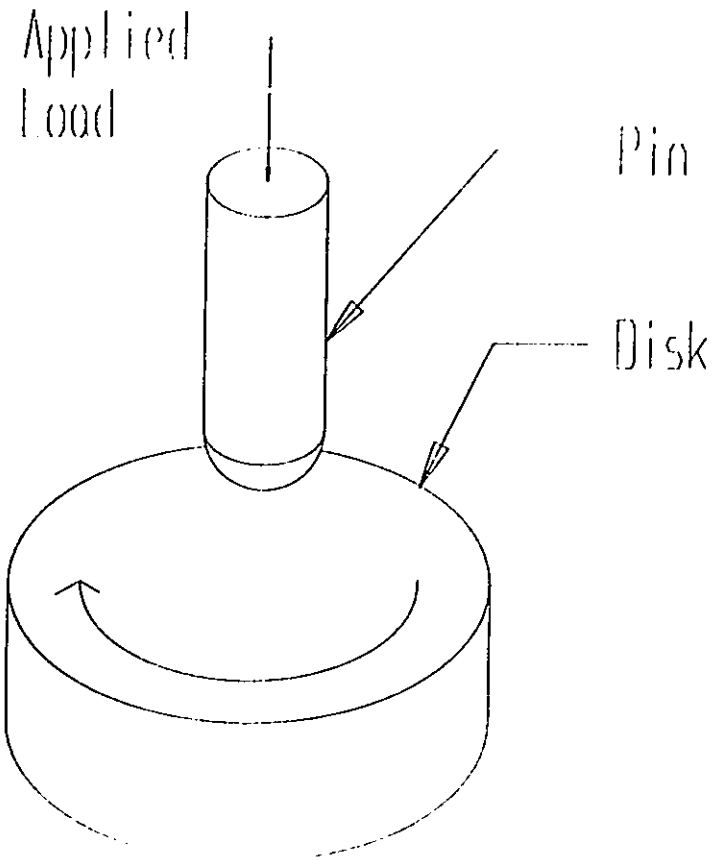

2.3: Pin on disk geometry

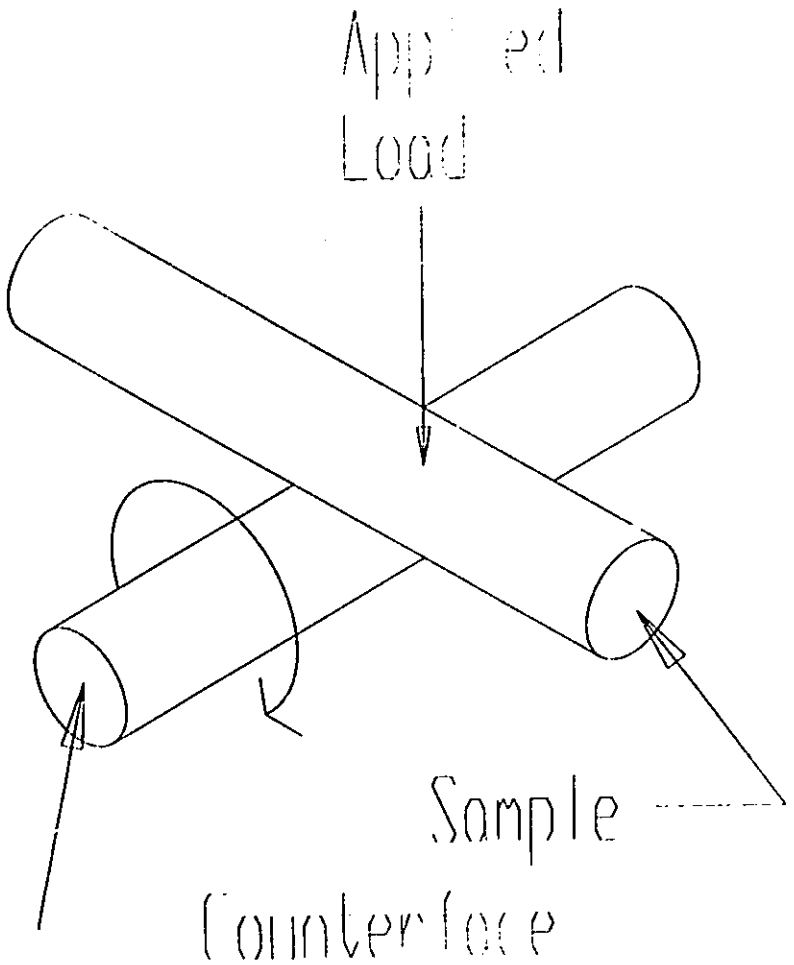

2.4: Crossed cylinder geometry

may be easily manufactured as a tube or cylinder. The sample cylinder is positioned perpendicular to a counterface cylinder. One cylinder rotates while the other is forced against it producing an elliptical wear scar.

Block-on-ring testing (Figure 2.5) uses a block sample which is forced against a rotating ring. The counterface produces a wear scar on the block sample allowing wear rate determination through calculation of the volume loss from wear scar dimensions. Alternatively the weight of the sample may be determined before and after the test yield the weight loss per unit sliding time or distance.

In each testing method the various factors that influence wear are normal load, sliding speed, sliding distance, ambient temperature, environment, counterface material, surface roughness, surface geometry and oscillating versus unidirectional motion [23]. Less obvious factors are machine stiffness and damping capacity. Increasing the machine stiffness yields results similar to increasing the load [23]. Increasing the damping capacity tends to decrease wear [23]. Interchanging the counterface and pin materials will often yield drastically different results [23]. Different results should be expected with different interface geometries such as flat-end pins and spherical-end pins [51]. The ability of debris to exit the contact surface has also been identified as a critical factor [51]. Considering these testing factors, along with the material and environmental factors, it may be concluded that close comparisons between published data may lead to inaccurate conclusions unless the

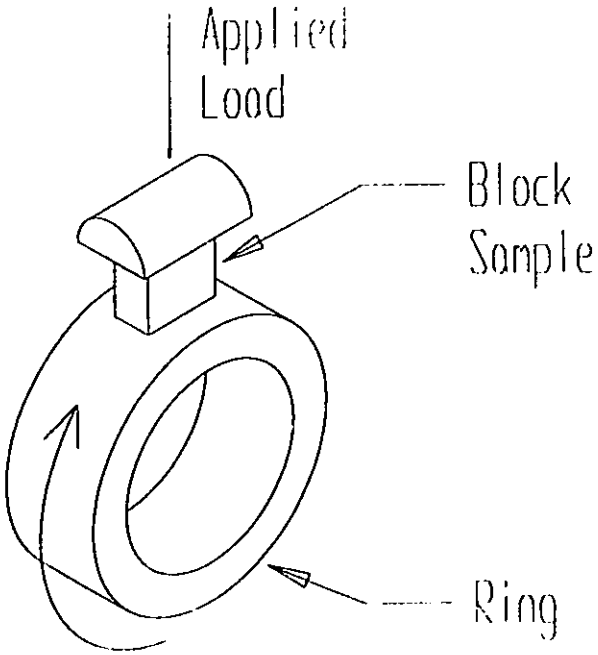

2.5: Block on ring geometry

testing procedures and conditions are similar.

2.4: Sliding Wear of Metals and Alloys

The dry sliding of metals and alloys upon a counterface results in groove, ridge and lapp formation on the worn surface due to ploughing by the counterface asperities or third bodies such as debris fragments. Material may be extruded from the contact surface and may fracture forming a debris fragment. Microscopically, debris may be formed by a lateral flow of surface material which is subsequently removed through a tearing mechanism [23]. The wear process is not limited to the surface. Damage is also accumulated in the subsurface, beneath the wear scar.

In ductile materials, large strains may be accommodated since the compressive hydrostatic stress opposes microvoid formation, coalescence and ductile fracture [53]. The strain decreases exponentially with depth [53,54] resulting in a severe strain gradient at the worn surface [23,55]. Research indicates that shear strains in the range of 10 to 100 may be possible [56]. The deformed layer may only be a few micrometers thick, at low loads, while greater loads result in highly deformed regions tens or hundreds of micrometers thick [23]. It has been proposed that the wear rate is indirectly related to the depth of deformation [54].

Initially equiaxed grains become elongated in the sliding direction due to the

plastic deformation which results in an increase in structural defects, such as dislocations and grain boundaries, enhancing diffusion which increases the rate of chemical reactions such as oxidation [57]. In fact steels oxidize much more rapidly when subject to sliding [57].

Dislocation substructures form within the deformed subsurface regions. Dislocation cells have been observed in high resolution electron microscopic studies of OFHC copper [58]. The cell walls are thick and have a high concentration of dislocations [58]. With further straining, the cells become smaller and the cell walls become more defined. The grain size of the surface material was only 4 to 5 nm [58]. In aluminum alloys, tested under vacuum, deformation structures such as dislocation cells, subgrains and other small dimension features were observed [56]. The dislocation substructure was mainly equiaxed subgrains with sharp walls.

One would expect that the highly deformed material would experience recrystallization due to the heat generated by friction. Subsurface grain recrystallization has been reported [59,60]. However, it is difficult to ascertain whether recrystallization occurred during sliding or after [56]. In fact, the surface layer of aluminum was not recrystallized and demonstrated a very small grain size (3 to 50 nm) [23].

The nanocrystalline layer has been shown to be a nanocomposite composed

of an intimate mixture of fragments from both sliding surfaces [23,56,61]. If second phase particles are present, they are broken up and tend to promote refinement of the nanocrystalline structure [23]. Rigney has proposed a description of transfer layer formation [23]. Fragments, normally tens of micrometers in size, are transferred to the opposing surface after short sliding distances. The composition of these fragments is the same as the sample of origin. Smearing of the transfer material occurs with continued sliding leading to initial mixing with the new substrate material. With further sliding, mixing continues resulting in an "intimate mixture" of the two materials. The resulting structure of the surface layer is a mixture of fine grains from both wear surfaces [23].

The inclusion of material from the opposite sliding surface may improve the properties of the sample. For instances, oxides may be incorporated in to the tribolayer increasing the flow strength of the deformed metal layer [54]. Transfer of iron oxides may lead to lubrication and a reduction in the wear rate. However, this typically occurs in materials with hard particles such as hypereutectic aluminum silicon alloys [62]. This transfer process may differ substantially from the process outlined by Rigney [23].

2.5: Sliding Wear of Al-Si Alloys

The tribological properties of aluminum silicon alloys have been studied due

to the promising wear behaviour they have demonstrated. The Al-Si system has a eutectic at 12% Si. Hypoeutectic, eutectic and hypereutectic compositions have been investigated yielding different results. Many researchers [62-65] have demonstrated that the eutectic composition displays the least wear (Figure 2.6) while other investigations [66] showed that the eutectic silicon content actually had a higher wear rate (Figure 2.7). Yet another investigation [67] concluded that the silicon content in the range of 4 to 24 wt% did not influence the wear rate in any detectable trend (Figure 2.8). Even though these contradictory results exist, the eutectic composition can in fact yield the best wear properties. From a consideration of Figure 2.8 it may be seen that the addition of silicon to the alloy does lower the wear rate compared to an alloy, of similar composition, without silicon [67]. However, high silicon content may lead to an increase counterface wear [63].

Al-Si alloys typically demonstrate two wear regimes; mild and severe [64-66]. In each regime the steady state wear rate increases with load (Figure 2.9) [64,66]. Oxidation [66] and delamination [36,64,68,69] theories have been used to describe mild wear. In the oxidative wear approach [66], the wear surface is covered with a layer of aluminum oxide or mixed oxide/metal. Wear occurs through the spalling of the oxide layer. This limits wear to the oxide layer, only, thus mild wear rates result.

In the delamination wear approach [36,64,68,69] subsurface cracks nucleate

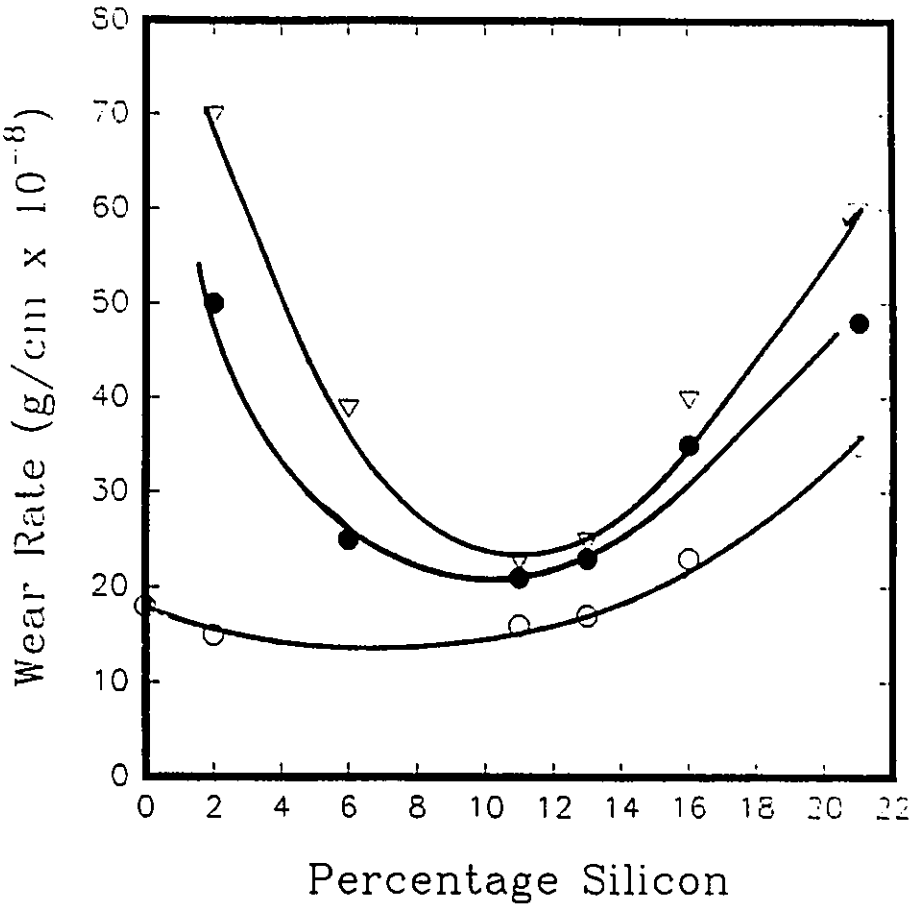

Figure 2.6: Wear Rate as a function of Si content at loads of 1 Kg (○), 1.5 Kg (●) and 2 Kg (▽) sliding against steel at 1.96 m/s [62]

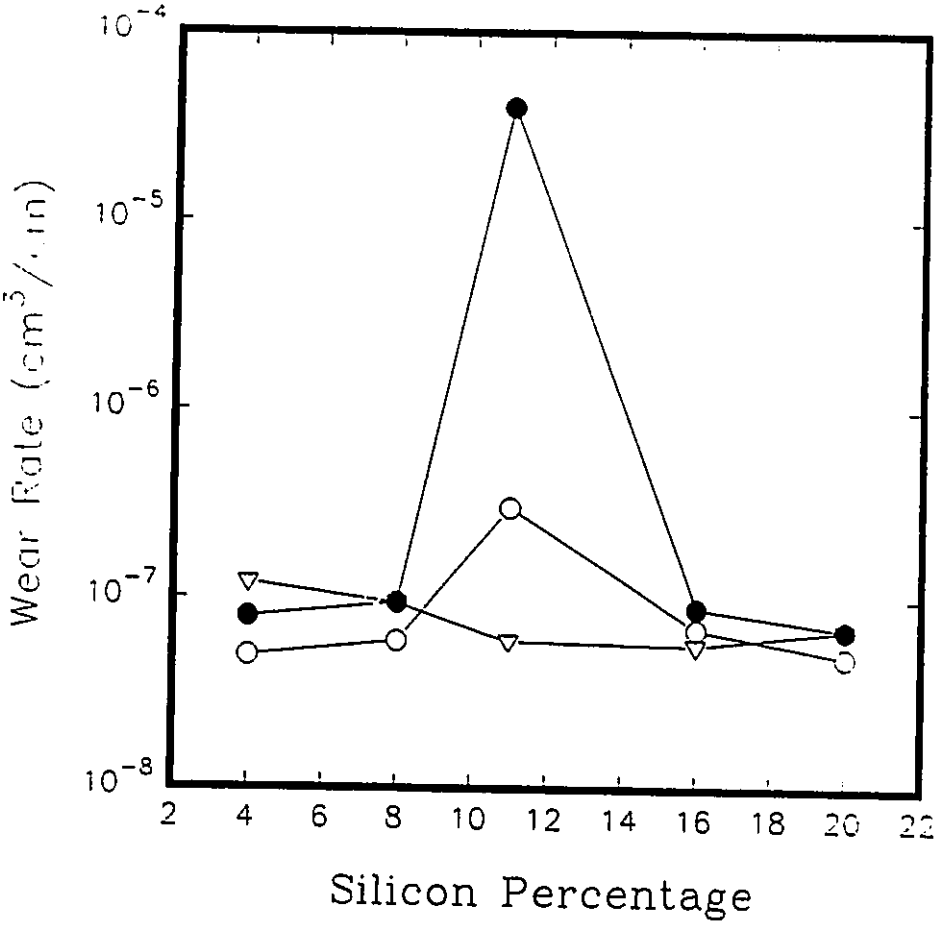

2.7: Wear rate as a function of Si content worn against steel at 1 m/s, 10 N (○), 20 N (●) and 60 N (▽) [66]

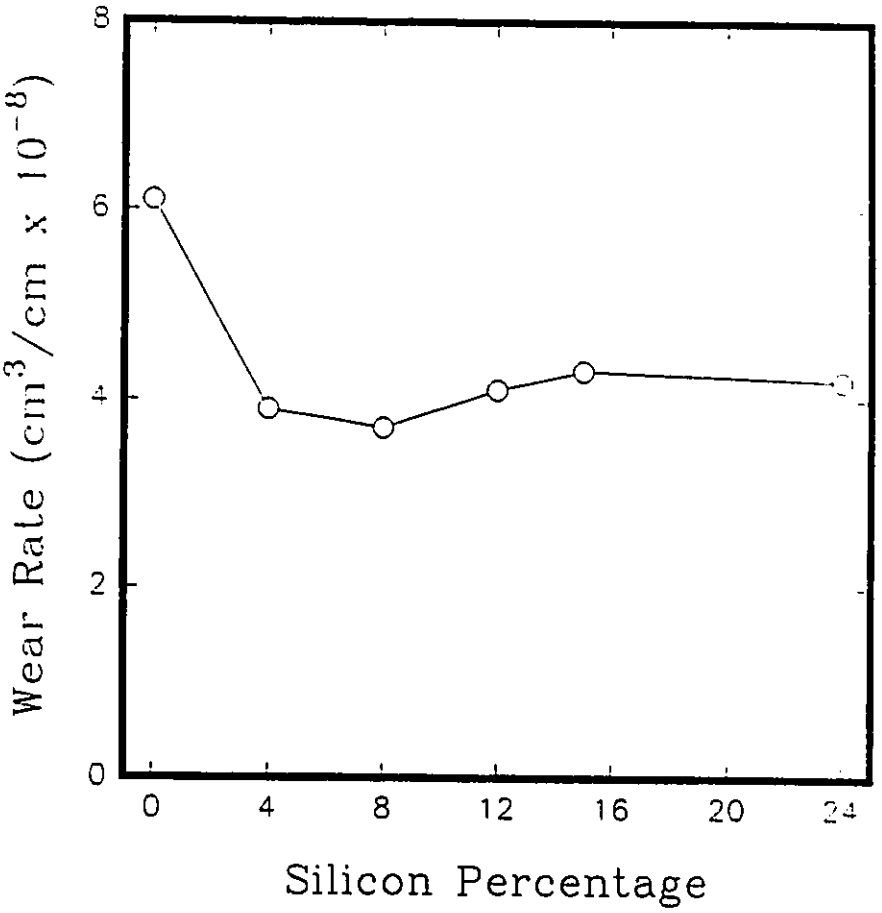

Figure 2.8: Wear rate as a function of Si content sliding at 5.2 m/s, 0.374 MPa against steel [67]

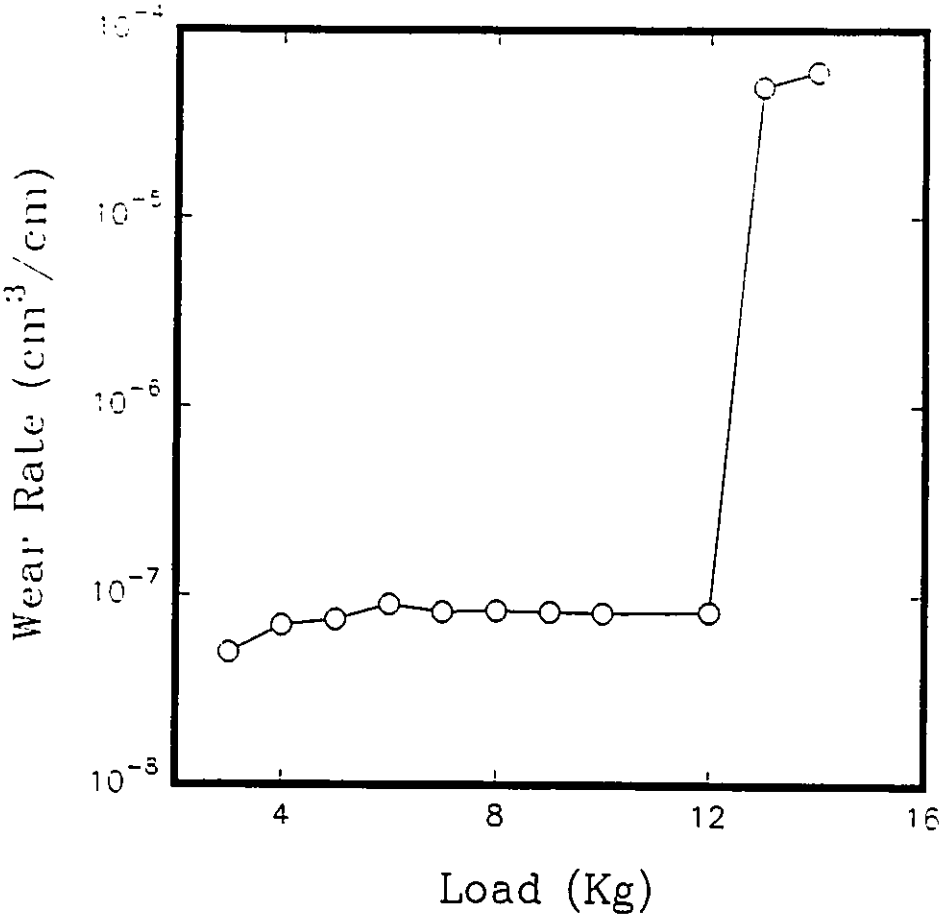

Figure 2.9: Wear of an Al-8%Si alloy slid against steel, 1m/s [66]

at the Al-Si interface and propagate parallel to the wearing surface at a depth of 10 to 20 μm [36]. Zhang and Alpas [36] have developed a model which considers the competition between the plastic strain which leads to void or crack nucleation and the hydrostatic pressure which opposes nucleation. With increasing load, and therefore hydrostatic pressure, the rate of void growth decreases but the depth of crack initiation increases yielding thicker debris. It has been shown that the thickness of the debris does increase with load (Figure 2.10)[68].

The deformation generated during mild wear results in the formation of three distinct subsurface zones (Figure 2.11)[68,70]. At the worn surface a zone of fractured particles exists in which crack nucleation and growth occurs. Adjacent to this is a region of plastically deformed material with some silicon particle fracture. Below this is the unaffected bulk material. It has been determined that the depth of plastic deformation increases with load at a greater rate than the debris thickness [68].

The debris formed during sliding against steel at low loads consists of aluminum, silicon, iron and a small amount of Al_2O_3 [71]. Macroscopically the debris is a finely divide powder with some metallic particles. Hypoeutectic alloys typically form laminar debris with one smooth surface due to interaction with the counterface and finer particulate debris (3 μm) [71,72]. The amount of flake type debris generated increases with load [69,71,72]. When a flake of surface material

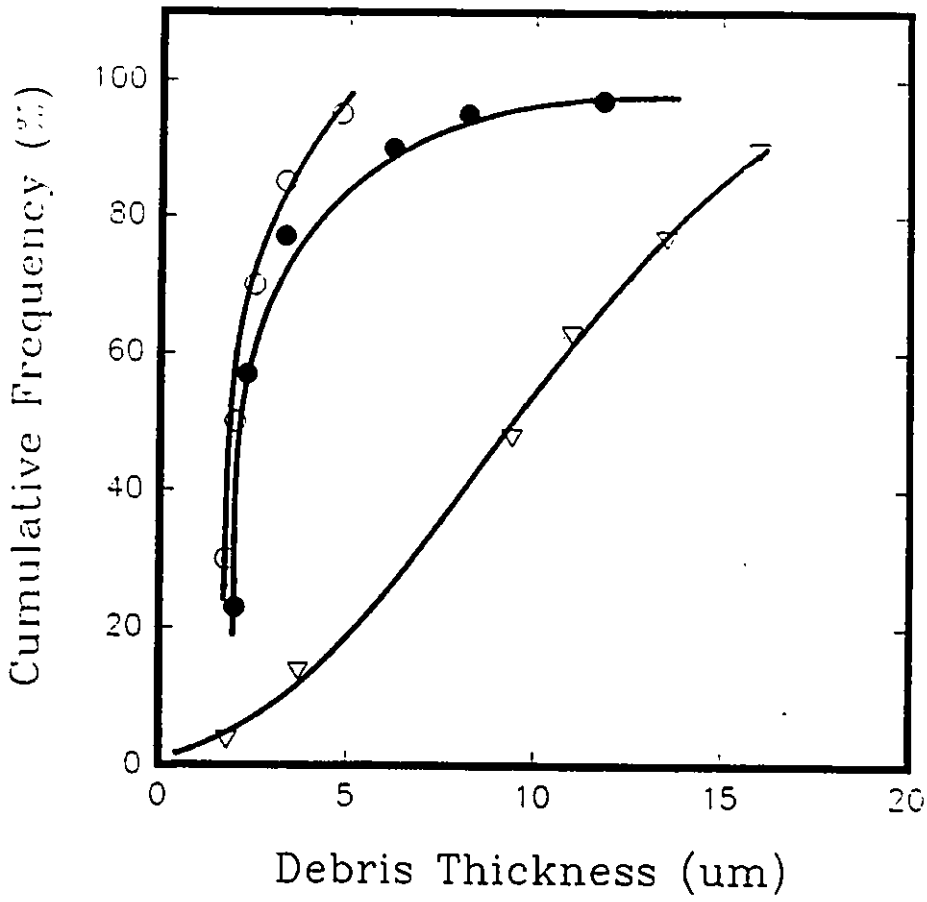

Figure 2.10: Debris thickness generated from an Al-8% Si alloy slid against steel at a velocity of 0.6 m/s and loads of 10 N (∘), 20 N (•) and 80 N (▽) [68]

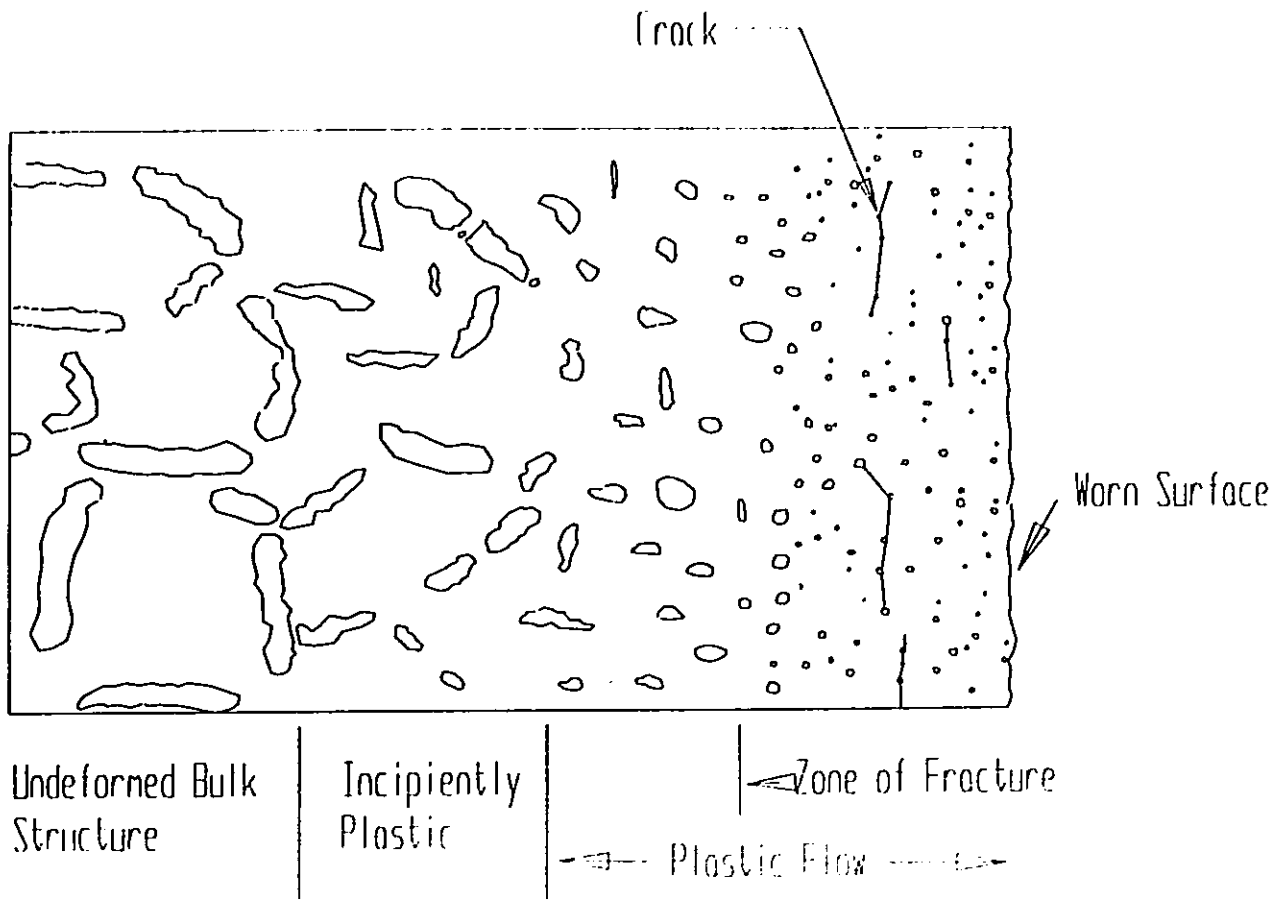

Figure 2.11: Schematic of the three subsurface zones generated during sliding of an Al-Si alloy [68]

is removed, a scar remains on the worn surface [71].

The surface material is a finely mixed layer of small particles (10 to 70 nm) of aluminum, silicon and iron particles [71]. The iron is introduced through the transfer and back transfer of material between the worn surfaces of the sample and the counterface [71]. At very high loads the surface may be protected from further damage by the layer of mechanically mixed material resulting in a lower wear rate [73].

Seizure occurs at high loads and is accompanied by gross plastic deformation and substantial material transfer. The transition load to severe wear increases with increasing silicon content (Figure 2.12)[66,74]. At this stage, transfer from the aluminum sample has resulted in a system where aluminum slide upon aluminum leading to very severe wear rates.

Mild wear rates have been shown to decrease with an increase in sliding speed [65,75]. It was determined that the steady state wear rate decreased with increasing sliding speed up to 2.5 m/s for aluminum alloys containing 7 to 22 wt% silicon [65]. This effect was greatest at low sliding speeds (Figure 2.13). This was believed to be due to the influence of sliding speed on the coefficient of friction which reduced the depth subsurface damage resulting in a decrease in wear [65].

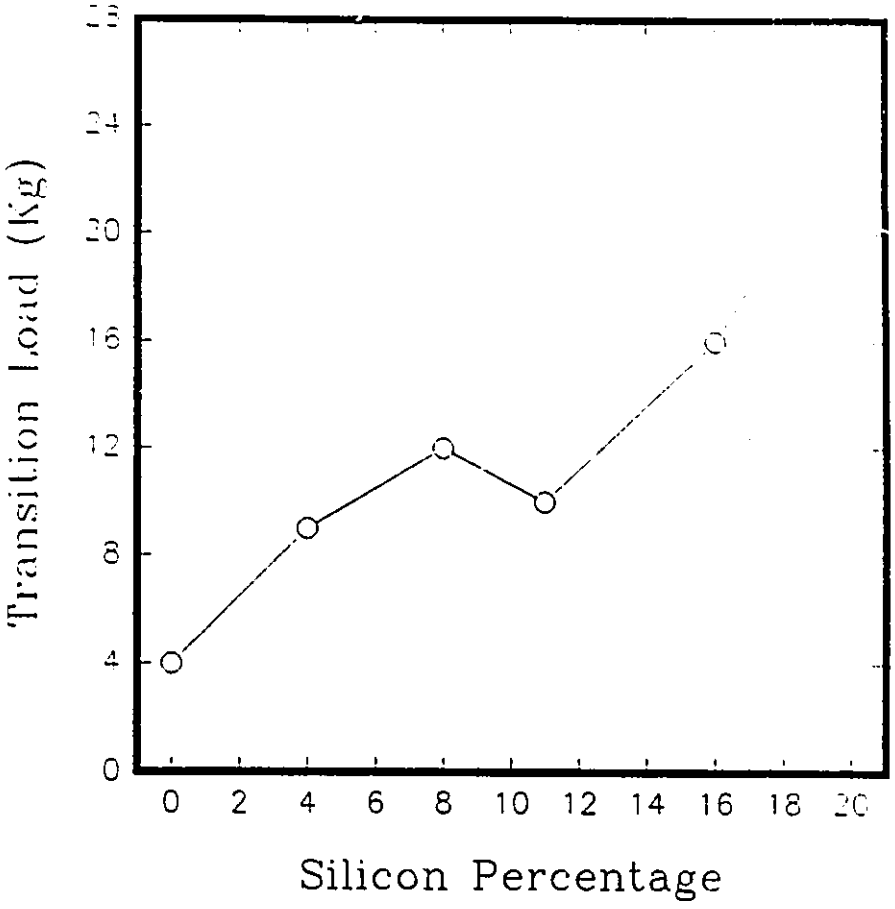

Figure 2.12: The effect of Si content on the transition load when slid against steel at 1 m/s [66]

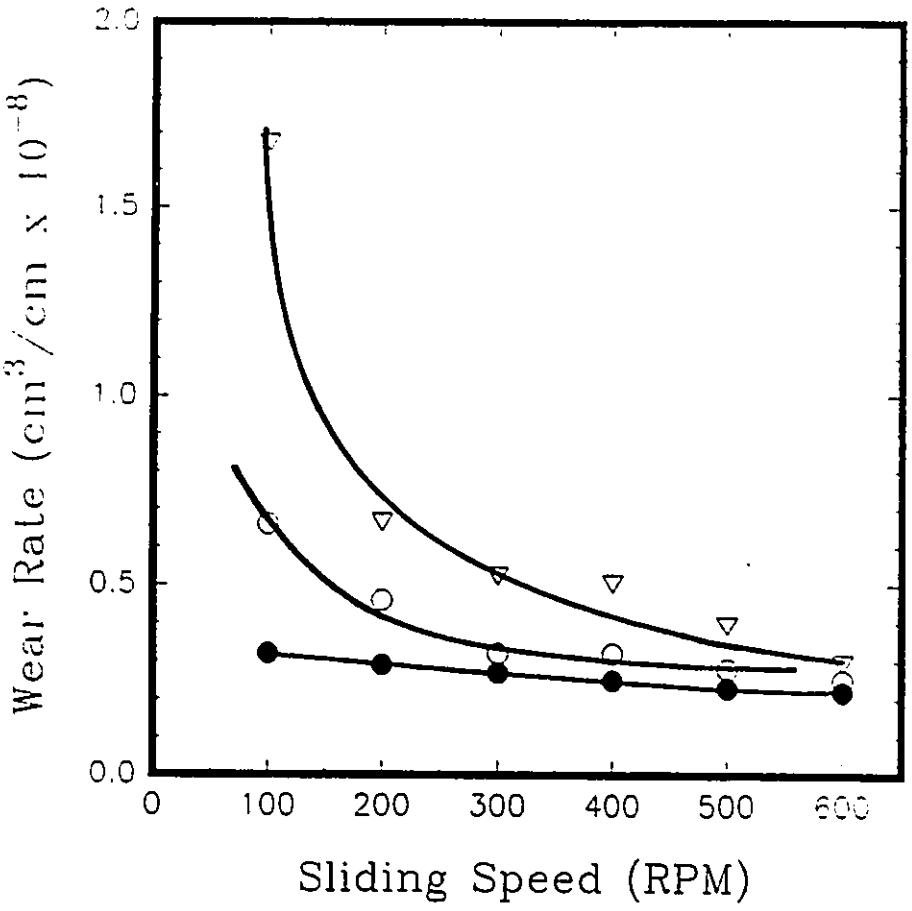

Figure 2.13: The relationship between sliding speed and wear rate of Al-7%Si (○), Al-13%Si (●) and Al-22%Si (▽) at 2 N load [65]

Investigation of the effects of sliding speed on the wear of an Al-12.3 wt% Si alloy showed that the wear rate decreased with sliding speed to a critical value after which the wear rate increased [76] (Figure 2.14). The author proposed that there are two competing processes occurring. As speed increases the strain rate increases resulting in an increase in the flow strength of the subsurface and a corresponding decrease in wear [76]. Opposing this process is the degradation of the flow strength as temperature increases due to the enhanced frictional heating as speed increases. It was concluded that the strain rate effect is dominant resulting in a reduction in the wear rate up to a critical speed. After this speed is achieved the temperature effect increases the wear rate of the alloy [76]. If this is true then the ability of the system to dispose of excess heat is critically important.

Heat may be transferred in to the counterface material. It has been suggested that a counterface which is a good heat conductor, is hard and less soluble in the sample material will result in less wear and an increase the transition load and speed for severe wear [77]. Figure 2.15 shows the normalized wear rates for an Al-12.3wt%Si alloy slid against steel and partially stabilized zirconia (PSZ). The ceramic counterface is not able to transfer heat as easily as the steel counterface resulting in increased wear [77]. Therefore frictional heating is an important factor in the friction and wear of these materials.

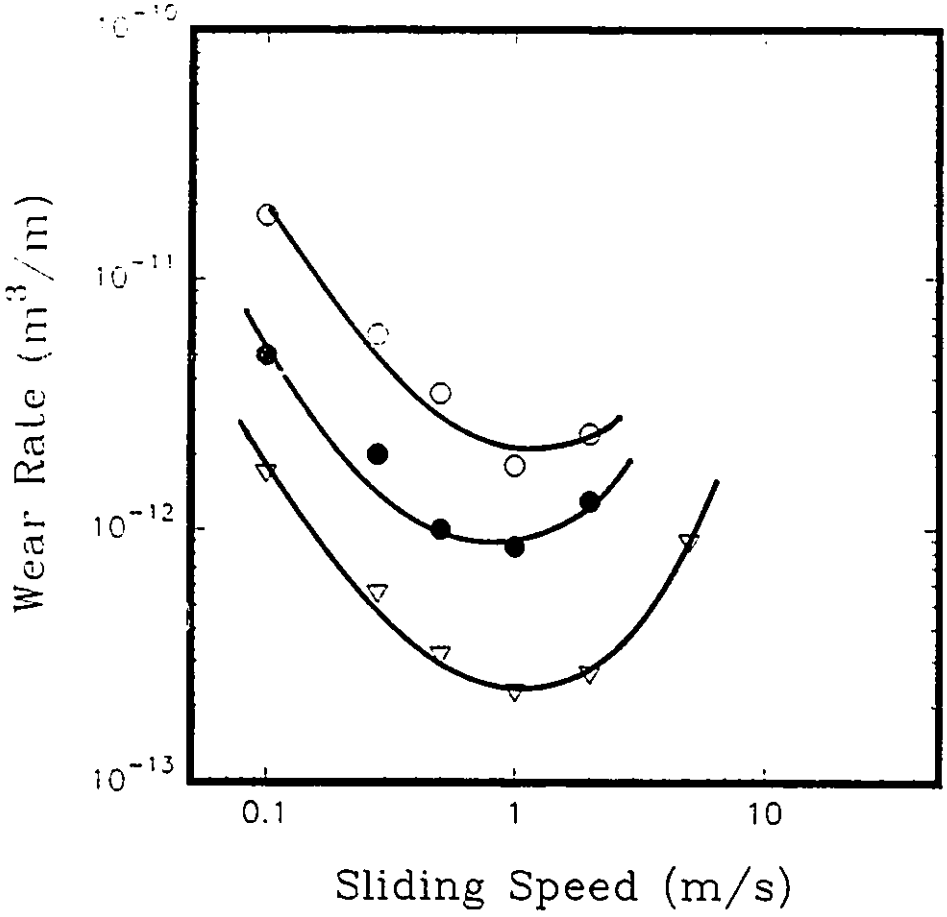

Figure 2.14: The variation of wear rate with sliding speed for an Al-12.3wt% Si alloy slid against Cu (∘), Cu-4.6%Al (•), Cu-7.5%Al (▽) at a load of 0.1 MPa [76]

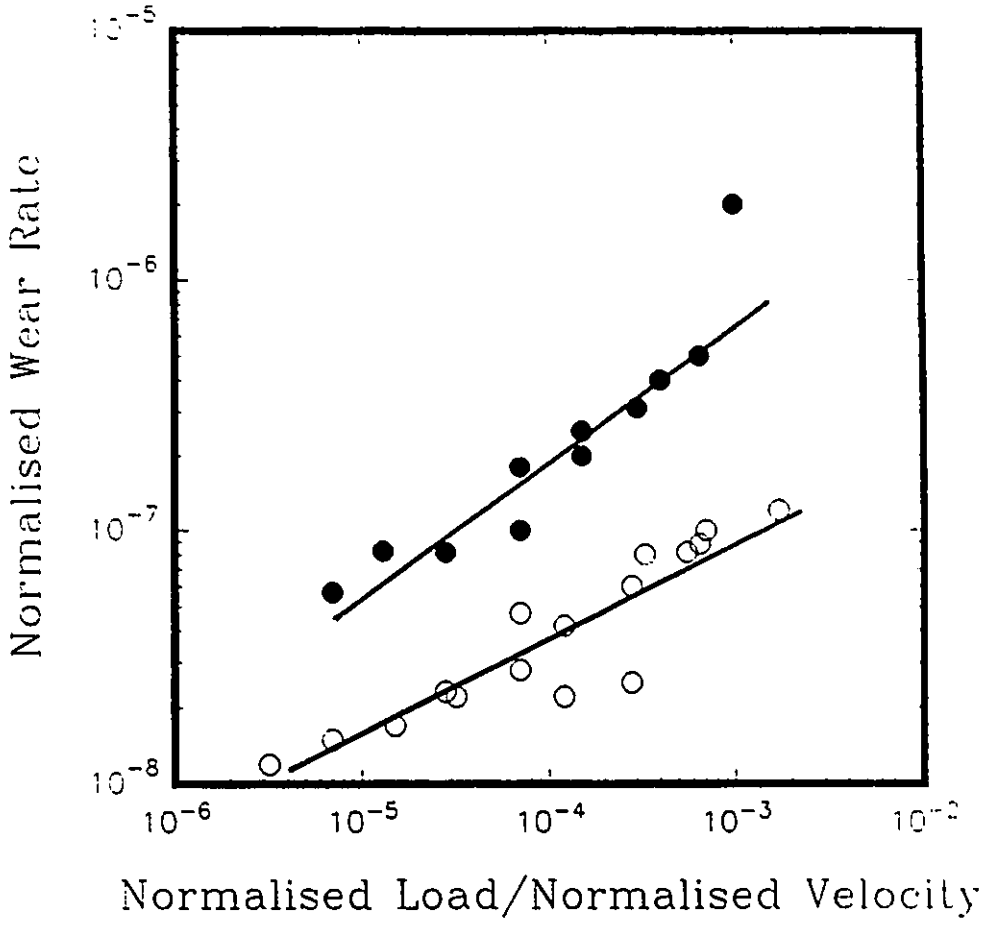

Figure 2.15: The variation of the normalised wear rate (W/A) with the normalised velocity (vr/a) and the normalised load (F/(HA)) for an Al-12.3wt% Si alloy slid against steel (∘) and PSZ (•) [77]

2.6: Sliding Wear of Metal Matrix Composites

The tribological properties of alloys reinforced with particles, whiskers, short fibres and continuous fibres have been investigated. Due to their greater cost effectiveness discontinuously reinforced composites are more frequently studied. Our discussion shall begin with composites with ceramic particulate reinforcement.

Particle Reinforcement

Composites containing SiC particulate [78-87] or Al_2O_3 particles [87-92] in an aluminum, magnesium or copper matrix have been studied. Most frequently the investigator determines that the reinforcement leads to a reduction in wear. In one study, commercially pure aluminum reinforced with 5 wt% Al_2O_3 particles demonstrated wear rates similar to eutectic and hypereutectic Al-Si alloys [87]. The addition of 20 wt% Al_2O_3 particles to a 2024 Al alloy resulted in a two order of magnitude reduction in weight loss [88]. When 20 vol% SiC particles were added to a 6061 Al matrix the reciprocating wear rate decreased up to 300 times [78]. When slid against steel, an Al-7% Si alloy reinforced with 20% SiC demonstrated wear rates similar to ductile iron [79]. Therefore, it would appear that the reinforcement of various alloys by hard ceramic particles reduces the dry sliding wear rate. However, this trend is not always factual.

Zhang and Alpas [80,81,89] observed wear rates similar to the unreinforced

material over a certain load range. This was attributed to a greater propensity for subsurface crack nucleation and growth in the composites as a result of the severe localized deformation. In the composites decohesion of the reinforcement-matrix interface nucleated a crack which propagated parallel to the worn surface along the particle-matrix interfaces. This process led to the delamination of a flake of surface material. The unreinforced material experienced a similar delamination process with nucleation of the cracks occurring at second phase particles [80,81,89]. The inclusion of the hard ceramic particles increased the number of sites for crack nucleation and decreased the fracture toughness leading to enhanced delamination wear in the composites. This offsets any beneficial effect of the reinforcement preventing any enhancement of the wear properties in this load range [80,81,89]. Similar results were achieved in the study of an Al_2O_3 reinforced copper alloy [92]. Poor interface bonding and an increase in delamination wear caused the wear rate of the composite to be as much as five times higher than the wear rate of the unreinforced alloy [92].

Ceramic particle reinforcement has been shown to increase the load required to achieve severe wear and seizure with respect to the unreinforced alloy [80-82,89]. It has been proposed that the transition to severe wear depends on the achievement of a critical transition surface temperature generated by frictional heating [80,81,89]. Typically the critical surface temperatures are between 390 to 420 K (approximately 0.4 T/T_m) for aluminum alloys [80,89]. For a 6061 Al composite with 20 vol% Al_2O_3 the critical transition temperature was 440±10 K. Work softening may occur in the

surface material leading to an increase in adhesion and wear. The ceramic reinforced composites are able to maintain mild wear to higher temperatures, and therefore higher loads, since the degradation of the mechanical properties is less in the composites with respect to the matrix alloy as temperature rises [80,81,83,89]. In fact, elevated temperature tests have shown that SiC reinforcement of an Al-7%Si alloy resulted in excellent wear rates up to 150 C (Figure 2.16) due to the "thermal stability" offered by the reinforcement [83].

At low loads the heat generated does not result in a significant rise in temperature. It has been shown that the hard particles in the subsurface are intact and able to support the load reducing the metal to metal contact [80,81,89]. The particles machine the counterface [79-81,89] resulting in the transfer of iron containing fragments to the wearing surface [80,81,89,90]. These fragments form a layer with some lubricating characteristics leading to an order of magnitude reduction in wear rates [80,81,89].

At higher loads the worn surface is composed of aluminum [80,81,89,90]. In the severe wear regime a layer is frequently formed adjacent to the worn surface of finely broken material. This layer may be established due to the high plastic strain in the immediate subsurface fracturing the particles ($\varepsilon \alpha D^{-3}$ where D is the particle diameter) [93], the re-imbedding of fractured ceramic particles in to the ductile matrix [90] or possibly transfer and back transfer of the composite components

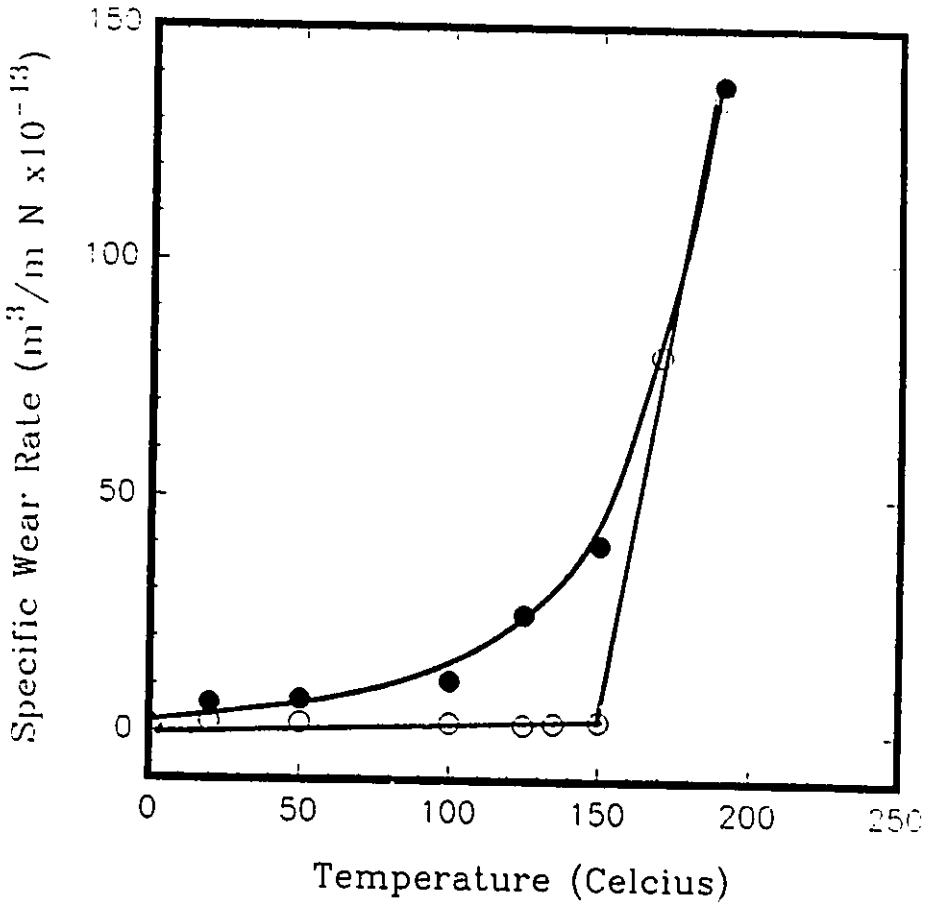

Figure 2.16: Comparison of the specific wear rates of Al-20%Si (•), Al-7%Si-20%SiC (○) with increasing temperature at a load of 25 N slid against steel [83].

which refines the morphology and results in the subsurface layer.

The transition from mild to severe wear also depends on the velocity. In the study of 7091 Al - SiC reinforced composites [84] the wear rate was found to be similar to the unreinforced alloy when tested at sliding speeds below 1.2 m/s. However, at higher velocities (up to 3.6 m/s) the composites demonstrated wear rates up to 25 times lower than the unreinforced material. Mild wear was observed at low velocities while a transition to severe wear occurred between 0.72 m/s and 3.6 m/s. The transition was attributed to a change in mechanism from surface- fatigue-related surface cracking to subsurface-cracking-assisted adhesive transfer [84].

In summary, the particulate composites appear to demonstrate three wear behaviours as load increases [81,89]. At low loads the particles are able to support the load and machine the counterface resulting in a decrease in wear with respect to the unreinforced alloy [80,81,89]. As load increases the particles fracture and lose their load supporting ability. Subsurface crack nucleation and growth occurs through a damage accumulation process leading to wear rates similar to the unreinforced alloy. The transition to severe wear occurs at higher loads in the case of composites [80-82,89]. Subsurface damage is evident and an interfacial layer forms consisting of fractured particles. Transitions in wear rate or wear mechanism may be caused by changes in velocity [84]. Severe wear is terminated by seizure. Similar trends are observed in fibre reinforced composites.

Fibre Reinforcement

Fibre reinforcement frequently results in a reduction in total wear but an increase in delamination wear [94]. In one investigation 20 vol% Al_2O_3 and 20 vol% SiC fibres were added to a 6061 Al alloy resulting in a decrease in the wear rate of 6% and 15% respectively [95]. Another study concluded with similar results [96]. It was reported that the wear resistance of a hypoeutectic Al-Si alloy could be improved over 50% by the addition of 8% to 17% Kaowool (Al_2O_3 SiO_2) or 10% Saffil (Al_2O_3) fibres [97]. A new concept is the introduction of two or more types of fibres into a single matrix resulting in a hybrid composite with superior properties. A 6061 Al hybrid composite of Al_2O_3 and SiC displayed better wear rates compared to composites with only one type of fibre when slid against 304 stainless steel at 0.94 m/s at a load of 31 N (Figure 2.17) [95].

The inclusion of ceramic fibres also increases the bearing capacity of the alloy. The addition of SiC whiskers to an aluminum alloy increased the bearing capacity 60%, compared to the unreinforced aluminum, which resulted in an increase in the load or velocity required to achieve severe wear [98]. This was due to the high hardness of the whiskers and the resistance they supplied to matrix deformation [98].

The effectiveness of the fibres to reduce wear has been shown to depend on

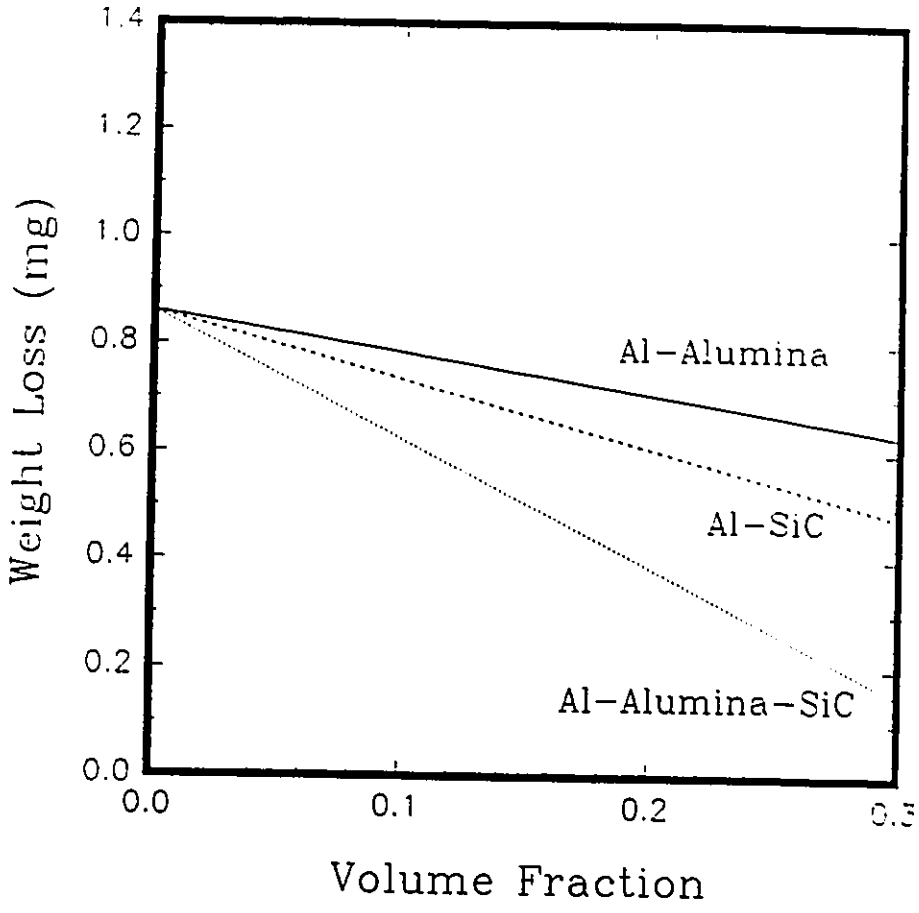

Figure 2.17: Effect of reinforcement on the wear properties of Al slid against 304 stainless steel [95]

the fibre orientation in SiC [95,96], Al_2O_3 [95,96,99] and graphite [100-102] fibre reinforced alloys. Composites which have fibres orientated normally to the wear surface display lower wear rates due to a reduction in fibre pull or roll out [100,102] or ease of subsurface deformation [98,99,101]. It has been observed that the fibres in the subsurface are forced to bend in the direction of sliding. Eventually the fibres fracture and rotate from the normal orientation to the parallel orientation due to the plastic deformation below the worn surface [98,101]. It has been suggested that the extra energy required to bend and break the normally orientated fibres is responsible for the improved wear resistance with respect to composites with the fibres orientated parallel to the contact surface [101]. Anisotropy of the fibre itself may also lead to orientation effects.

The type of fibre is very important. Superior wear rates have been observed in composites with SiC fibres compared to composites with Al_2O_3 fibres [95]. Graphite fibres have a layer lattice structure which is very anisotropic. In one direction, graphite fibres resist shear. Perpendicular to this direction the layers of the lattice structure readily slide past each other when subject to shear. The result is solid lubrication due to the fibres which has been shown to reduce both friction and wear [101,103,104]. However, the degree of graphitization in carbon fibres depends on the starting materials and the manufacturing process. Before a discussion of the wear properties of graphite reinforced alloys may be undertaken a consideration of the various types of carbon fibres and particles must be

performed.

2.7: Carbon Fibres

Carbon fibres may be roughly divided in to two categories: graphitic carbon fibres and non-graphitic carbon fibres. Both fibre types consist of carbon atoms, however, the graphitic fibres have undergone a heat treatment procedure to produce a crystalline state with a high degree of long range order. In general the treatment process [105] starts with a setting treatment under oxidative control. The temperature is increased resulting in a carbonization reaction. Finally the treatment temperature is raised to temperatures of the order of 2400 K at which point graphitization occurs [105]. The details of this process depend on the starting material.

Three common precursor materials are rayon, polyacrylonitrile (PAN) and pitch. Rayon and PAN are polymer molecules. Pitch is a complex mixture of aromatic compounds [105]. Pitch is the least expensive of the common precursor materials for carbon or graphite fibre production [106].

PAN precursors are frequently used to produce high modulus or high strength graphite fibres for use in high strength composites [106]. The properties of the fibres, and hence the composite, depend on the processing technique and, in

particular, the final graphitization temperature [106].

Pitch may be used to produce low strength, low modulus carbon fibres simply by extrusion followed by a dehydrogenation condensation reaction at about 600 K [105]. The fibres produced in this manner are non-graphitizing, isotropic carbon fibres. Graphite fibres may be produced from pitch although this requires the intermediate step of producing a highly anisotropic mesophase pitch [105]. Upon heating at high temperatures, graphitization occurs resulting in graphite fibres. Table 2.2 compares the properties of a pitch based fibre after carbonization and graphitization and a non-graphitizing pitch based fibre. From Table 2.7.1 it may be concluded that the addition of a non-graphitic pitch based carbon fibre to an aluminum matrix must be considered fundamentally different than the addition of a graphite fibre which posses a much high degree of long range order.

2.8: Manufacture of Aluminum-Carbon Composites

Several problems arise during the fabrication of these materials [106]. Firstly there is an interfacial reaction. Secondly, carbon fibres are not wetted by molten aluminum leading to a poor interface. Lastly, the carbon fibre will oxidize at elevated temperatures in air.

It has been shown that at temperatures above 800 K, carbon will react with

Table 2.7.1: Properties of pitch based carbon fibres.* Carboflex is the trade name of non-graphitic carbon fibres produced by Ashland Petroleum Co. of Ashland Kentucky, USA.

	Carbonized[105]	Graphitized[105]	Carboflex[107]
Interlayer Spacing	3.40-3.43 Å	3.36-3.37 Å	
Density (g/cm^3)	2.1-2.2	2.1-2.2	1.57
Tensile Strength	835-950 MPa	1490-2080 MPa	400-600 MPa
Elastic Modulus	150-210 GPa	450-720 GPa	30-40 GPa

aluminum to produce the brittle compound Al_4C_3 [106]. This results in the degradation of the fibre and a resultant degradation of the mechanical properties of the composite (Figure 2.18)[108]. Increasing the time of infiltration, melt temperature or infiltration pressure promotes aluminum carbide formation [106].

Another problem encountered is poor wetting. This is overcome by the modification of the chemical composition of the melt or the fibre surface, increasing the working temperature or modification of the atmosphere [106]. Metallic coatings, of copper [109] or nickel [108,110], are often applied to the fibres resulting in an improvement in the reinforcement-matrix interface coherency of the composite.

Oxidation of the carbon fibres is reduced by lowering the fabrication temperature or with a metallic coating [106].

2.9: Wear of Graphite Reinforced Aluminum Alloys

In the study of graphite particle reinforced aluminum composites it has been observed that the wear rate tends to decrease. In a 2014 Al-50% graphite particle composite, slid against steel at a speed of 0.1 m/s and a load of 10 N, the wear rate of the composite was 20% of the wear rate of the unreinforced alloy [111]. A hypoeutectic Al-Si alloy (LM6) displayed a 50% reduction in wear when 3% graphite particles were added [112]. The seizure pressure increased from 2.0 MPa

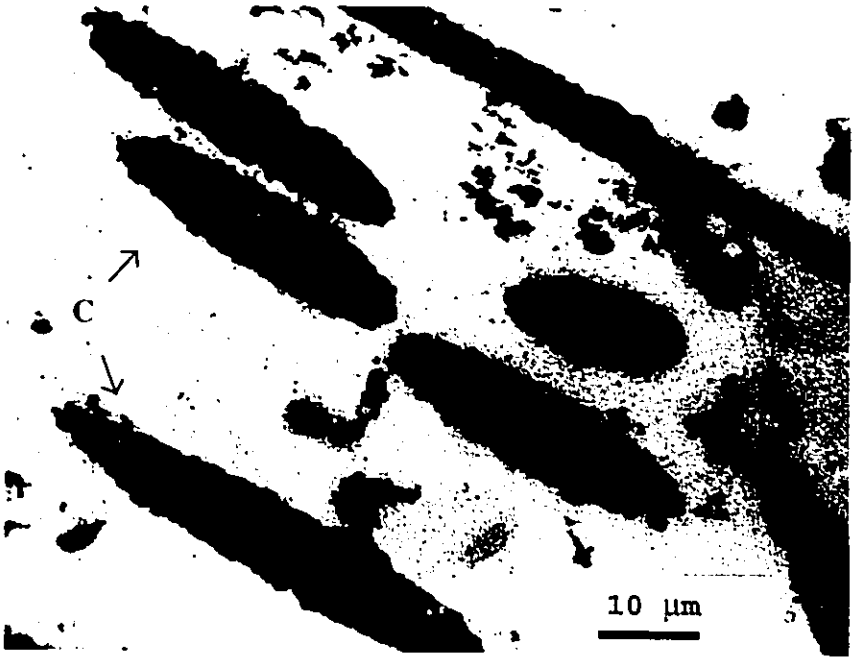

Figure 2.18: Degradation of the carbon fibres as a result of interfacial carbide reaction (used with permission [108])

in the unreinforced alloy to 3.2 MPa in the graphitic composite [112]. It has also been shown that the weight loss decreases with increasing amounts of graphite (Figure 2.19) in a 2014 Al matrix composite [113]. Friction displays a similar trend.

The coefficient of friction decreases to a stable value of 0.2 when the graphite content exceeds 20% [114]. When less graphite is available the coefficient of friction depends on the matrix composition [114]. Studies have determined that the reduction in coefficient of friction and wear is due to the formation of a graphite film on the wear surface [111-114]. The correlation between the area covered by graphite and the reduction in coefficient of friction as sliding distance increases supports this statement [114].

The graphite film formed on the wear surface was shown, using AES and XPS, to consist of carbon oxide, air deposited carbon, graphitic carbon and aluminum particles [111]. The primary constituent was graphite suggesting that the film must behave as a solid lubricant resulting in the lower friction force and wear rates [111].

Film formation has been proposed to occur through a series of steps [113]. Due to the layer lattice structure of the graphite particles, layers will be preferentially removed. As sliding continues the plastic deformation of the subsurface causes the subsurface graphite particles to be squeezed out on to the

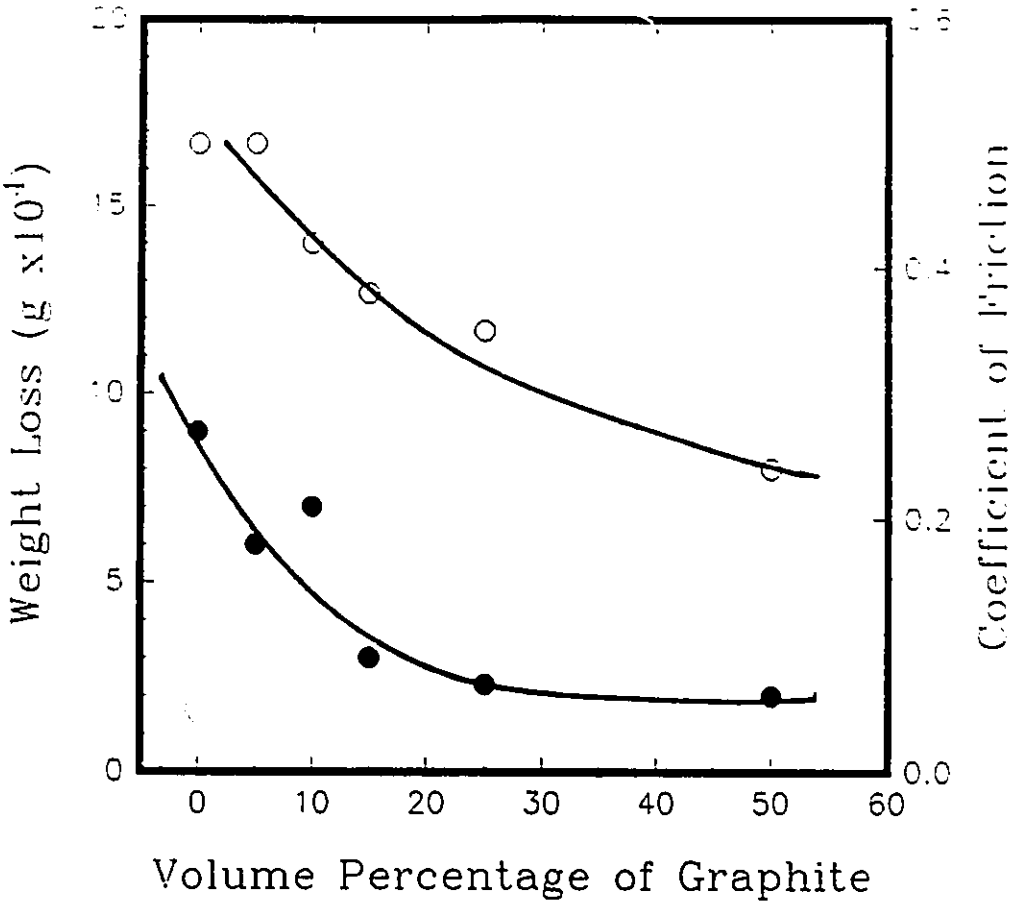

Figure 2.19: Weight loss (•) and friction coefficient (○) as a function of the graphite volume fraction slid against steel at 15 N, 1 m/s for 5 minutes [113]

wearing surface. The extruded graphite is sheared off and smeared on the wear surface covering a larger area than the volume fraction of graphite would predict [113].

The thickness of the graphite film has been measured using Auger Electron Spectroscopy (AES) and X-ray Photoelectron Spectroscopy (XPS) profiling techniques. In an Al 319-10% Gr composite the film was 5 to 10 nm thick after sliding for 7.5 m at 10 N [115]. In an Al 2014-50% Gr composite the thickness was 10 to 20 nm [111] with some variations in thickness. A significant lubricating film was formed after only 2 m of sliding. In an Al-10% Gr composite the thickness was 10 to 20 nm [116]. More significant is that 30% of the surface was covered with graphite which shows that the 10% graphite has smeared out over the wear surface [116].

The graphite smears on to the wear surface but there is a competing process in which the aluminum smears overs the graphite preventing lubrication [114,115]. Larger graphite particles are more difficult to cover and lead to more effective lubrication [114].

The lubricating film is also transferred to the counterface. Transfer of iron from the counterface to the wear surface of the composite has been reduced through the addition of graphite to the sample [115].

Other factors, related to the introduction of graphite, may overshadow the beneficial effects of lubricating film formation. A reduction in strength and ductility has been observed and was cited for an increase in the wear rate in one investigation [117]. In composites manufactured via powder metallurgy, the porosity has been observed to increase with graphite addition which also lead to an increase in wear [118].

The lubricating effects of graphitic carbon depend on the long range order of the graphite layer lattice structure. Other factors such as humidity [43] and environment do influence the lubricating ability of graphite. However, amorphous and non-graphitic carbons do not have the graphite structure and cannot be considered to have solid lubricating characteristics.

2.10: Wear of Non-Graphitic Composites

In a study of an aluminum alloy reinforced with 10% naturally occurring non-graphitic microcrystalline carbon particles it was observed that the wear rate was higher in the case of the composite when slid at 7.5 N load, 0.2 m/s [119]. The coefficient of friction of the unreinforced and composite materials were similar. The non-graphitic carbon did not form a lubricating film and it was concluded that the carbon was ineffective in improving the tribological characteristics [119]. This points out the importance of a graphitic structure for solid lubrication by carbon to occur.

In summary, there are two general types of carbon fibres. These are graphitic and non-graphitic regardless whether the starting material was PAN, pitch or rayon. These fibres may be incorporated in to an aluminum matrix. The problems of Al_4C_3 formation, fibre oxidation and poor wetting may be overcome by applying a metal coating on to the fibre or particle [106]. The friction and wear properties of composites made with graphite fibres are improved due to the formation of a solid lubricating film [111-116]. Carbon fibres or particles which do not have a layer lattice structure, viz. non-graphitic carbon, can not act as solid lubricants [119].

Chapter 3: Experimental Methods

3.1: A356-Carbon Fibre (CF) Composite Fabrication

These composites were manufactured by INCO of Mississauga Ontario, Canada, using a low pressure infiltration apparatus (Figure 3.1). Carbon fibre paper, purchased from Ashland Petroleum Company, was cut such that the carbon fibres could be stacked in a quartz tube producing a fibre preform. The density of the preform and the resultant volume fraction of carbon fibres was determined by the density of the carbon fibre paper used. Prior to infiltration the preform was heated to approximately 623 K.

The charge was a molten A356, Al-7%Si-0.35%Mg-0.11%Fe-0.20%Ti-0.05%Mn-0.5%Zn alloy. The alloy was at a temperature of approximately 923 K in the crucible. The apparatus was under vacuum to prevent oxidation of the aluminum. The heated crucible was raised to form a seal with the quartz tube. An inert gas (Ar) was then added to the system which applied pressure (0.7 to 1.9 MPa) to the surface of the molten alloy causing the fluid to flow up the tube and infiltrate the carbon fibre preform. The preform was then cooled and machined to produce wear samples.

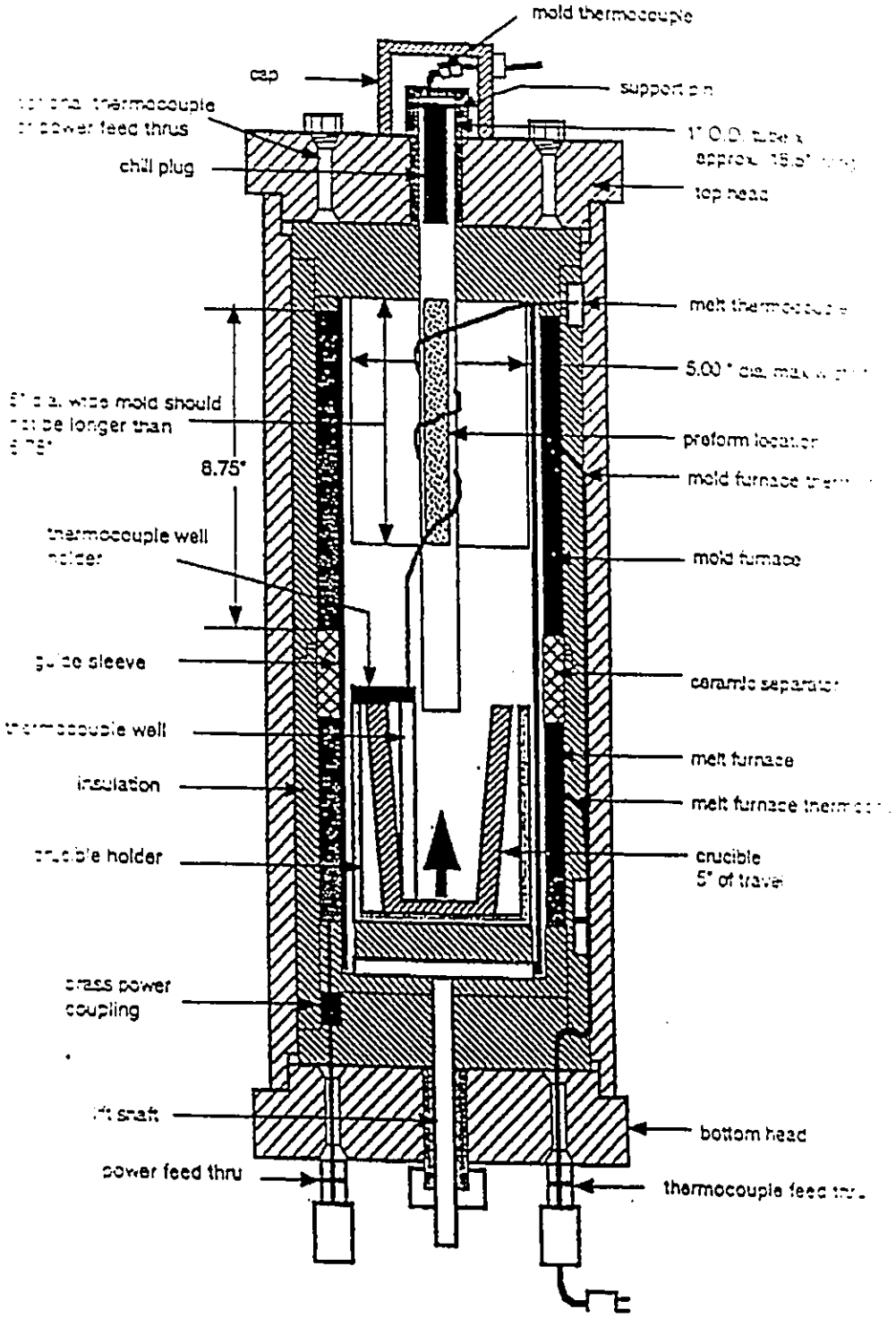

Figure 3.1: PCast low pressure infiltration apparatus (compliments of T. Stephenson)

A nickel coating was applied to the fibres in order to improve the wetting characteristic of the carbon-aluminum system resulting in a more coherent interface upon solidification. The application of the nickel coating was performed through the decomposition of a nickel containing gas [94].

Nickel carbonyl decomposes at relatively low temperatures (below 575 K) [94]. This decomposition reaction yields solid nickel and carbon monoxide:

$$Ni(CO)_4\ (g) \rightharpoonup Ni\ (s) + 4(CO)\ (g)$$

The solid nickel was deposited on the carbon fibres resulting in a coating thickness of the order of one micron and a nickel loading of approximately 62 wt% [94]. Figure 3.2 is a secondary electron image of the nickel coated carbon fibres. The structure of the infiltrated preform may be observed in Figure 3.3.

3.2: A356-Gr-SiC Composite Fabrication

Composites containing 3 or 10 vol% graphite and 20% SiC particulates were manufactured via a molten metal mixing process. An A356-20 vol% SiC composite was produced by Alcan Int., Kingston, Ontario, using the Duralcan process. This composite was remelted so that graphite particles could be added. Prior to graphite addition to the melt the graphite particles were coated with nickel, to improve wettability, using the same nickel carbonyl decomposition technique described in section 3.1.

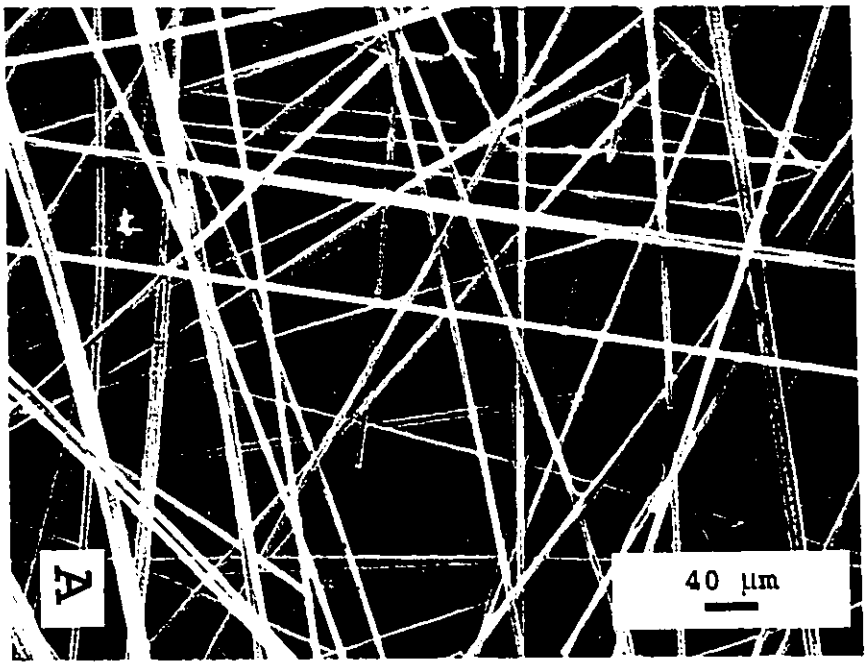

Figure 3.2: Nickel coated carbon fibres (compliments of T. Stephenson)

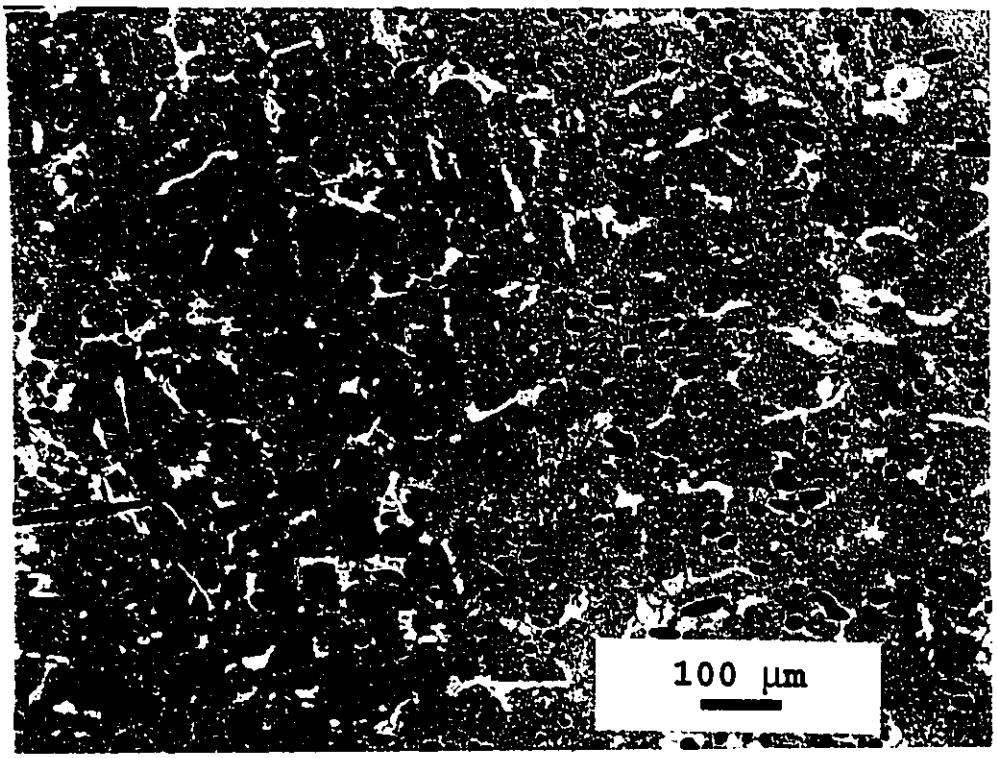

Figure 3.3: Composite structure after infiltration. Black circles are the carbon fibres. Light phases are the intermetallics.

3.3: Wear Testing

Wear tests were performed using a block on ring wear machine designed and manufactured at the University of Windsor (Figure 3.4). The machine consists of a rotating bearing steel ring upon which a stationary composite sample is forced. A one horsepower DC motor (1750 RPM max) was used to drive the rotating ring. The applied normal loads varied from 5 N to 441 N. Typical testing conditions were a sliding speed of 0.5 m/s and a sliding distance of 1000 m in the ambient atmosphere. Some tests deviated from these standard conditions. For instance, sliding speeds of 0.1 m/s and 1.0 m/s were used. The sliding distance varied up to 9000 m in some cases. The sliding speed was determined using a contact tachometer to measure the rotational velocity of the steel ring in revolutions per minute (RPM). The sliding distance was calculated from the sliding velocity and the duration of the test.

The bearing steel ring was a SAE 52100 steel of nominal composition 1% C, 0.35% Mn, 1.45% Cr, 0.25% Si, 0.04% max S, 0.035% max P and the balance iron. The outside diameter of the ring was 30 mm and the width was 12 mm. The ring was treated to a hardness of 63 HRC. Prior to each test the counterface was polished with 240, 320, 400 and 600 grit SiC abrasive papers resulting in a arithmetic average surface roughness (R_a) of 0.9 μm. The surface roughness was determined using a Mitutoyo Surftest 401; a stylus type apparatus. The ring was

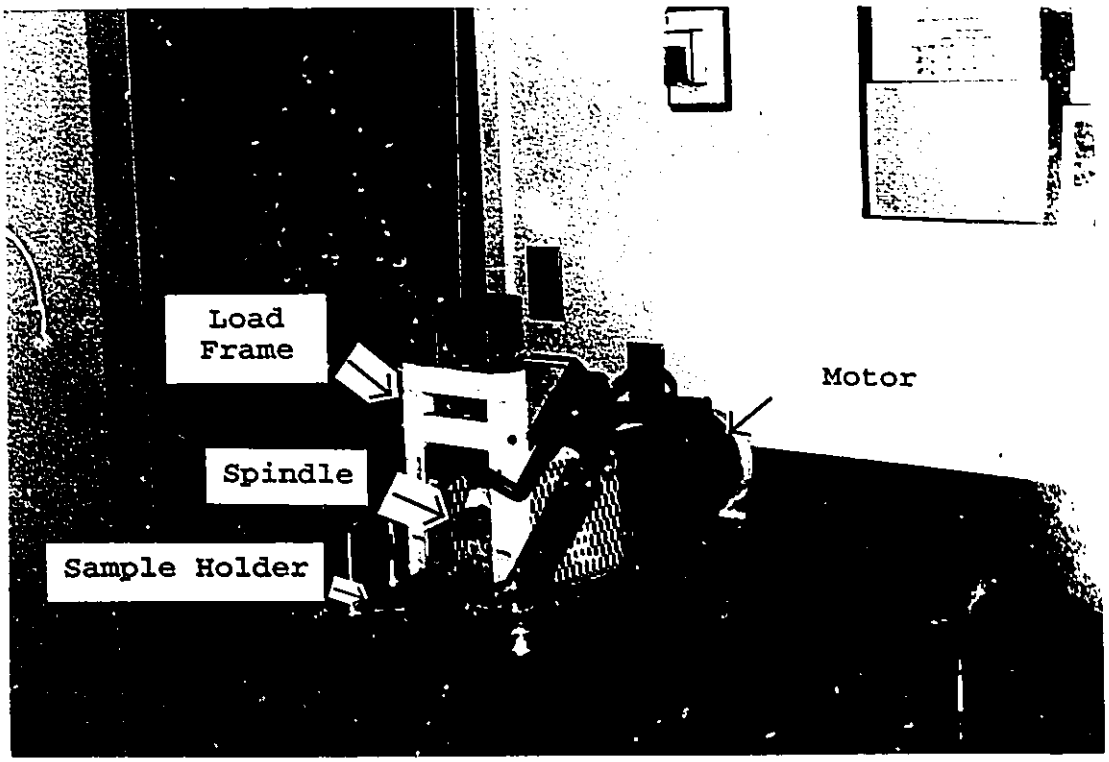

Figure 3.4: The block on ring wear machine

then ultrasonically washed in acetone.

The composites were machined in to wear samples 10x10x5 mm^3 in size. A narrow face of each sample was then polished with 400 and 600 grit SiC paper and 1 μm alumina slurry. The resulting surface roughness values (R_a) were 0.7 μm and 1.2 μm for the A356-CF and A356-Gr-SiC composites respectively. The samples were also ultrasonically washed in acetone and their weight determined.

The weight difference before and after the test was measured to determine the average weight loss per unit sliding distance. This was converted to the volumetric wear rate (mm^3/m) using the appropriate densities. The density of each composite was measured using an immersion technique (ASTM D792-86). Basically this involved determining the weight of the sample in air and in water at 293 K. The difference can be related to the buoyancy force and hence the volume of the sample. The density of each composite is displayed in Table 3.1.

Most of the wear rate data was obtained for composites tested in the as received condition. However, some of the hybrid A356-Gr-SiC composites were solutionized and artificially aged to the peak aged condition. The solutionizing treatment was four hours at 813 K followed by artificial aging for nine hours at 428 K. These samples were tested at a load of 10 N only.

Table 3.1: Densities of the composite materials

	Density
A356-CF	2.62 g/cm^3
A356-3%Gr-20%SiC	2.78 g/cm^3
A356-10%Gr-20%SiC	2.75 g/cm^3

3.4: Contact Surface Temperature Measurement

The temperature of the contact surface during wear was measured using a grounded chromel-alumel wire thermocouple probe with a stainless steel sheath of diameter 0.25 mm. The probe was inserted through a hole drilled through the sample from a narrow face adjacent to the wearing surface. The hole was drilled with a solid carbide bit (0.7 mm diameter) in a high speed drill press. The thermocouple was placed such that it was either in contact with the steel counterface or trapped in the tribolayers of the sample. The data was recorded, manually, at thirty second intervals. Measurement became difficult at high loads since the velocity fluctuated to a greater degree during severe wear. The thermocouple tended to fail due to damage caused by the wear process at high loads.

3.5: Microscopic and Spectroscopic Analysis

X-ray diffraction studies were performed on the as received samples and the wear debris. A Rigaku X-ray diffractometer with Cu-α radiation was most often used. Secondary electron images were obtained employing a Semco Nanolab 7 Scanning Electron Microscope (SEM) fitted with a tungsten filament. SEM samples were coated in a acetone soluble lacquer and then mounted in a cold epoxy mount in order to improve edge retention and reduce damage to the wear surface during polishing. Accompanying the SEM was a Kevex-ray 5100C X-Ray Energy

Spectrometer which was capable of detecting elements with atomic numbers greater than 12. In order to detect carbon, Auger Electron Spectroscopy was performed on the worn surface.

Auger Electron Spectroscopy (AES) was performed at McMaster University utilizing a Perkin-Elmer PHI 600 Scanning Auger Multiprobe. The samples were sputter cleaned, with argon, to remove any air deposited carbon. Surveys of small areas were able to identify the local atomic composition. Some of this data was treated to yield the atomic ratios of C:Fe:O without consideration of any other element.

Particle size was determined using a microscope with a graduated eyepiece. The maximum and minimum dimensions of approximately 200 particles were measured and used to determine the average maximum and average minimum dimension. A Buehler Micromet II Hardness Tester was employed to measure Vickers and Knoop hardness values. The loads varied from 25 g to 200 g depending on the application. The volume fraction of various constituents were determined using a metallographic point counting technique described in ASTM standard E562-89.

Chapter 4: A356-CF Composites

Part A: Experimental Results of the A356-CF Composites

4.1: Material Characteristics

The carbon fibre - aluminum matrix composites were produced using low pressure infiltration. The matrix was an A356, Al-Si casting alloy of nominal composition 7.0% Si, 0.35% Mg, 0.11% Fe, 0.20% Ti, 0.05% Mn, O.05% Zn and the balance aluminum. The carbon fibres were produced from petroleum pitch through a melt blowing technique (section 3.1). These fibres are non-graphitizing, isotropic carbon fibres. The distribution of the fibre diameter is shown in Figure 4.1. The average maximum and minimum dimensions were 16.2 μm and 10.5 μm respectively. The fibre length was not evident from standard metallography. Etching away the matrix revealed that the fibres were at least 600 μm long. Prior to infiltration the carbon fibres were coated with nickel to improve the wetting characteristics of the system.

In Figure 4.2 one observes the distribution of carbon fibres in the matrix. The carbon fibres were randomly orientated in planes which were either parallel (Figure 4.2 a) or normal (Figure 4.2 b) to the contact surface. Higher magnification allowed other phases to be discernable in the matrix (Figure 4.3).

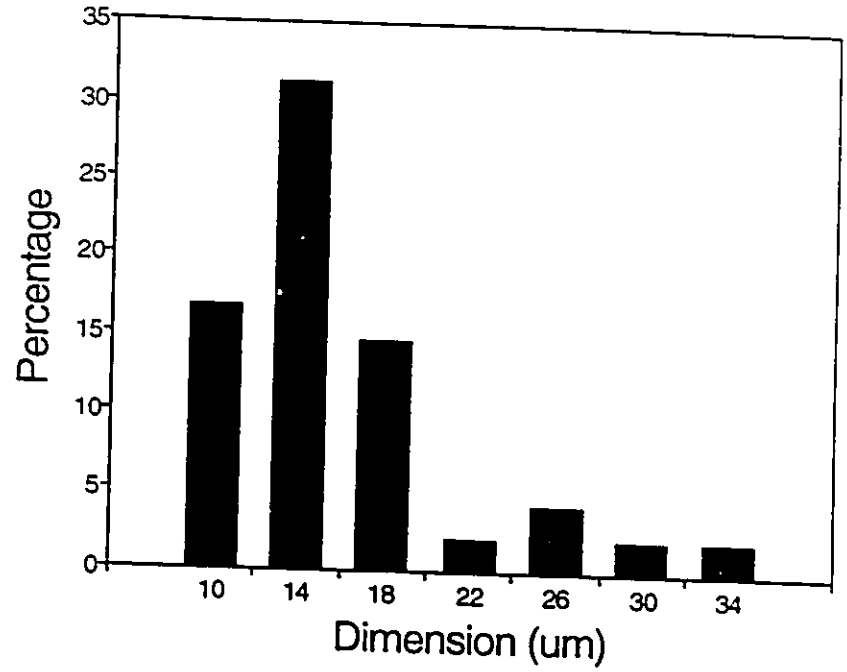

(a)

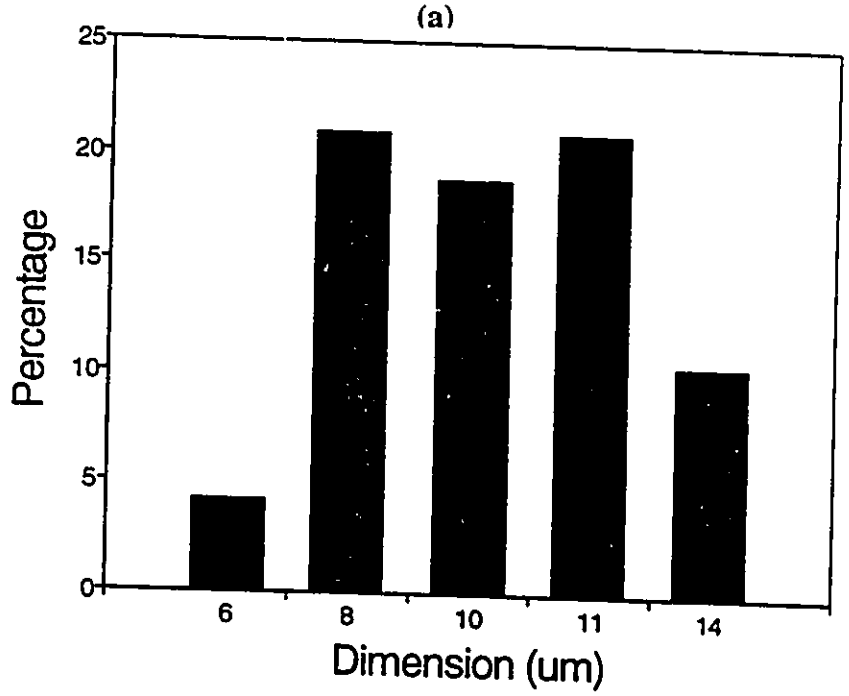

(b)

Figure 4.1: Distribution of the carbon fibre diameters a) maximum diameter and b) minimum diameter

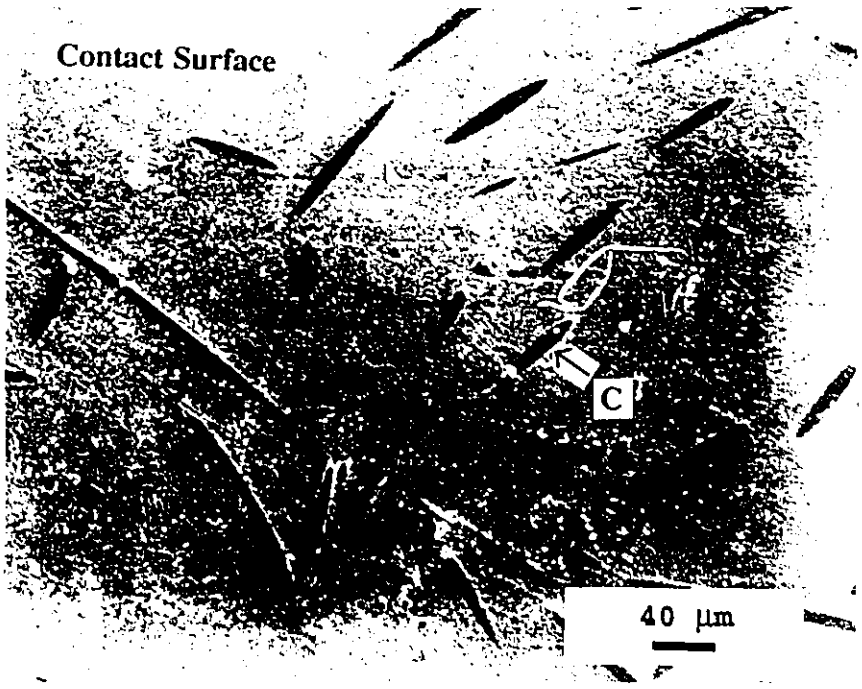

(a)

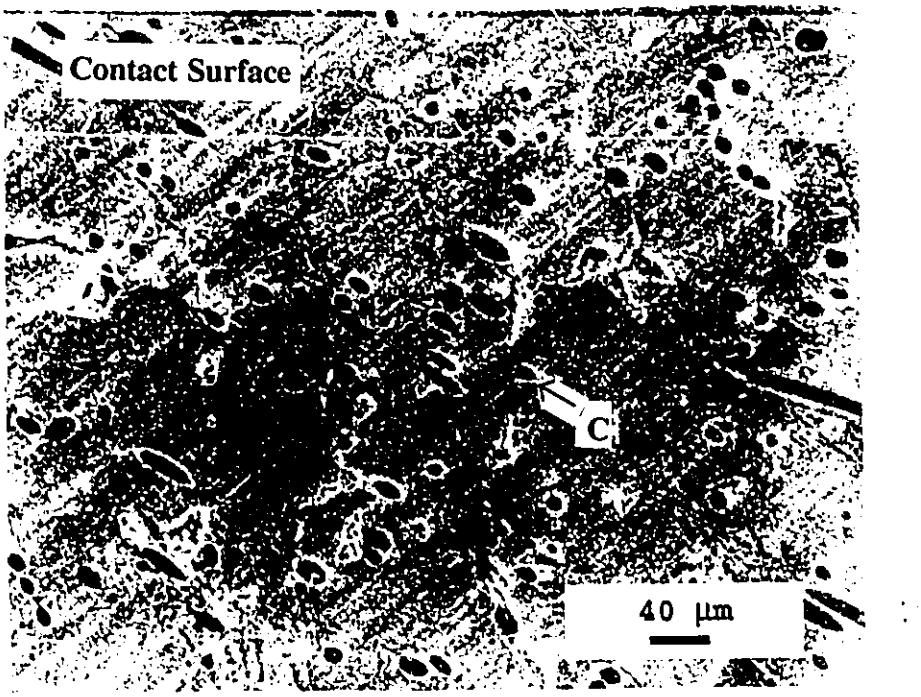

(b)

Figure 4.2: Microstructure of the composites with fibres orientated a) parallel and b) normal to the contact surface

Figure 4.3: Microstructural constituents

In the matrix the coated carbon fibres are readily distinguished. Irregularly shaped, finger-like, particulates in the matrix were identified as silicon (dark grey) and an intermetallic phase (light grey).

Phase identification was performed using X-Ray Diffraction (XRD). The results of the XRD experiments indicated the presence of Al, Si and an intermetallic phase, Al_3Ni (Figure 4.4). A peak for elemental nickel was not observed suggesting that the majority of the nickel had reacted with the aluminum matrix. The carbon fibres did not produce a peak due to the low volume fraction of fibres and their non-graphitic structure.

The microhardness values and volume fraction of each constituent is shown in Table 4.1. The hardness of the intermetallic is very high compared to the hardness of either the carbon fibres or the matrix. The volume fraction of the intermetallic is approximately two times the volume fraction of the carbon fibres. The silicon particles in the matrix are comparable to the intermetallic in regards to hardness and volume fraction.

In summary the composite consisted of several components. These were a relative soft aluminum alloy (0.3% Mg) matrix with hard silicon particles dispersed throughout, carbon fibres of somewhat higher hardness and a nickel aluminide

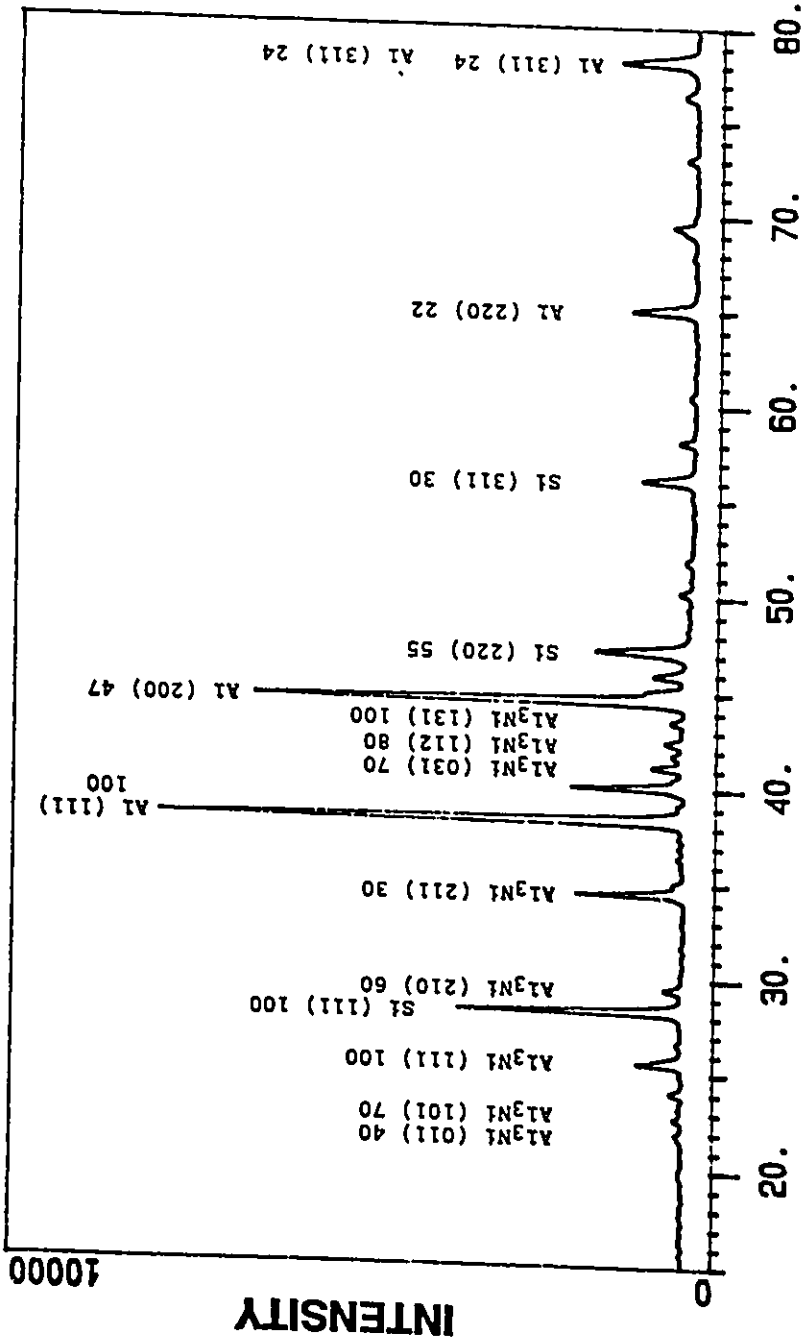

Figure 4.4: XRD Pattern of the A356-CF composite

Table 4.1.1: Hardness and volume fraction of the carbon fibre composite's constituents

	Hardness	Volume Fraction
Al-0.3wt% Mg	74.1 ± 8.1 VHN, 25g	Balance
Carbon Fibres	180 VHN [91]	0.04 ± 0.01
Al_3Ni	610-770 VHN [104]	0.1 ± 0.03
Si	715-1450 VHN [104]	0.07

intermetallic phase. The wear behaviour was observed to be dependant on the presence of each component.

4.2: Wear Rates

The dry sliding wear rates of the A356-4%CF composites as a function of load are depicted in Figure 4.5. The composites demonstrated two wear regimes, mild and severe. At low loads typical wear rates of $7x10^{-4}$ mm^3/m at 10 N and $1x10^{-3}$ mm^3/m at 130 N were observed. The wear rates, W_d (mm^3/m), increased linearly on a log-log plot suggesting the curve fit equation:

$$W_d = C \cdot L^n \qquad (4.2.1)$$

where C and n are the intercept and the slope of the line respectively and L is the applied load. The constants, C and n, and the correlation coefficient, r, for this equation are shown in Table 4.2 for both orientations.

Mild wear occurred until a transition load was reached. The transition load was identified by a change in the debris morphology. This was also accompanied by an increase in the slope of the wear rate-load curve indicating a change in the wear mechanism. Examination of the wear rate data suggests that the transition from mild to severe wear occurred at loads from 150 to 200 N. Extrapolation of the wear

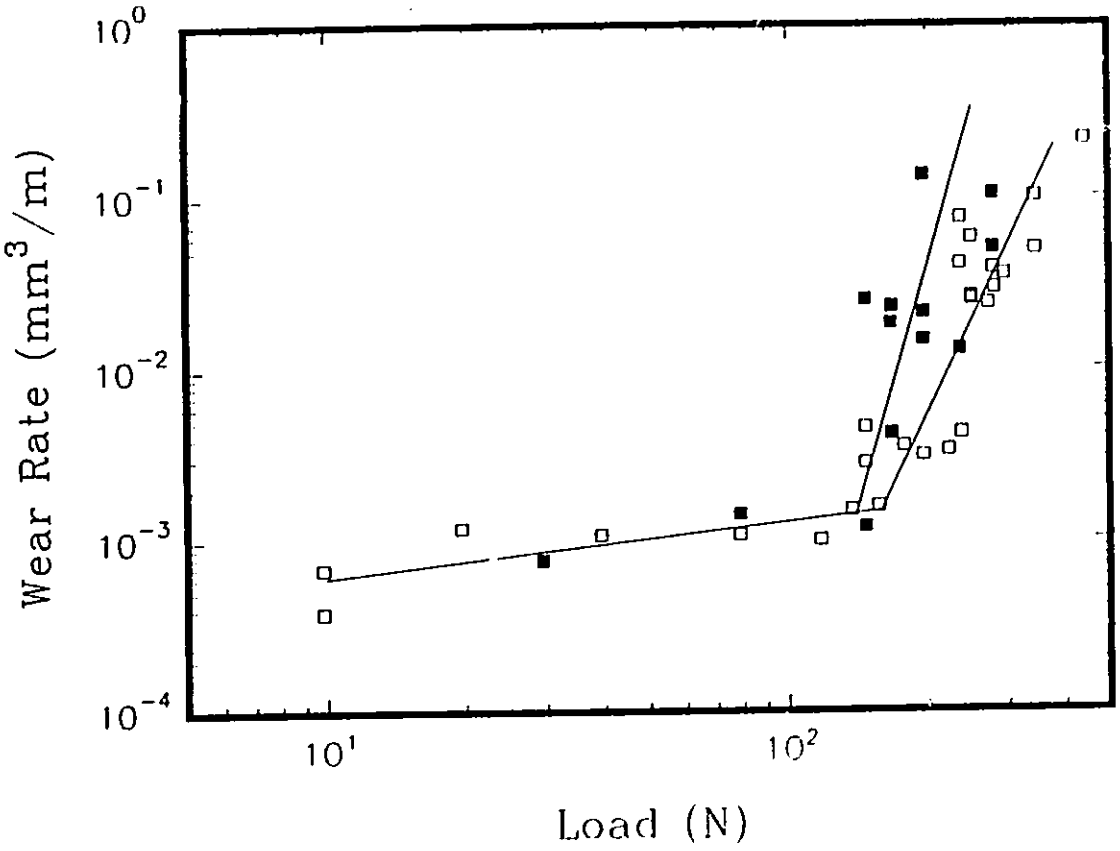

Figure 4.5: Wear rate of the composites with normal (□) and parallel (■) fibres as a function of load

Table 4.2: Curve fit parameters C and n and the correlation coefficient r for the Al-Si - CF composites in the mild wear regime.

	C	n	r
Parallel Fibre Orientation	2.12×10^{-4} $\pm 2.1 \times 10^{-4}$	0.27±0.68	0.72
Normal Fibre Orientation	3.04×10^{-4} $\pm 1.5 \times 10^{-4}$	0.32±0.17	0.82

Table 4.3: Curve fit parameters C and n, and the correlation coefficient r for the Al-Si - CF composites in the severe wear regime.

	C	n	r
Parallel Fibre Orientation	10^{-31}	13	0.49
Normal Fibre Orientation	10^{-21}	8	0.46

data and observation of the debris suggested that fibre orientation may affect the transition load. The possible dependence of the transition load on fibre orientation will be discussed later.

Once the transition to severe wear occurred, higher wear rates of $3x10^{-1}$ mm^3/m at 200 N and $9x10^{-2}$ mm^3/m at 300 N were typical. Once again the wear rate increased with load indicating that severe wear may also be described by equation 4.2.1. The parameters C and n, as well as the correlation coefficients are shown in Table 4.3.

Composite samples, with the fibres orientated parallel to the contact surface, were tested for sliding distances up to 1800 m (Figure 4.6). At a load of 78 N the volume loss increased linearly at a wear rate of $1.1x10^{-3}$ mm^3/m indicating mild wear. However, at a load of 196 N, which is above the transition load, a rapid increase in wear was observed at a sliding distance of 1100 m. This increase in volume loss was accompanied by massive deformation and rapid material transfer indicating seizure. The slope of the curve suggests a wear rate of $4.1x10^{-1}$ mm^3/m.

Therefore, Figure 4.5 demonstrates the two wear regimes, mild and severe. The transition load, identified by a change in debris morphology, denoted an increase in the slope of the wear rate-load plot. Figure 4.6 showed that there are two different behaviours. At low loads the volume loss increased linearly with

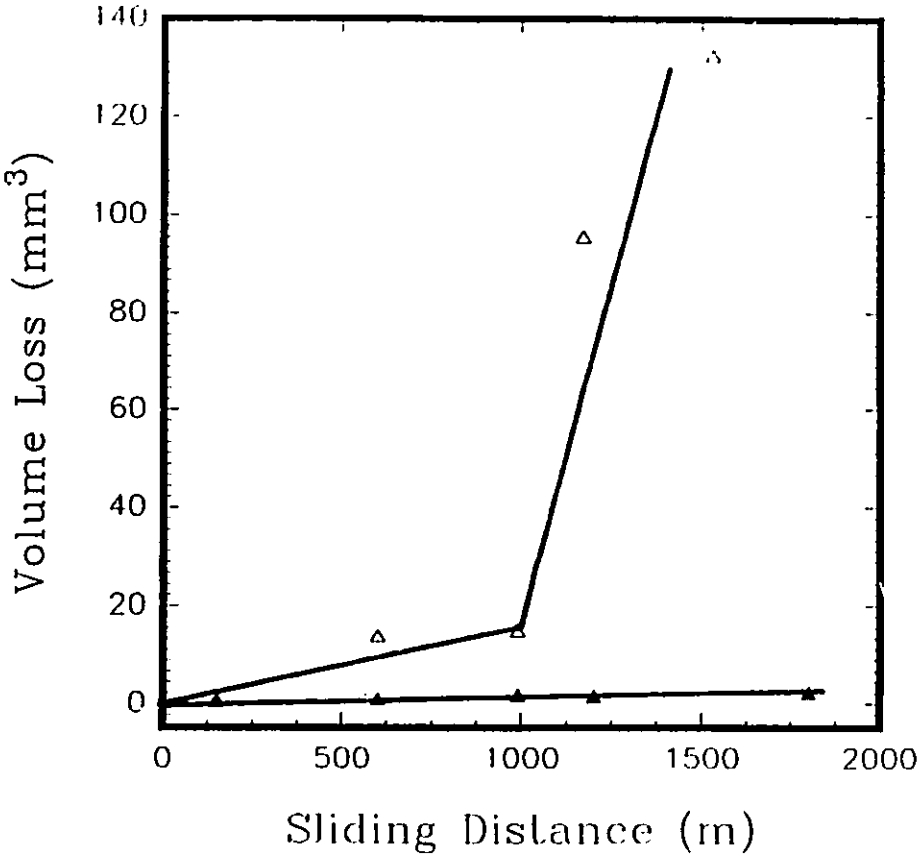

Figure 4.6: Volume loss as a function of sliding distance for the A356-CF composite with fibres parallel to the contact surface at loads of 78 N (▲) and 196 N (∧)

sliding distance at a relatively low wear rate. At high loads there was an increase in volume loss at high sliding distances indicating seizure.

Seizure and wear of the composite samples affected the wear of the SAE 52100 steel counterface (Figure 4.7). In the mild wear regime, wear of the counterface resulted in a weight loss which increased in the relatively small range of $2.5x10^{-3}$ g to $1.5x10^{-2}$ g over 1000 m of sliding. However, once the transition load (150 to 200 N) was surpassed the counterface gained weight. This weight gain was due to the transfer of surface material from the composites to the steel counterface. At a post transition load of 196 N (Figure 4.5), the majority of the metal transfer occurred during seizure (Figure 4.8). When seizure developed the wear track on the steel ring was almost completely covered with an adherent layer of aluminum (EDS) (Figure 4.9). However, the counterface wear data indicates that transfer also occurred prior to seizure. This is supported by metallographic evidence. The fact that transfer to the steel counterface occurred in the severe wear regime, prior to seizure, is significant in the interpretation of the operating wear mechanisms and will be discussed in section 4.8.

4.3: Temperature Rise During Sliding

The mechanism of debris generation is affected by the interface temperature generated during sliding. Figure 4.10 documents the surface temperature as a

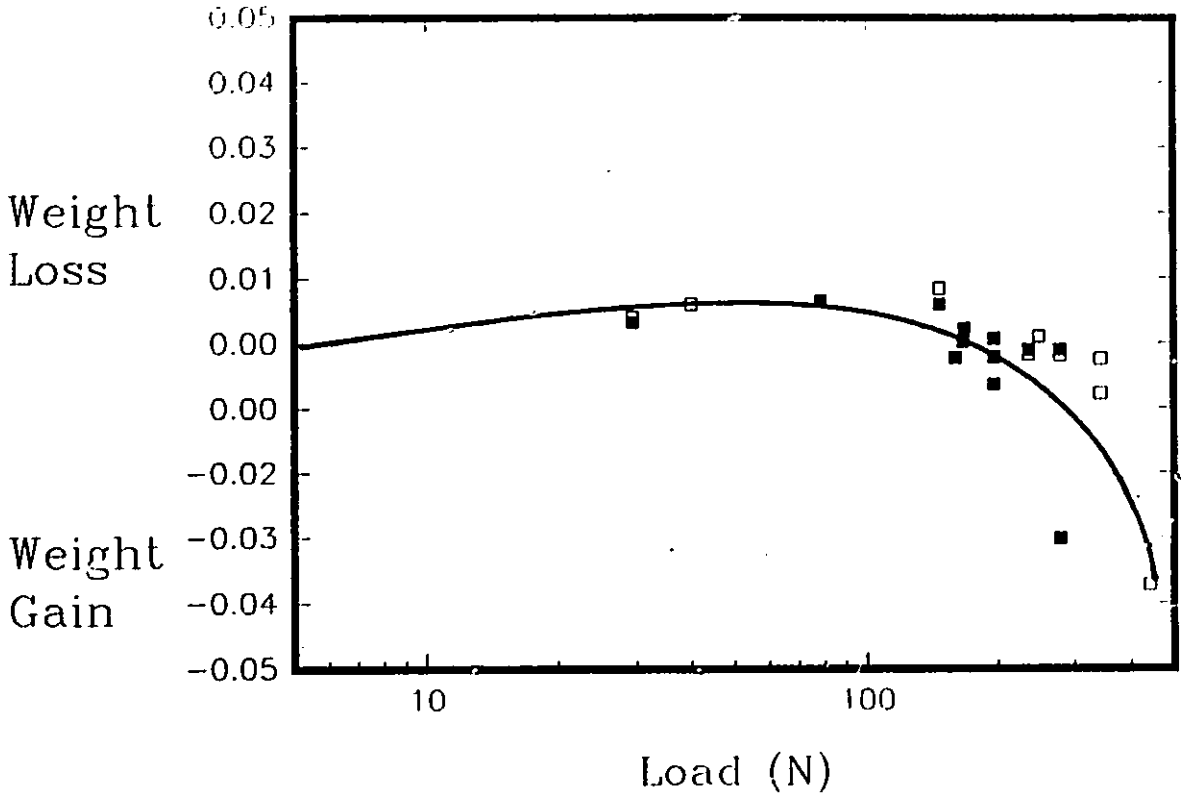

Figure 4.7: Counterface wear as a function of load for the normal composite (□) and the parallel composite (■)

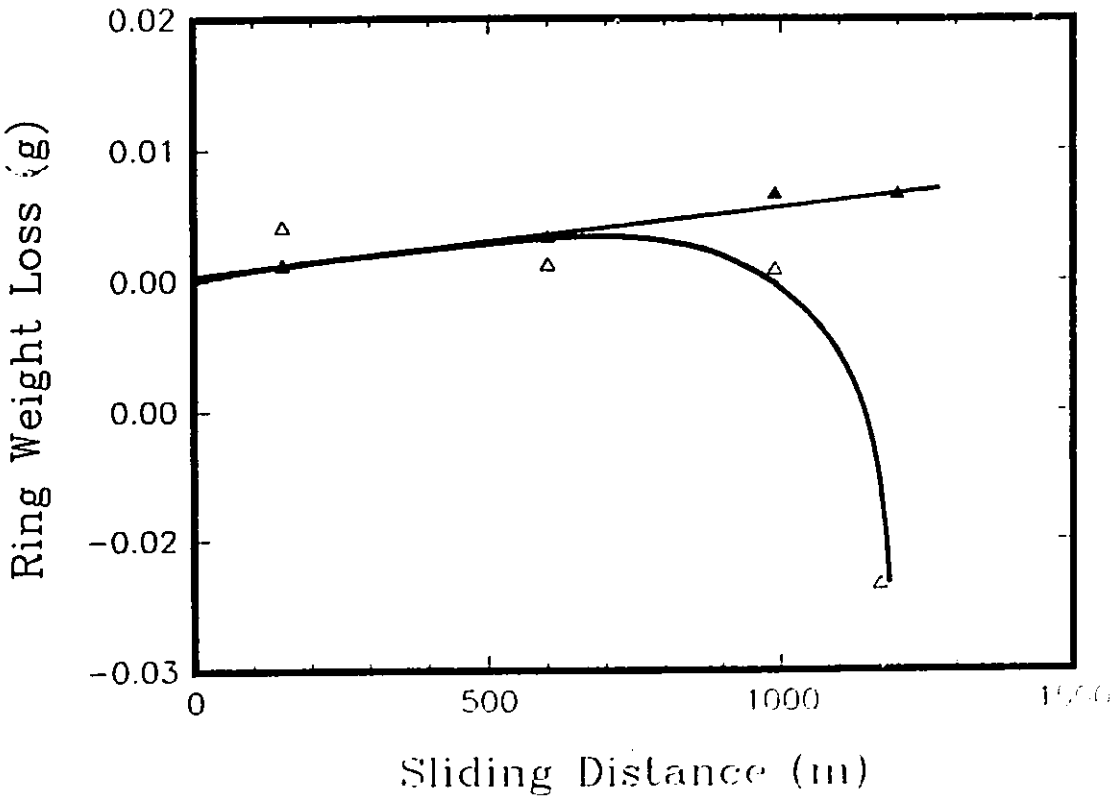

Figure 4.8: Counterface wear as a function of sliding distance, load 78 N (▾) and 196 N (▿), parallel fibres

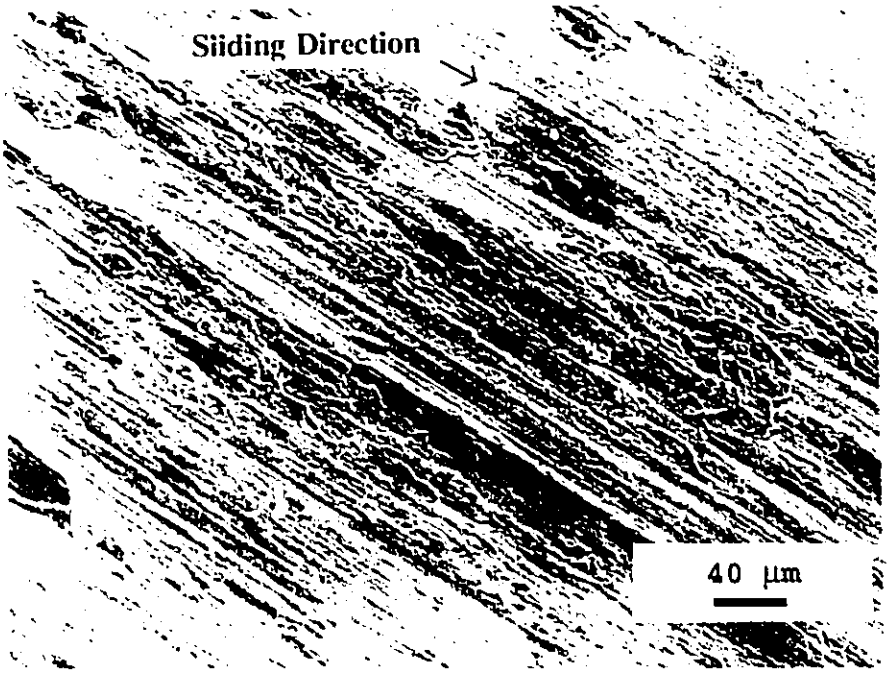

Figure 4.9: Ring surface after seizure occurred when slid against a composite with parallel fibres

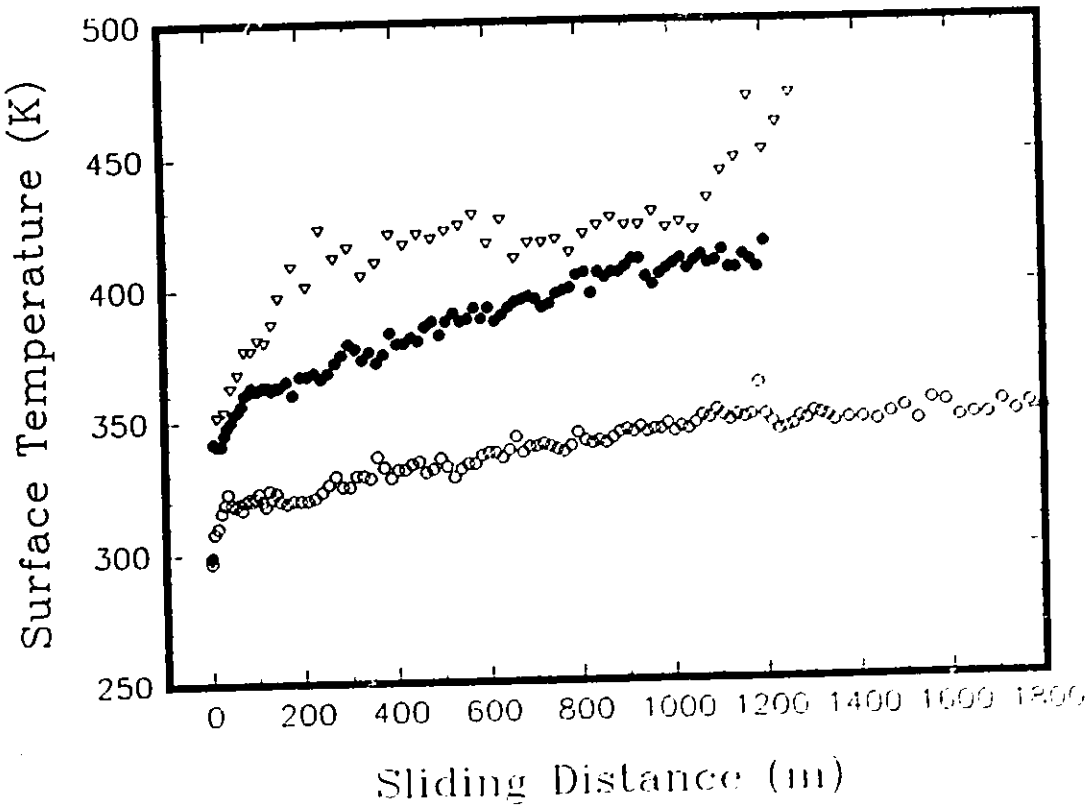

4.10: Contact surface temperature as a function of sliding distance for composites slid at loads of 78 N (○), 196 N (•) and 226 N (▽)

function of sliding distance for a pretransition load (mild wear) and two post-transition loads (severe wear).

In the mild wear regime (78 N) the interface temperature initially increased, rapidly, followed by a gradual increase thereafter. After 1800 m of sliding the temperature had increased approximately 50 K to 350 K. However, in the severe wear regime, the temperature rise was significantly greater. When tested at 196 N, the interface surface temperature of the sample increased 120 K after 1200 m of sliding. This sample did not demonstrate the high wear rates, gross plastic deformation or material transfer characteristic of seizure because the test was stopped prior to seizure. When the load was increased to 226 N, a greater surface temperature (425 K) was observed after 1000 m of sliding. Most significant was the further temperature rise generated during seizure. When seizure started to occur at 1100 m, the rate of temperature rise increased. The test was stopped since seizure resulted in large vibrations in the testing machine. At this point the surface temperature exceeded 475 K.

The temperatures generated during severe wear were sufficiently high to cause degradation of the load carrying ability (ie. strength) of the aluminum matrix [121]. This fact is very important in understanding the severe wear mechanism and the presence of the transition load between mild and severe wear regimes and will be discussed in detail.

4.4: Characteristics of the Wear Debris

The morphology and composition of the debris generated by wear can often yield significant clues as to the mechanism by which the debris was formed. Since two different wear regimes were observed, indicating at least two different wear mechanisms, it was expected that the morphology and composition of the debris would be significantly different in the two wear regimes.

In the mild wear regime the debris from the composite was observed to be a black powder to the unaided eye. SEM secondary electron images indicated that the debris consisted of many flake-like particles (Figure 4.11). A few larger flakes (approximately 500 μm) were also observed suggesting that the smaller particles may have initially been larger flakes. Alternatively, the larger flakes may have been composed of the small debris flakes. When these flakes were released from the surface, deformation and fracture of the flakes occurred as the debris exited the tribo-system. This processing of the debris likely broke the majority of the large flakes into smaller flake-like particles.

The composition of the debris particles was determined through X-Ray Diffraction (XRD) studies. In the mild wear regime the debris was observed to consist mainly of elemental iron and aluminum (Figure 4.12). The broad X-Ray peaks suggest the possibility that non-stoichiometric and/or amorphous iron and/or

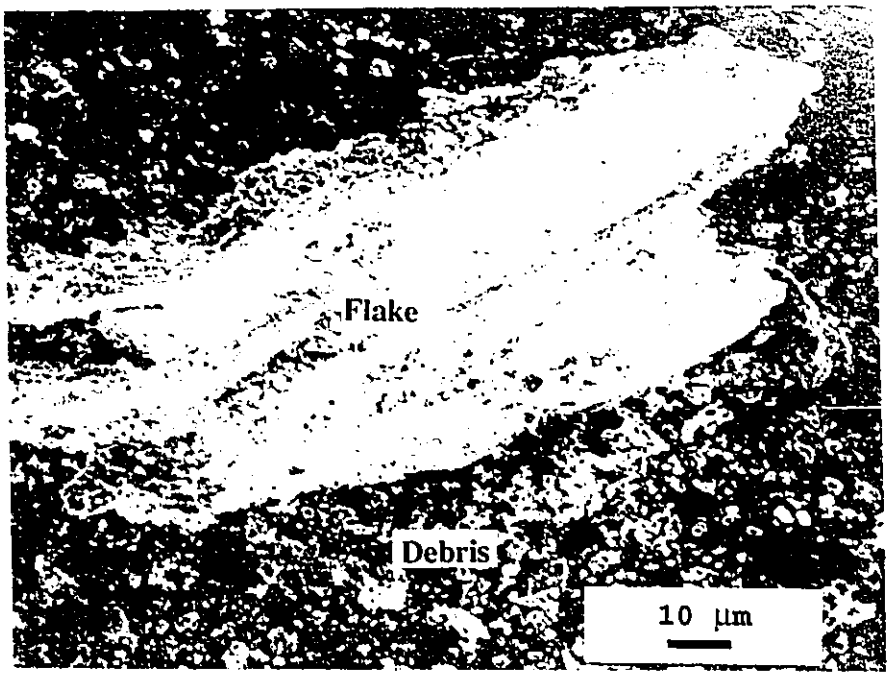

Figure 4.11: Morphology of the debris from a low load test

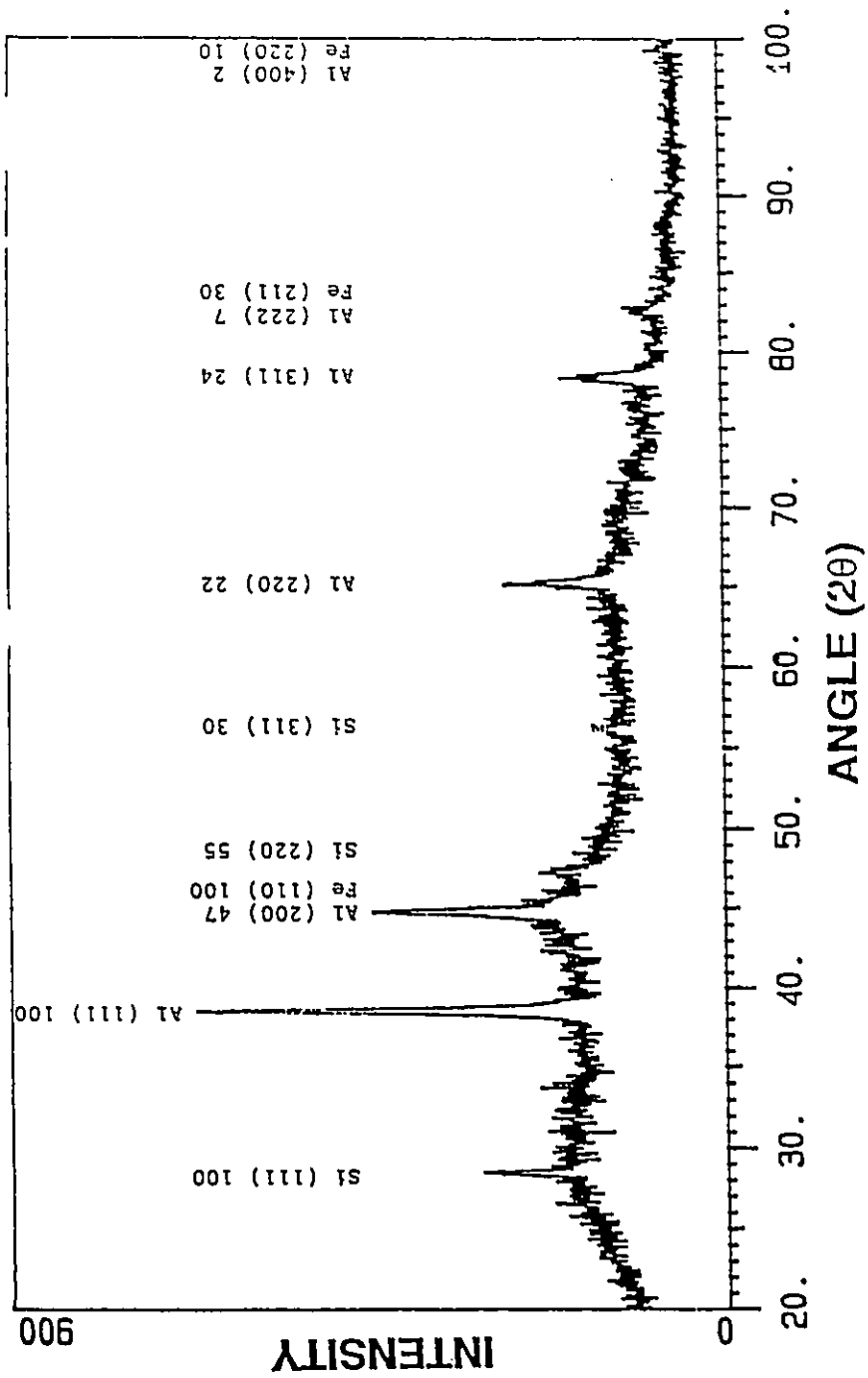

Figure 4.12: XRD pattern of the debris formed at low loads

aluminum oxides may have been formed due to the low contact surface temperature (less than 350 K) generated during sliding at low loads.

Once the transition to severe wear had been achieved, the debris from the composites was flake-like with some chunk material of the order of 1 mm in diameter, 0.1 mm thickness (Figure 4.13). The debris material appeared to be metallic to the unaided eye. Energy Dispersive Spectrometry (EDS) determined that the severe wear debris was mainly aluminum with smaller amounts of iron. This agrees with the observation that aluminum transfer to the steel ring results in a system where aluminum slides against aluminum preventing any significant transfer of iron on to the sample wear surface during severe wear. The flakes appeared to be formed through extrusion of the surface layers which built up outside the contact surface and were then fractured off.

Severe wear was terminated by seizure. When seizure occurred a large proportion of the debris was transferred to the steel counterface (Figure 4.9). The debris that was not captured by the counterface was irregular in shape and larger. The largest dimension of the debris fragments was 1 to 8 mm. The large size of the debris was indicative of the severe plastic deformation that the seized worn surface experienced.

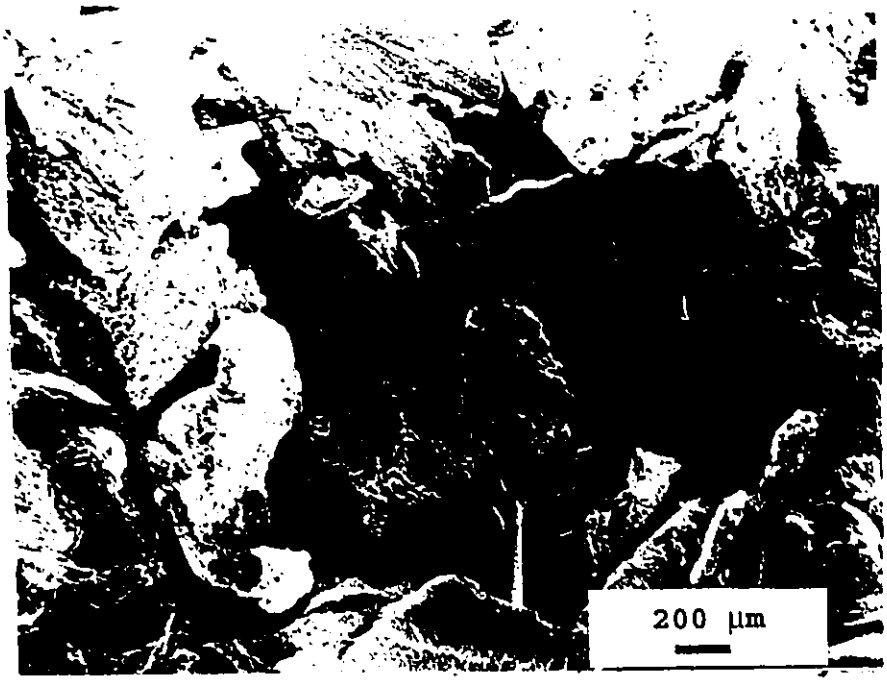

Figure 4.13: Debris from a high load test (196 N)

4.5: Characterization of the Worn Surfaces

In the mild wear regime, scoring or grooving of the surface occurred (figure 4.14). Plastic deformation of the surface material resulted in the build up of aluminum at the exit edge of the wear scar in a process analogous to extrusion. Pits of granular appearance were dispersed in the grooved surface (Figure 4.15). The carbon fibres were observed to have fractured at the wear surface of composites with parallel fibres (Figure 4.16) and normally orientated carbon fibres (Figure 4.17). Although these fibres fractured, decohesion or fibre pull out was not observed. Debris particles (1 to 3 μm) of aluminum, iron and oxides were found on the surface at higher magnifications (Figure 4.18). Energy Dispersive Spectrometry (EDS) was used to identify the composition of these particles. The EDS system used was not capable of detecting elements with atomic numbers less than 12. Hence Auger Electron Spectroscopy (AES) was performed to detect carbon on the worn surface.

The purpose of performing the AES analysis was to determine whether the non-graphitic carbon fibres had formed a solid lubricant film on the surface analogous to the behaviour of graphite [95-98]. Figure 4.19 is the AES survey of a sample tested at a load of 10 N (mild wear). Sputtering was performed to remove all adventitious (air deposited) carbon (section 3.5). The results indicate that the worn surface consisted of aluminum and silicon from the matrix, oxygen from the atmosphere and carbon from the fibres. The argon and nitrogen peaks were

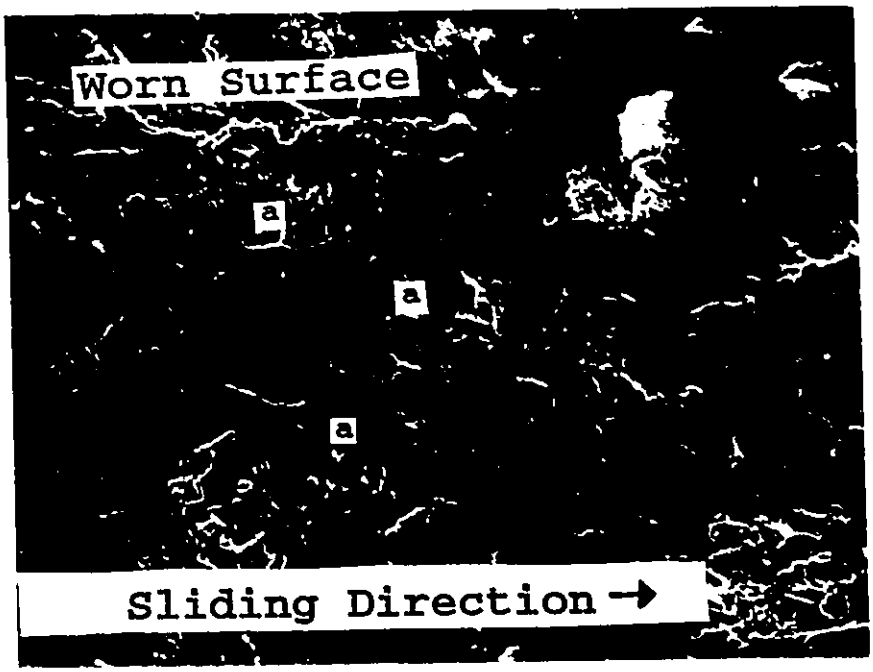

Figure 4.14: Worn surface of a composite slid at 10 N. Broken carbon fibres on the surface are denoted by 'a'. (sliding direction is left to right)

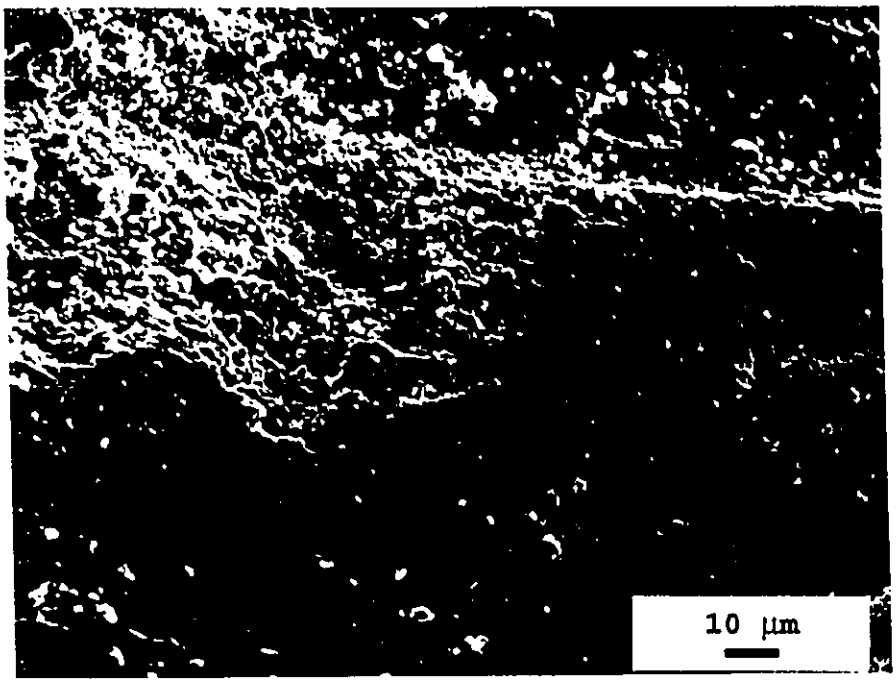

Figure 4.15: Worn surface slid at 78 N (sliding left to right)

Figure 4.16: Fractured fibre orientated parallel to the worn surface (10 N)

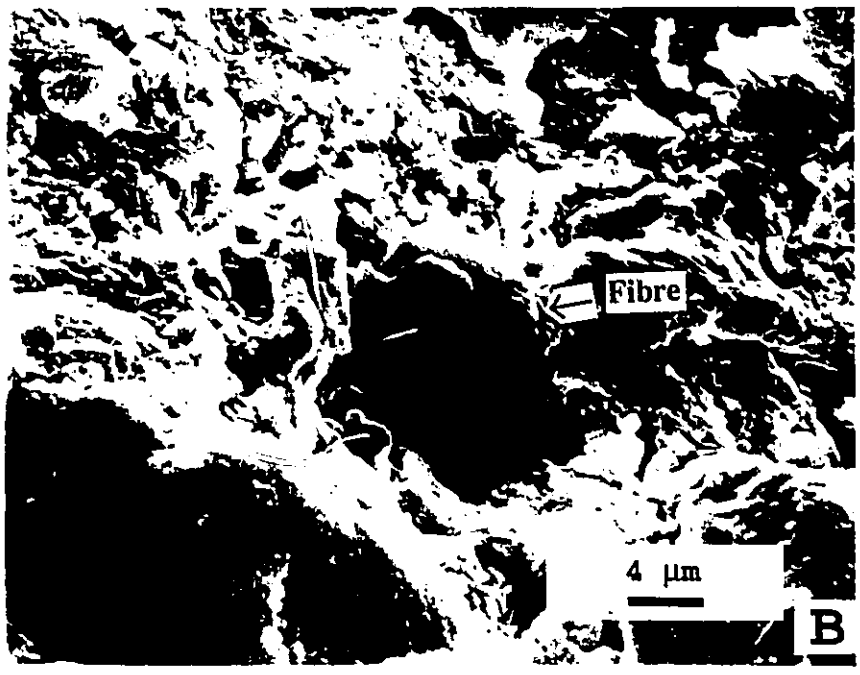

Figure 4.17: Fractured fibre orientated normal to the worn surface (10 N)

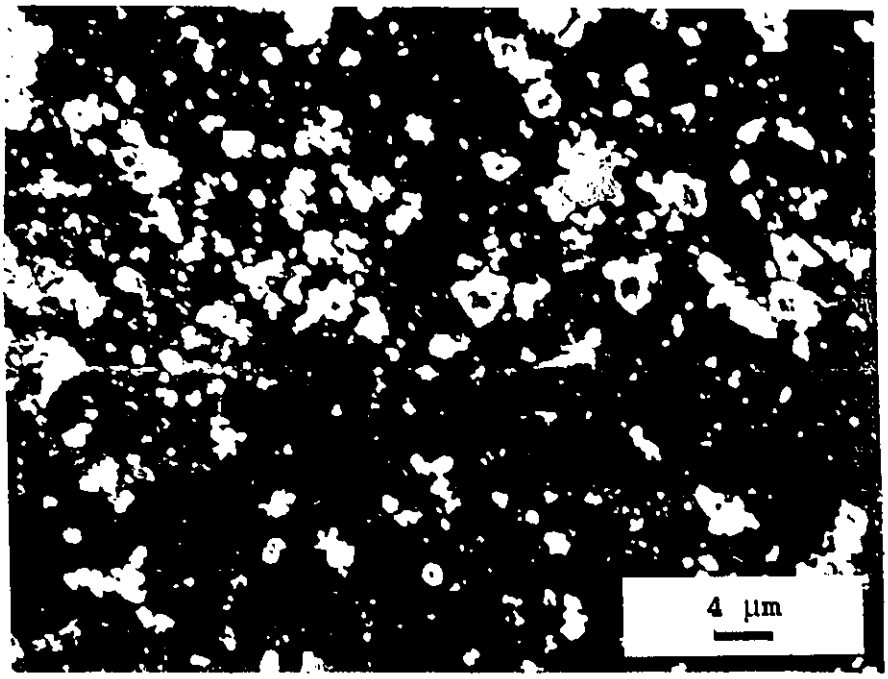

Figure 4.18: Debris particles on the worn surface of a composite slid at 78 N (sliding direction left to right)

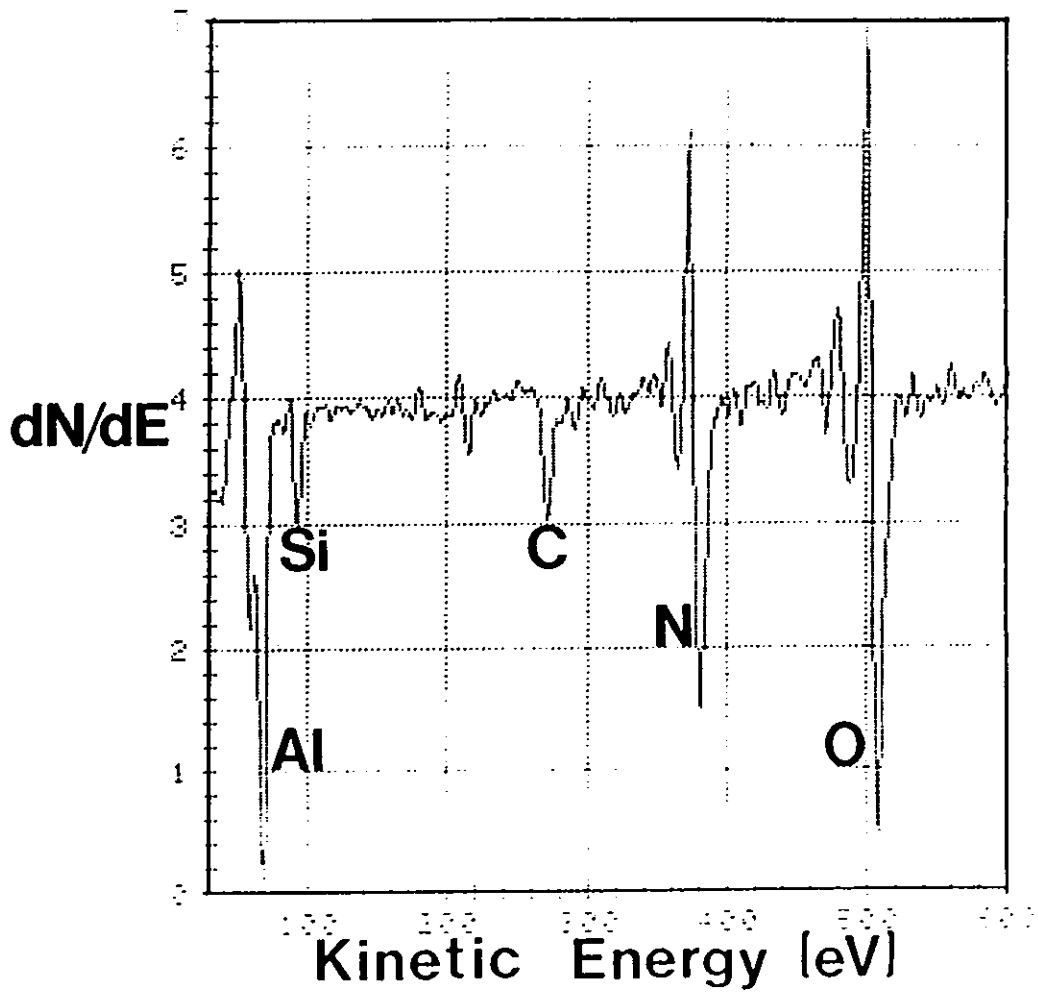

Figure 4.19: AES survey of the worn surface after sliding at 10 N.

believed to be artifacts. Since the carbon peak persisted with further sputtering it was initially assumed that the fibres had indeed formed a lubricating film at low loads. The validity of this statement will be discussed later.

In the severe wear regime the worn surfaces of the composite samples displayed a metallic appearance. Deep longitudinal grooves were readily observable to the naked eye (Figure 4.20). Microscopically these grooves were coupled with rather severe plastic deformation (Figure 4.21). The surface layers were extruded at the exit, the entrance and the sides of the wear scar (Figure 4.22). Qualitative EDS of the worn surface demonstrated the presence of aluminum and silicon without significant amounts of iron. Once again AES was performed to detect carbon species on the worn surface.

The AES survey of a severely worn sample is shown in Figure 4.23. After a period of sputtering, to eliminate the adventitious carbon, the carbon peak was nearly indiscernible from the background of the survey. The absence of carbon suggested that film formation did not occur or that the plastic deformation of the ductile aluminum matrix had covered the fibres preventing their detection. Plastic deformation became even more severe when seizure occurred.

Seized surfaces are dominated by macroscopic features, reminiscent of ridges, running perpendicular to the sliding direction indicating the gross deformation

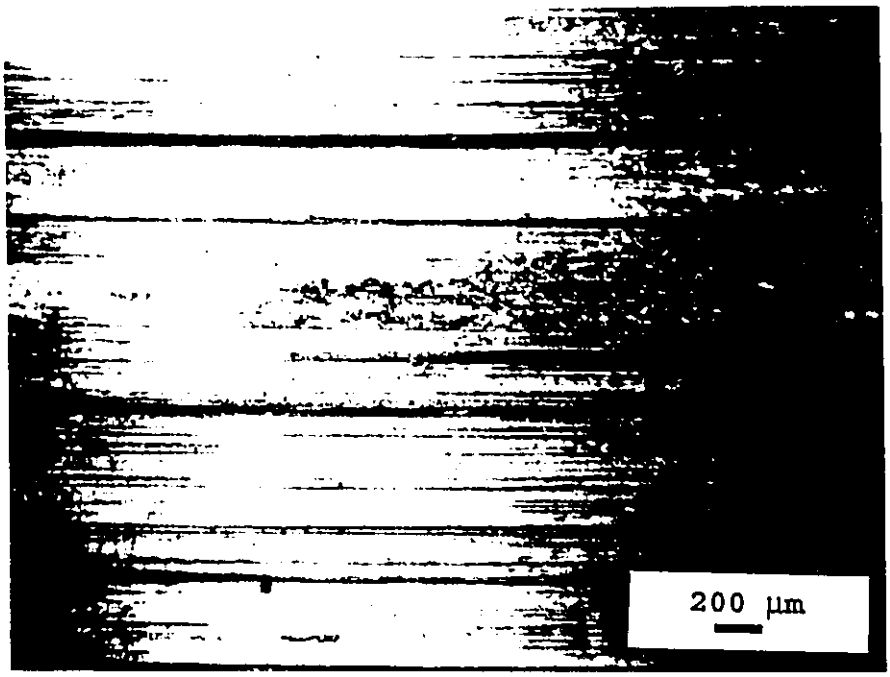

Figure 4.20: Severe wear surface slid at 237 N (sliding direction left to right)

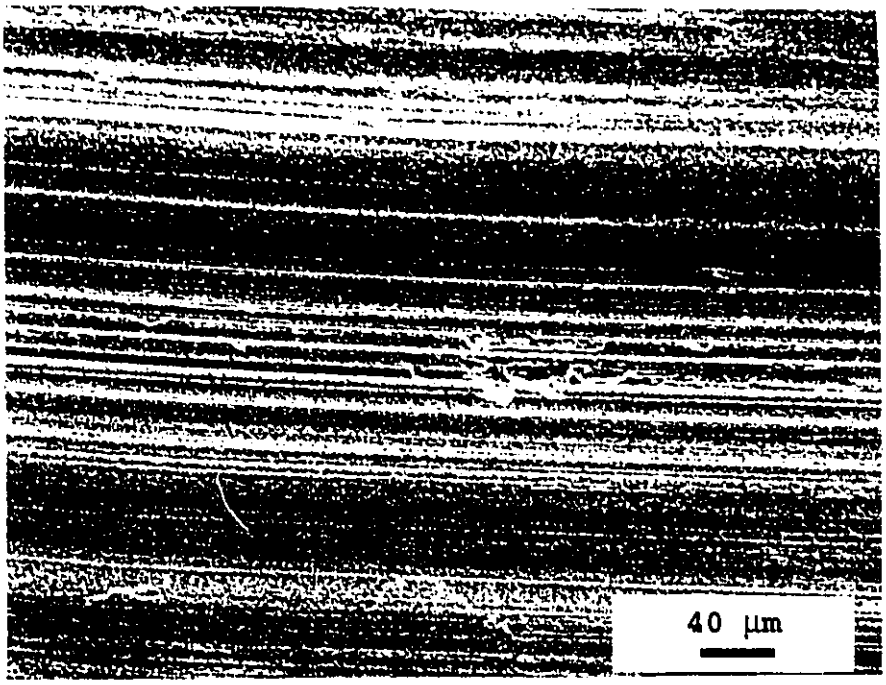

Figure 4.21: Severely worn surface showing grooving and plastic deformation caused by sliding at 196 N (sliding direction left to right)

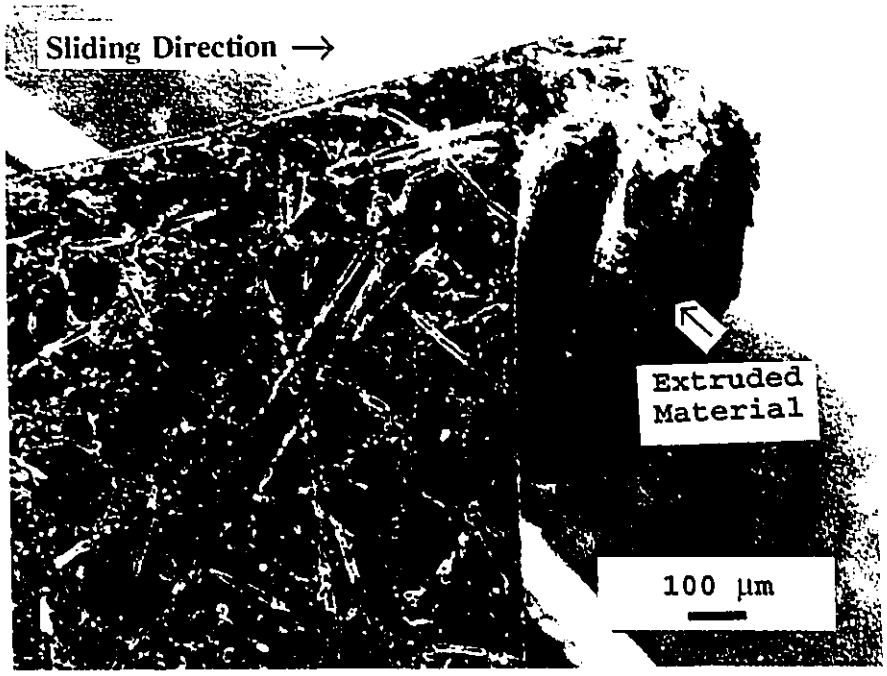

Figure 4.22: Section showing the extruded material at the exit of the wear scar, 235 N

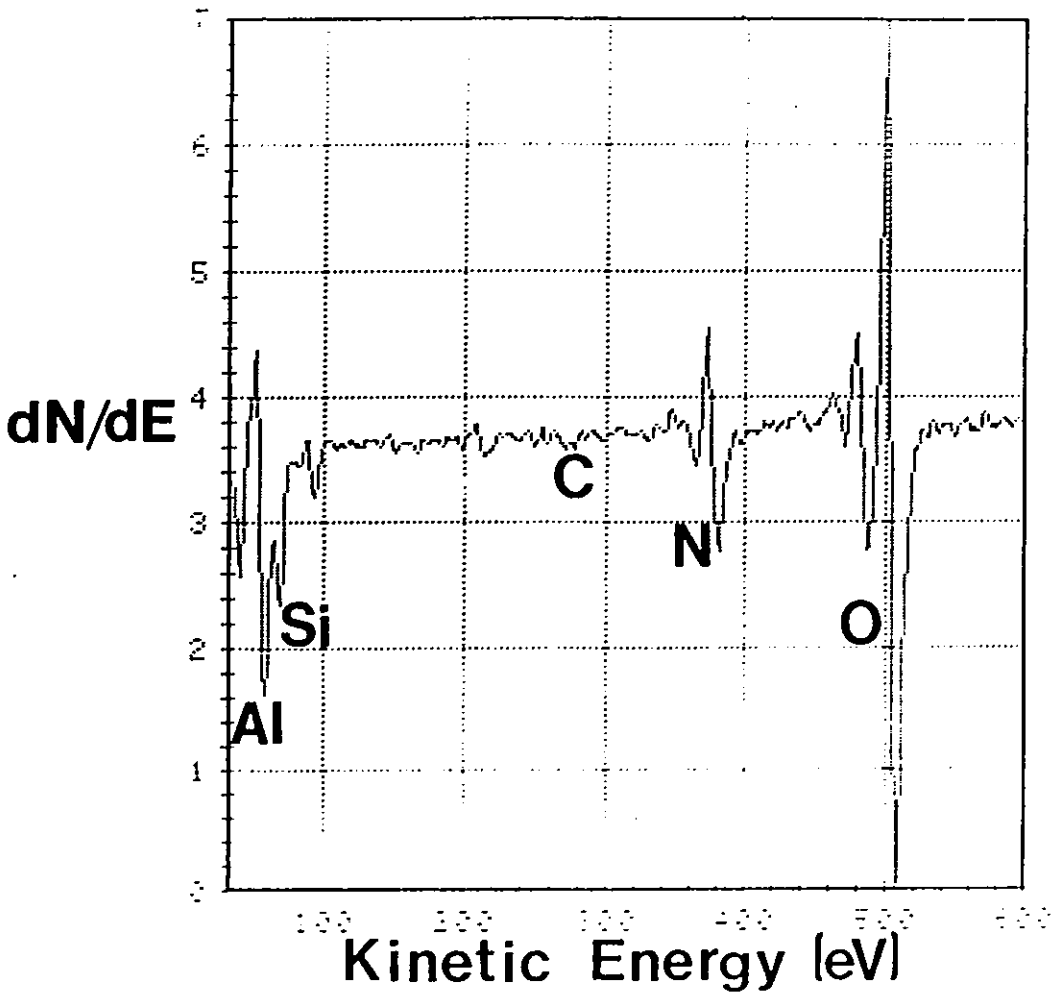

Figure 4.23: AES survey of the worn surface slid at 225 N

damage that is characteristic of seizure (Figure 4.24). The surface of the sample had been torn away leaving deep scars. The damage caused by seizure is more evident when one examines the subsurface.

4.6: Subsurface Characterization

The depth of subsurface damage is very limited during mild wear. The carbon fibres extend to the wear surface without significant subsurface fracture (Figure 4.25). Strain developed in the subsurface tends to bend the fibres in the sliding direction (Figure 4.26). This effect became more dramatic at higher loads in the mild wear regime. Subsurface cracks 10 to 20 μm below the worn surface appeared to propagate parallel to the worn surface until crack lengths of 200 to 400 μm were achieved. The flake of material above the crack was delaminated when the crack intersected the surface. Figure 4.27 is a secondary electron image of a flake of surface material prior to delamination. Removal of similar flakes left pits on the worn surface.

In the severe wear regime the subsurface demonstrated three distinct regions (Figure 4.28). Furthest from the wear surface was the unstrained bulk material. This region did not show any damage due to the wear process. The intermediate region (80 to 350 μm deep) was a region of plastic deformation resulting in the fracture of the carbon fibres. Immediately adjacent to the worn surface, a layer of

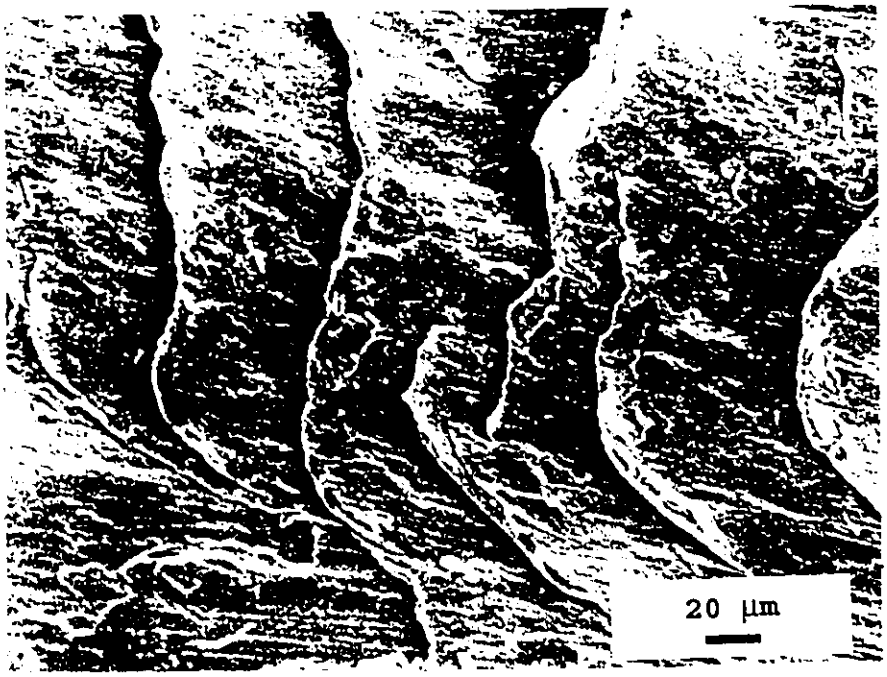

Figure 4.24: Wear scar after seizure at 196 N, 1530 m of sliding (left to right)

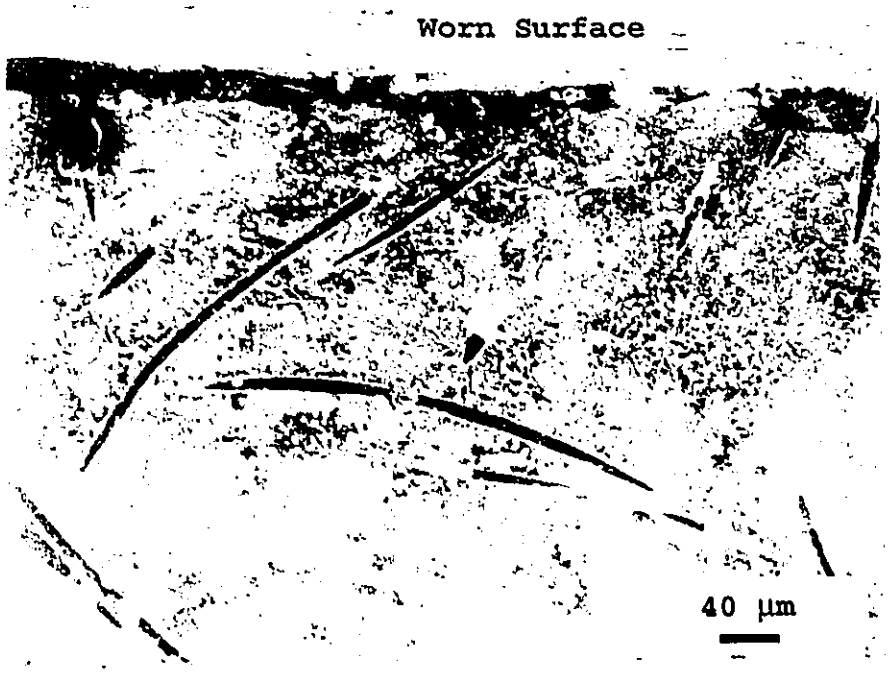

Figure 4.25: Section of a sample slid at 147 N (sliding direction left to right)

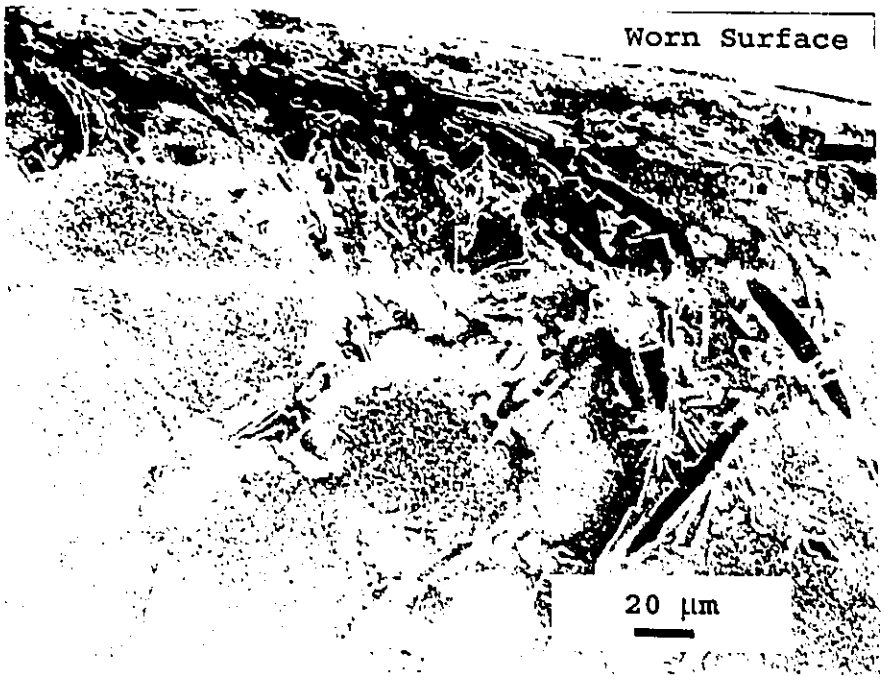

Figure 4.26: Section of a sample slid at 147 N (sliding direction left to right)

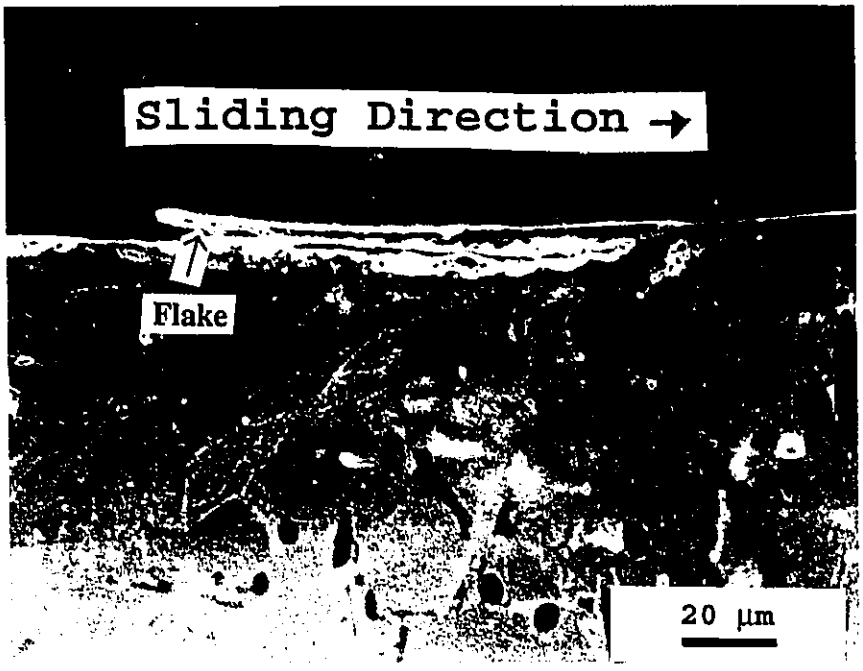

Figure 4.27: Delamination flake being generated during sliding at low loads (20 N) (sliding direction left to right)

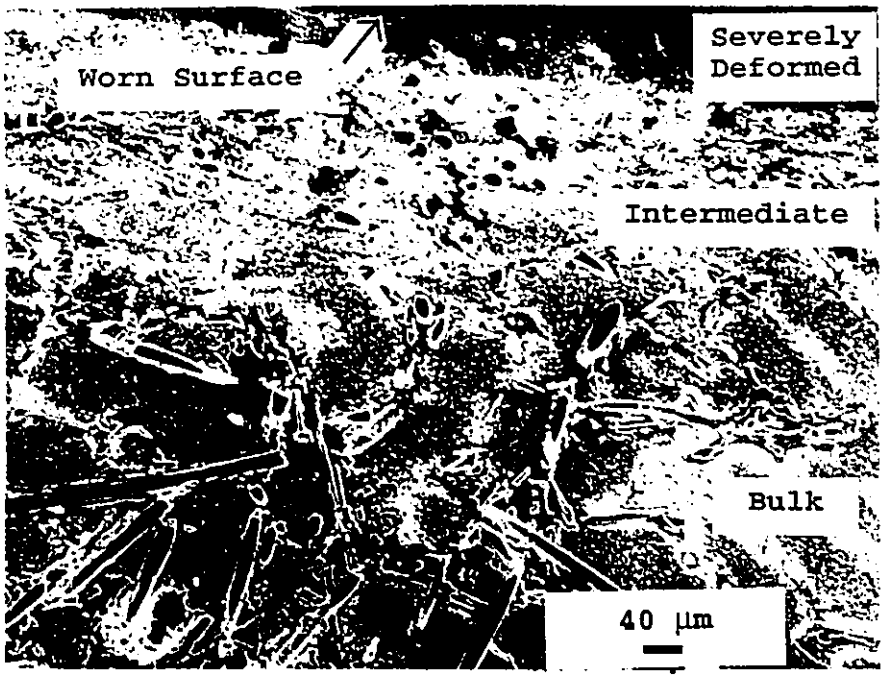

Figure 4.28: Section of a sample which experienced severe wear at 235 N (sliding left to right)

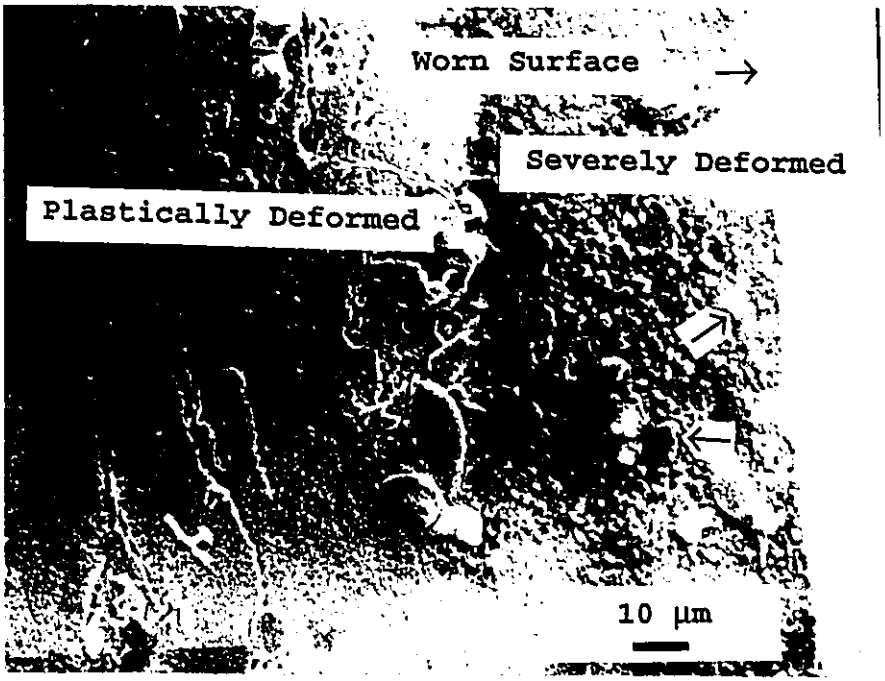

Figure 4.29: View of the interface between the highly fractured layer and the plastically deformed layer

severe deformation was observed up to 80 μm thick.

The severely deformed surface layer consisted of a mixture of finely broken particles (Figure 4.29). This communitated material most likely formed due to the very high plastic strains (20 to 50 strain [38]) immediately below the worn surface. The hardness gradient below the worn surface (Figure 4.30) indicated that the hardness increased near the contact surface. The near surface measurements revealed a hardness of 120 VHN(150 Knoop) at a depth of 40 μm, however, this measurement included the influence of the broken particles. It was not possible to differentiate the effects of work hardening of the matrix, particle hardening or softening due to the elevated temperature. Therefore the matrix may have been harder or softer when severe wear occurred.

When seizure occurred the plastically deformed regions adjacent to the wear surface were violently torn away (Figure 4.31). Seizure damage extended more than 250 μm below the worn surface. Plastic strain bent the fibres in the sliding direction (Figure 4.32). The ridge-like features observed on the seized surface (Figure 4.24) were formed through crack propagation in to the sample as the surface is lifted away (Figure 4.33). This characterizes the severe rapid damage which occurred during seizure.

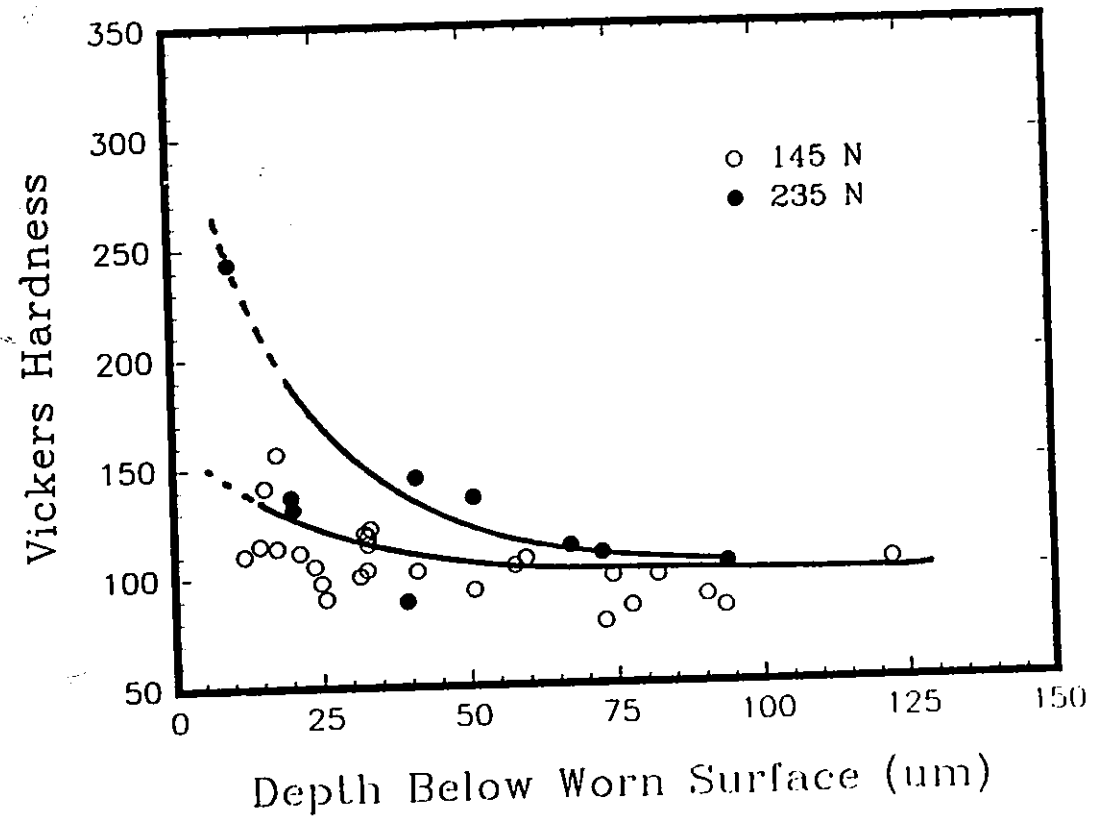

Figure 4.30: The variation of hardness with increasing depth below the severely worn surface

Figure 4.31: Section of a seized sample after sliding at 196 N (sliding direction left to right)

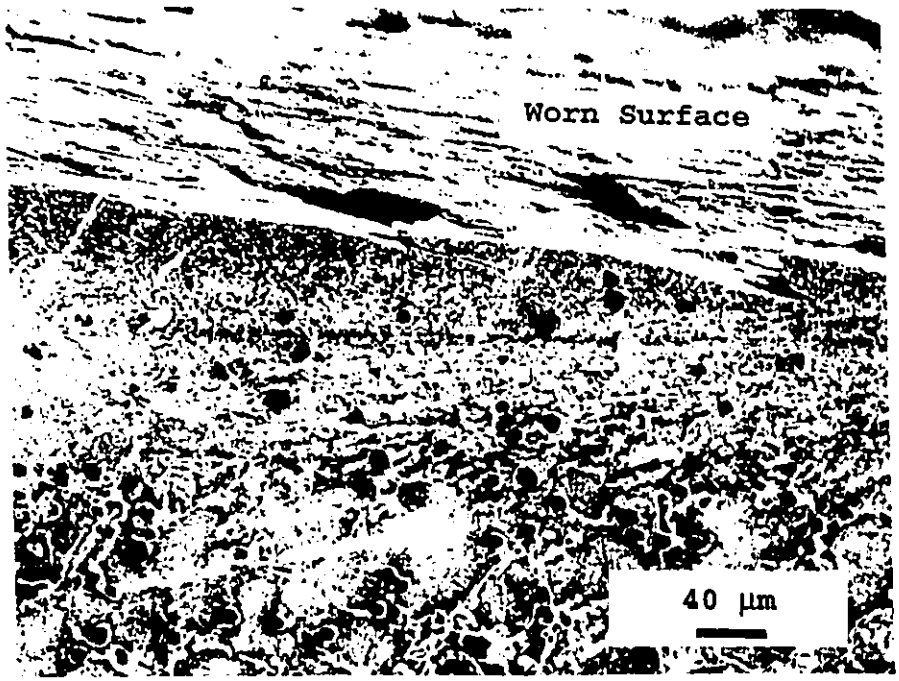

Figure 4.32: Section of a seized sample after sliding at 196 N showing the heavy subsurface deformation (sliding direction left to right)

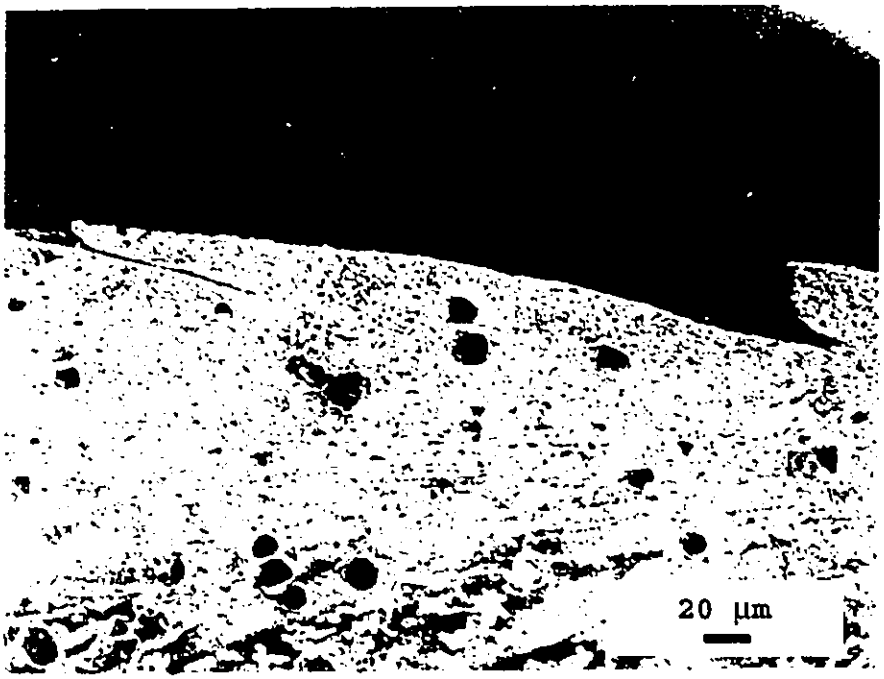

Figure 4.33: Section of a seized sample showing cracks extending into the deformed region of the sample.

4.7: Summary of Observations

A356-4%CF composites demonstrated two wear regimes as load increased: mild and severe wear. Severe wear was terminated by seizure. A transition load between mild and severe wear was determined, by a change in debris morphology, and was found to depend on the fibre orientation. The contact surface temperature increased as the load increased. When seizure occurred the temperature jumped to temperatures exceeding 475 K.

In mild wear grooved worn surfaces with granular pits were observed. AES determined the presence of carbon of the worn surface. The debris was shown to consists of aluminum, iron and oxides (EDS & XRD). The subsurface did not show evidence of subsurface fibre fracture even though plastic deformation was observed. Cracks propagated parallel to the worn surface delaminating a flake of surface material.

In the severe wear regime the worn surface had a metallic appearance with deep grooves and evidence of plastic deformation. Carbon was not identified on the worn surface. The subsurface showed three distinct regions: a communitated layer adjacent to the worn surface, a plastically deformed layer in which fibre fracture occurred and lastly, the unaffected bulk material.

When seizure occurred the surface of the sample was torn away and transferred to the counterface resulting in a net increase in weight of the counterface. The subsurface displayed cracks running in to the sample and severe straining. At the onset of seizure the test had to be stopped to prevent damage to the equipment.

Part B: Discussion of the Results

4.8: Wear Mechanisms

Examination of the worn surfaces and the debris indicated that at least two different debris formation processes occurred in the mild wear regime. Figure 4.18 documents the presence of fine particles 1 to 3 μm on the worn surface. EDS and XRD analysis showed that these particles consisted of aluminum, iron and oxides. Abrasive wear likely generated these particles.

The abrasives, in this case, were the hard asperities of the steel counterface and the composites. When these asperities slid upon the mating surface, gouging and ploughing occurred resulting in the formation of fine particulate debris from the contact surfaces of both the samples and the counterface. The debris, formed from this mechanism and others, may have also behaved abrasively leading to further particulate formation.

A second debris formation mechanism, delamination, was observed in the mild wear regime. The plastic strain developed in the subsurface likely nucleated cracks at second phase particles. Cracks were not observed to nucleate at the carbon fibre - matrix interface. Once nucleated these cracks propagated parallel to the wearing surface, at a depth of 10 μm to 20 μm, until the cracks intersected the surface (Figure 4.27). Crack lengths of 200 μm to 400 μm were achieved before the material delaminated. The flake of material was removed leaving pits of granular appearance on the worn surface (Figure 4.15).

The removed debris flakes did not exit the tribosystem immediately. Debris examination indicated that the flakes were broken in to smaller flakes by the interaction of the steel counterface and the sample surface. The debris fragments may have acted as third body abrasives and may have increased the rate of abrasive wear, although a definitive conclusion cannot be made.

The onset of severe wear corresponds to a degradation of the load carrying capability of the composite as temperature increased. Severe wear is believed to occur due through the achievement of a critical interface temperature [74,80,81,89]. The transition load of the composites was increased through the retention of load carrying ability at elevated temperatures due to the reinforcing phases (see section 4.11). Transfer and adhesion of communitated composite material to the steel ring took place. The surface layer was also extruded at the edges of the contact surface

and then fractured from the sample. The significance of this wear mechanism increased with increasing load conditions.

Post transition loading and long sliding distances resulted in seizure. The steel counterface, once largely covered with a layer of aluminum, likely displayed greater solid state welding between the sample and the counterface resulting in fracture and easy transfer of the surface layer from the composite. The surface layers were torn from the sample resulting in rapid volume loss. Localized build up of transferred material on the counterface resulted in topography that varied 2 to 3 mm from spot to spot resulting in large scale ploughing. This caused severe vibrations and the conclusion of the test.

4.9: Lubrication Effects

Upon fabrication of these carbon fibre composites, the carbon fibres were thought to posses solid lubricating characteristics similar to graphite. However, the non-graphitic structure of the carbon fibres suggested that the lubricating ability of these particular fibres was very limited.

Graphite is soft (61 VHN) and easily shearable leading to efficient lubrication. Contrary to this, the carbon fibres were substantially harder (180 VHN) and lacked the layered lattice structure required for lubrication. Microscopic evidence

suggested that the carbon fibres did not smear on to the wear surface when deformed but fractured instead (Figures 4.16 and 4.17). Intact fibre segments were found in the debris at high loads (Figure 4.34). More evidence was obtained through very limited pin on disk friction experiments.

The graph of friction coefficient against sliding distance is displayed in Figure 4.35. The curve starts at a value of 0.18 followed by a steep rise. It has been suggested that a steep rise will occur in a friction plot when debris particles begin to form [26]. The debris particles may become entrapped resulting in ploughing and an increase in the coefficient of friction. Adhesion forces may also increase due to the new material exposed [26]. After reaching a maximum coefficient of friction of 0.24, the friction force decreases. This may be due to a general smoothing of the harder surface [26]. If a lubricating film formed on the surface, the coefficient of friction should decrease as the film covers a greater area on the surface. Sliding did not result in a significant reduction in friction force. In fact the steady state friction coefficient was comparable to the initial friction coefficient. This suggests that a triboinduced lubricating film was not formed. Therefore, the carbon fibres and intermetallic acted as reinforcements leading to improved wear behaviour.

4.10: Orientation Effects

The Al-Si-CF composites were manufactured such that two different fibre

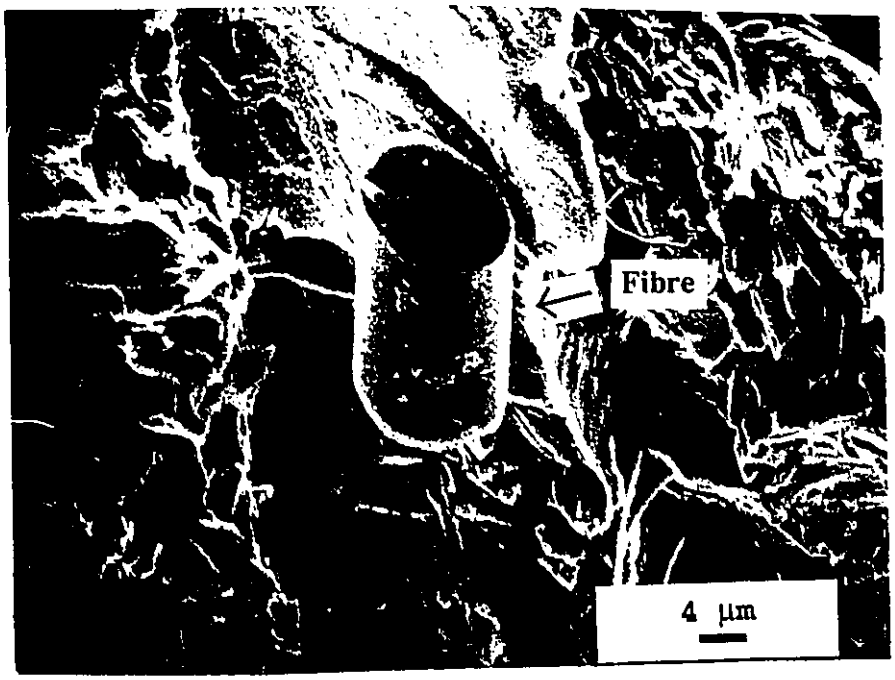

Figure 4.34: Fibre segments in the high load wear debris

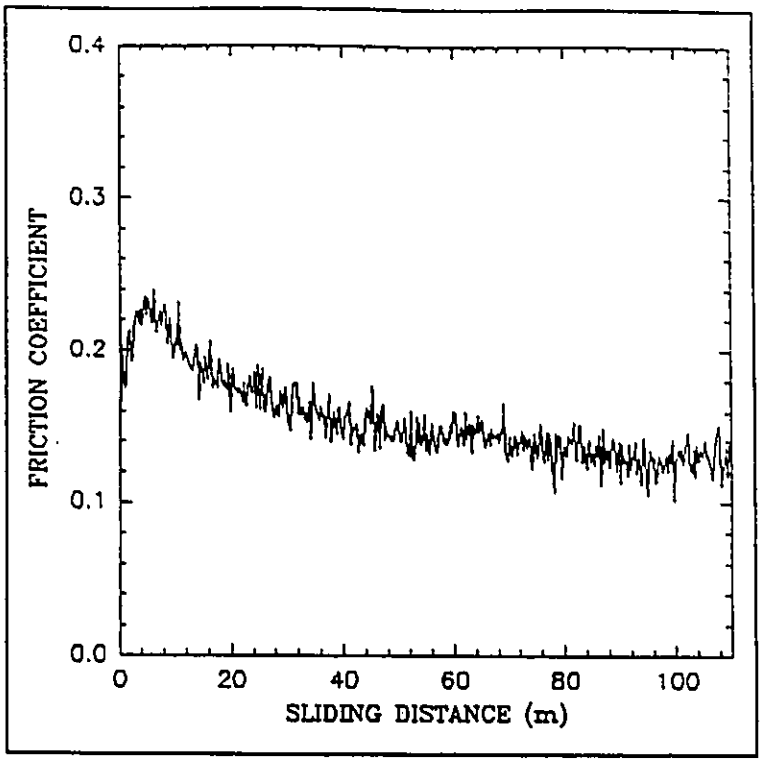

Figure 4.35: Coefficient of friction as a function of sliding distance at a load of 2 N

orientation were possible. The fibre orientations were described as normal and parallel in relationship to the wear surface. However, this description does not fully explain the fibre orientation. In the composites the fibres were orientated in parallel planes but the fibres were randomly distributed in those planes (Figure 4.36). Therefore the designations, as either normal or parallel, are not exactly correct.

Anisotropy was observed in the bulk hardness values of the composites. Sample surfaces which had parallel fibres demonstrated a lower hardness (83 VHN; 38±3 30-T) compared to the surface with normally orientated fibres (90 VHN; 44±2 30-T). Therefore the composites with normally orientated fibres at the wear surface may have possessed superior load carrying capabilities which may have increased the load required to initiate severe wear.

The onset of severe wear occurred at a transition load of 150 to 200 N. Considerable scatter in the wear rate data existed, however, extrapolation suggested that the composite with fibres orientated normal to the surface may have demonstrated a higher transition load. This was supported by the observations of the debris morphology. The higher load capacity of the composite with normal fibre orientation likely delayed the onset of severe wear to higher loads than in the case of the composite with parallel fibres. A second, and supporting, reason for this difference in transition load was observed microscopically. Figure 4.29 showed the cross section of a sample with normally orientated fibres tested in the severe wear

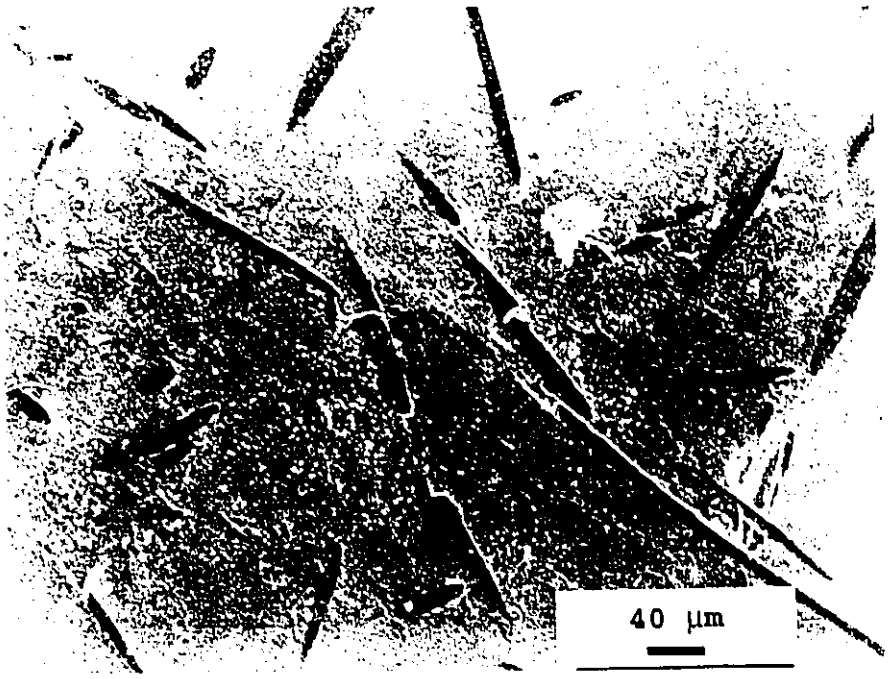

Figure 4.36: In the planar random structure the fibres are orientated in a plane parallel to the worn surface but randomly distributed in that plane.

regime. Furthest from the worn surface was the bulk material. Above this was a region in which the fibres had fractured due to the subsurface strain. Closer examination of this region reveals that the circular ends of the fibres are now facing out of the page indicating that a rotation had occurred. Figure 4.37 illustrates that the carbon fibres segments have in fact rotated from the normal orientation to the parallel orientation. The process of fibre fracture (due to the strain gradient) and subsequent rotation occurs only in the composites with normal fibres. This process requires additional energy and thus creates a barrier to subsurface strain development and severe wear. Therefore two factors appear to influence a possible orientation dependence on the transition load. Firstly there is the anisotropy of indentation hardness and secondly, the extra energy requirement for subsurface deformation in the normally orientated composites.

4.11: Comparison With the Unreinforced Material

Zhang and Alpas [37] investigated the wear behaviour of A356, Al-7%Si alloy in a similar block on ring testing apparatus under similar conditions. Their results of wear rate as a function of load are compared with the results of the A356-CF composites in Figure 4.38. It may be seen that the unreinforced alloy also demonstrates two wear regimes separated by a distinct transition load. In mild wear, the Al-Si alloy demonstrated wear rates of 9×10^{-4} mm^3/m at 10 N and 3×10^{-3} mm^3/m at 70 N resulting in the formation of black powder debris. Subsurface

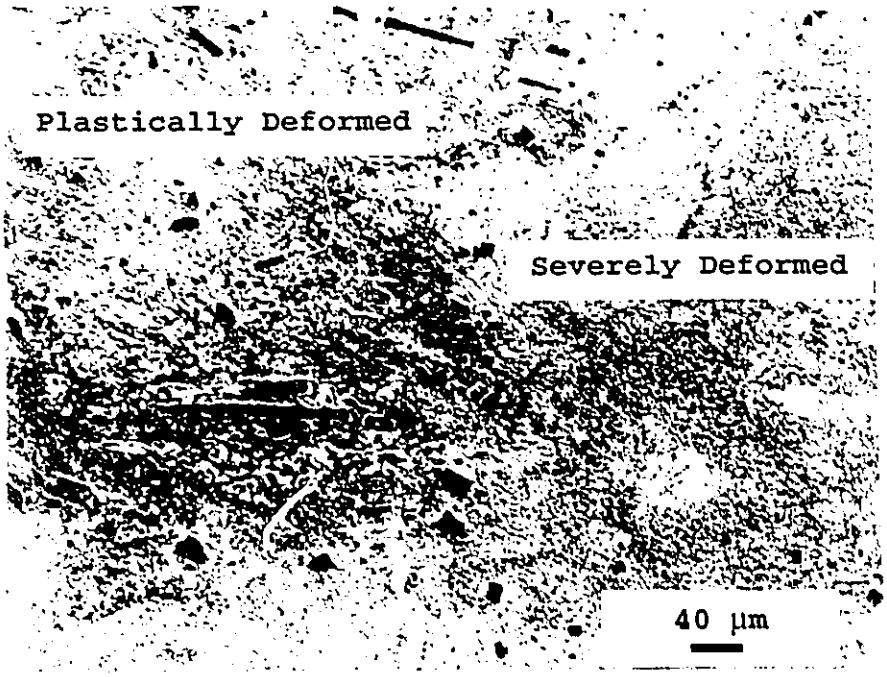

Figure 4.37: Section taken parallel to the worn surface demonstrating that the fibre fragments in the plastically deformed subsurface layer have rotated so that the long axis of the fibres are parallel, rather than normal, to the worn surface.

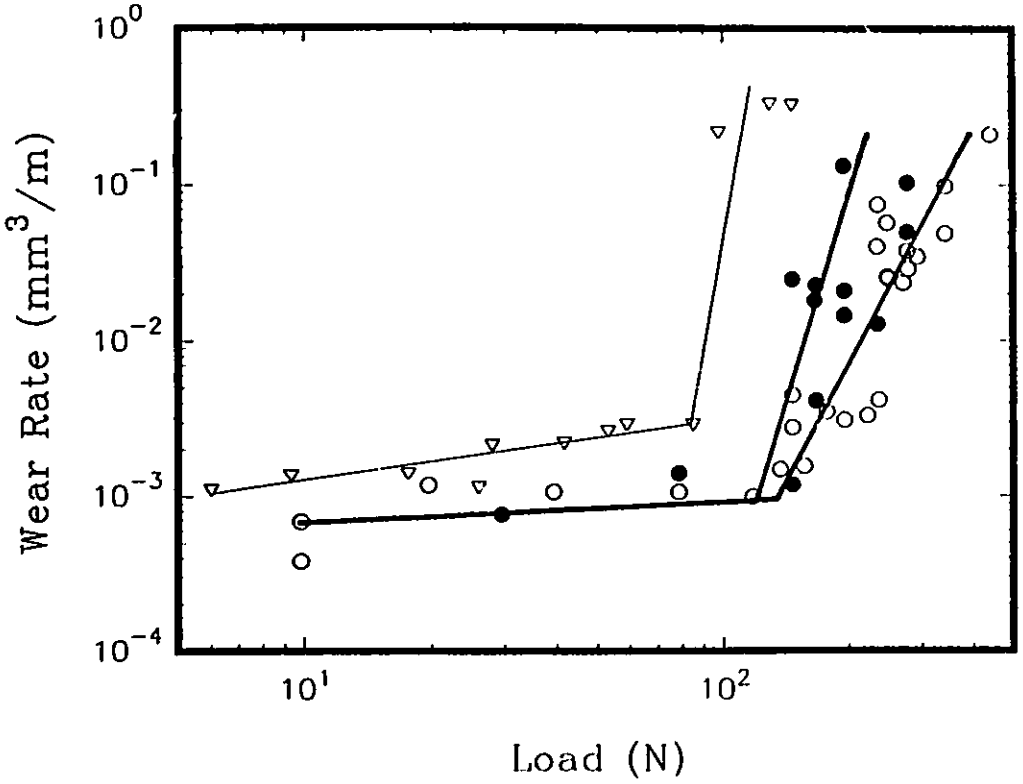

4.38: Wear rate comparison of the unreinforced A356 (▽) and the A356-CF composites with parallel (•) and normal (○) fibres as a function of load

delamination and abrasion of the surface by hard silicon particles were shown to be the two major wear mechanisms.

The onset of severe wear occurred at 80 N and resulted in the formation of metallic aluminum debris. A typical wear rate was 3 x 10^{-1} mm^3/m (100 N). Transfer occurred rapidly from the sample to the steel counterface analogous to the severe wear of the carbon fibre reinforced composites.

The A356-CF composites displayed wear rates one to three times lower than the unreinforced alloy in the mild wear regime. This was due to the superior load carry capability of the composites as a result of the intermetallic and fibre additions. The maximum theoretical hardness of the composites, 143±60 VHN, was calculated using a linear rule of mixtures; $H_c = V_m \cdot H_m + V_f \cdot H_f + V_i \cdot H_i$ where V is the volume fraction of each phase, H is the hardness of each phase (see Table 4.1) and the subscripts c,m,f,i refer to the composite, matrix, carbon fibres and nickel aluminide intermetallic respectively. The minimum theoretical hardness, 83±35 VHN, was calculated using the inverse rule of mixtures; $H_c^{-1} = V_m \cdot H_m^{-1} + V_f \cdot H_f^{-1} + V_i \cdot H_i^{-1}$. In fact the experimental hardness was very similar to the theoretical minimum. It may be concluded that the reinforced alloy should have a higher load carrying capacity but the more significant observation is that the greatest influence on the hardness was due to the nickel aluminide intermetallic. Therefore the addition of the hard intermetallic particles and the carbon fibres led to a decrease in the wear rate in the

mild wear regime.

It has been proposed [98] that the introduction of hard particles or fibres could result in an increase in the rate of crack nucleation resulting in increased wear. Since the wear rates of the composites were in fact two to three times lower than the unreinforced material, the beneficial effect of carbon fibre reinforcement must outweigh any increase in crack nucleation.

The increased load capacity of the composites allowed mild wear to prevail to higher loads. The transition load increased from 80 N in the Al-Si alloy to 150 to 200 N in the carbon fibre composites. Hence, at a load of 100 N the composites experienced mild wear while the unreinforced material encountered severe wear resulting in nearly three orders of magnitude difference in their wear rates. This denotes the significance of increasing the transition load to severe wear through reinforcement.

It has been suggested [80,81] that the transition to severe wear is dependant on the achievement of a critical surface temperature in the sample material. The temperatures generated during severe wear were in excess of 400 K (0.5 T_m). Therefore the load carrying ability of the composite should be considered under the elevated temperature conditions. This was not practical in this investigation although an indication of the composites elevated temperature behaviour may be deduced from the behaviour of the constituents.

Figure 4.39 shows that the ultimate tensile strength of the Al-Si matrix decreases rapidly with elevated temperature [121]. Contrary to this behaviour, the strength of the carbon fibres increases up to 470 MPa at 480 K and only then begins to decrease [107]. The hardness of the Al_3Ni intermetallic (Figure 4.40) does not decrease until a temperature of 563 K is obtained [120]. Therefore it is likely that the degradation of the load carrying ability of the composites, due to thermal softening of the matrix, is reduced due to the introduction of carbon fibres and Al_3Ni. Consequently, the composites have higher strength at room temperature and at elevated temperatures, with respect to the unreinforced Al-Si alloy, resulting in a higher load required for the transition to severe wear.

The only severe wear mechanism observed in the unreinforced alloy was seizure. The carbon fibre composites demonstrated a period of sliding in the severe wear regime prior to seizure. Considering the subsurface of the severely worn composites, a layer was observed which was made up of broken fibres, intermetallic particles and silicon particles adjacent to the worn surface. This layer was effectively particle hardened to values exceeding 700 VHN. The particle hardened surface was likely more resistant to the massive flow and material transfer to the counterface characteristic of seizure. Thus the onset of seizure was delayed to higher sliding distances in the composite materials.

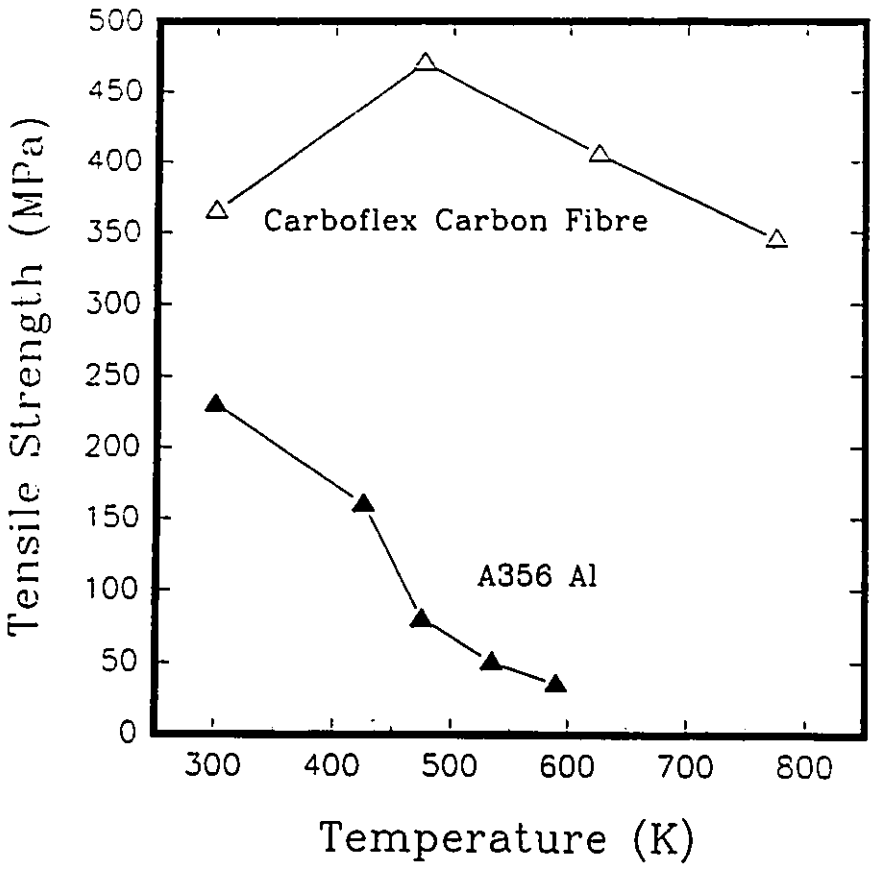

Figure 4.39: Effect of temperature on the strength of the matrix [121] and fibres [107].

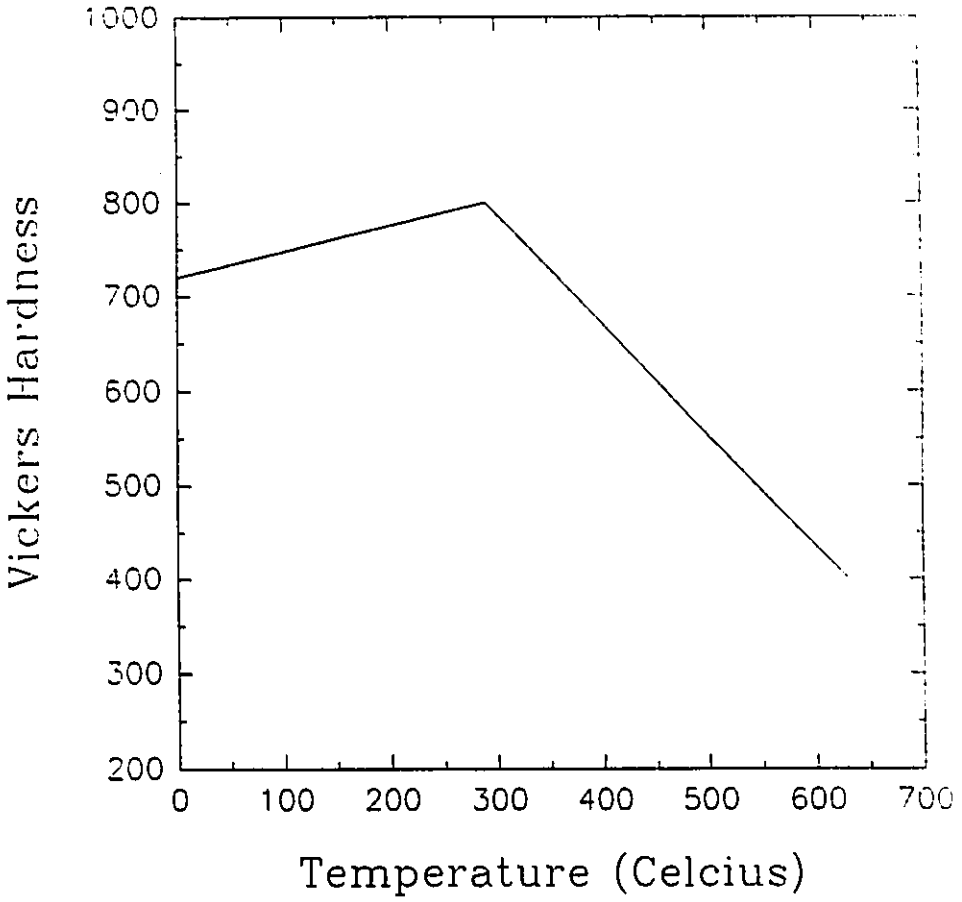

Figure 4.40: Effect of temperature of the hardness of the Al_3Ni intermetallic [120]

4.12: Comparison With Other Al Matrix Composites

Figure 4.41 contrasts the wear rate of several metal matrix composites, adapted from the literature, and the A356-CF composites. The wear rates of a 6061 (Al-1%Mg-0.6%Si-0.3%Cu-0.2%Cr) alloy composite reinforced with SiC whiskers was investigated by L.Cao et al [98] using a pin on disk machine at a velocity of 1.5 m/s and a sliding distance of 300 m. In comparison, the A356-CF composites demonstrated substantially lower mild wear rates (approximately six times lower). In relation to an A356-15%SiC_p composite investigated by Pramila Bai et al [85]; velocity 0.5 m/s,sliding distance 450 m, the A356-CF composites displayed wear rates three to seven times lower in the mild wear regime. The different testing conditions make direct comparison difficult, however, it appears that the wear resistance of the A356-CF composites is comparable or somewhat superior to aluminum matrix composites with hard ceramic reinforcement.

An alternative to ceramic reinforcement is lubrication through the addition of solid lubricants. Figure 4.42 compares the tribological behaviour of the A356-CF composites with graphite containing aluminum based composites. At high loads the wear rates appear to be similar. However, at lower loads, below approximately 100 N, the graphite containing materials tend to display lower wear. This is likely due to lubricating film formation due to the graphite. The reader must be cautioned that direct comparisons must be treated with discretion.

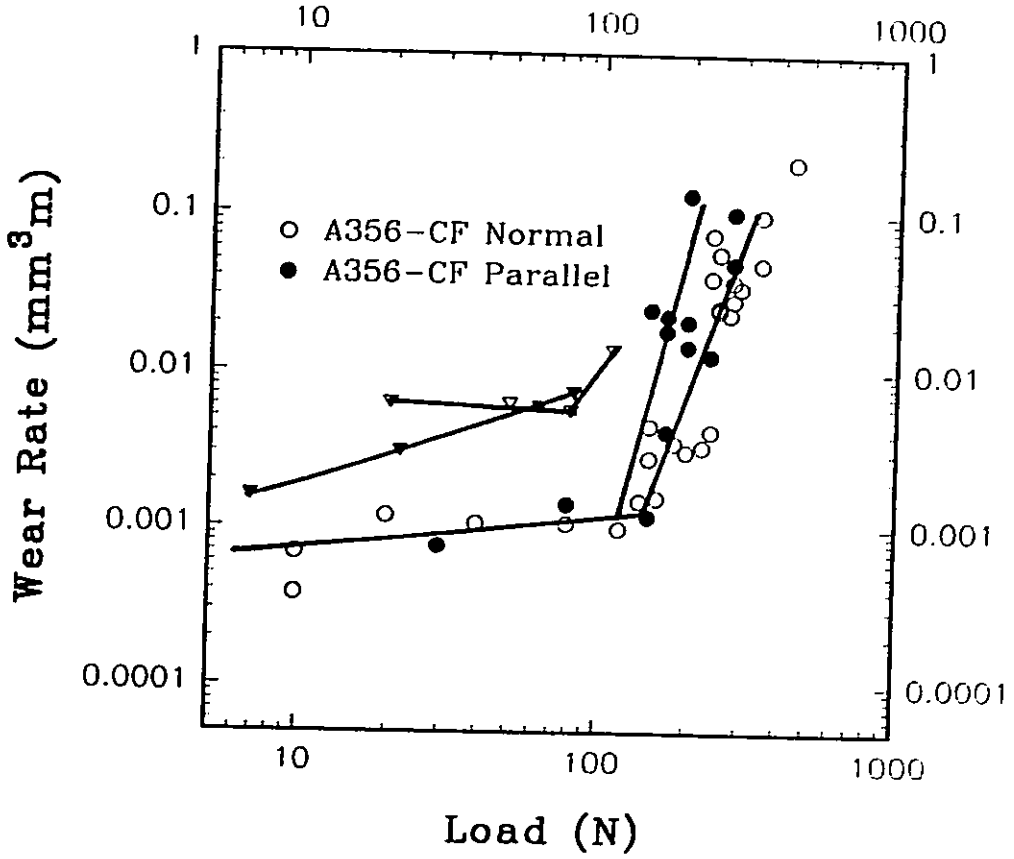

Figure 4.41: Wear rate comparison of composites with hard particle reinforcement. (▽) 6061-20% SiC_w, 1.5 m/s, 300 m, against WC-8%Co [98]; (▾) A356-15% SiC_p, 0.5 m/s, 450 m, against steel [85]

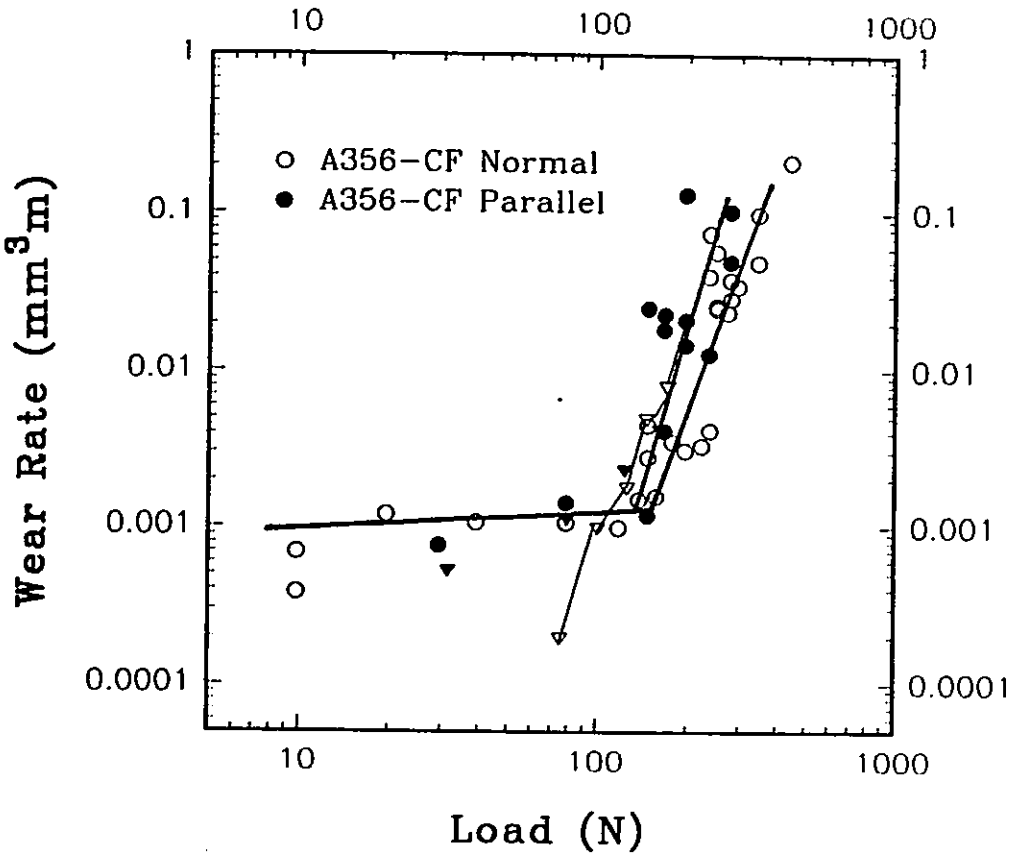

Figure 4.42: Wear rate comparison of MMCs with graphite particle lubrication: (▽) Al-4.5Cu-0.12Fe-3% Gr, 2.68 m/s, 500 m, against steel [122]; (▾) Al-12% Si-2% Gr, 1 m/s, 1800 m, against steel [117]

It appears that the use of pitch based, non-graphitic, isotropic carbon fibres in an aluminum matrix leads to an improvement in the wear properties with respect to the unreinforced alloy. The magnitude of this improvement is comparable, or even superior to other metal matrix composites based on aluminum alloys.

Chapter 5: A356-Gr-SiC Composites

Part A: Experimental Results of the Hybrid MMCs

5.1: Material Characterization

The SiC and graphite particulate reinforced aluminum matrix composites were produced through a molten metal mixing process. The matrix was an A356, Al-Si casting alloy of nominal composition 7.0% Si, 0.35% Mg, 0.11% Fe, 0.22% Ti, 0.05% Mn, 0.05% Zn and the balance aluminum. The graphite particles were coated with nickel by INCO Ltd. The particles were subsequently mixed in to a remelted A356-20%SiC composite by Alcan Int.

Figure 5.1 is a secondary electron image of the microstructure of the composite. The size distribution of the SiC particles was measured and it was determined that the average maximum and minimum dimensions were 12.8 μm and 9.1 μm respectively (Figure 5.2). The size distribution of the graphite particles was also investigated. The average maximum and minimum dimensions were 110 μm and 44 μm respectively (Figure 5.3).

X-ray diffraction analysis was used to identify the phases present in the composites. The analysis determined the existence of aluminum, silicon and SiC.

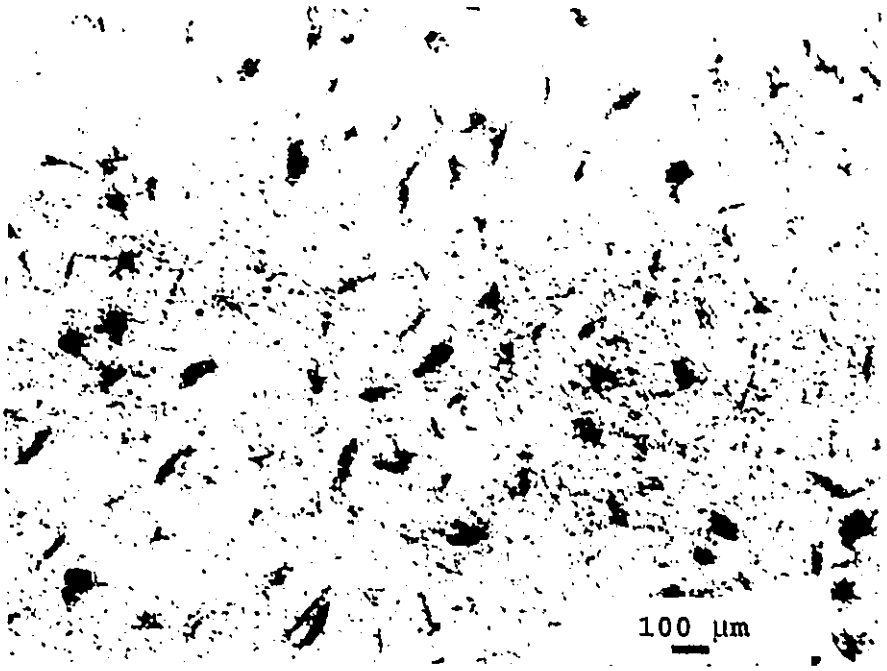

Figure 5.1: Microstructure of the A356-10%Gr-20%SiC composite. Large black particles are graphite particles. Smaller, lighter particles are SiC.

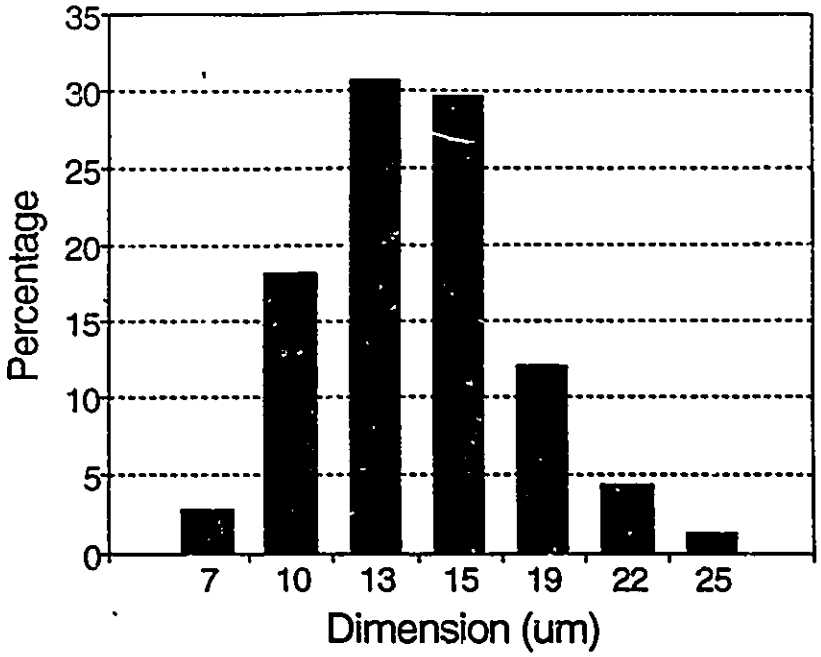

(a)

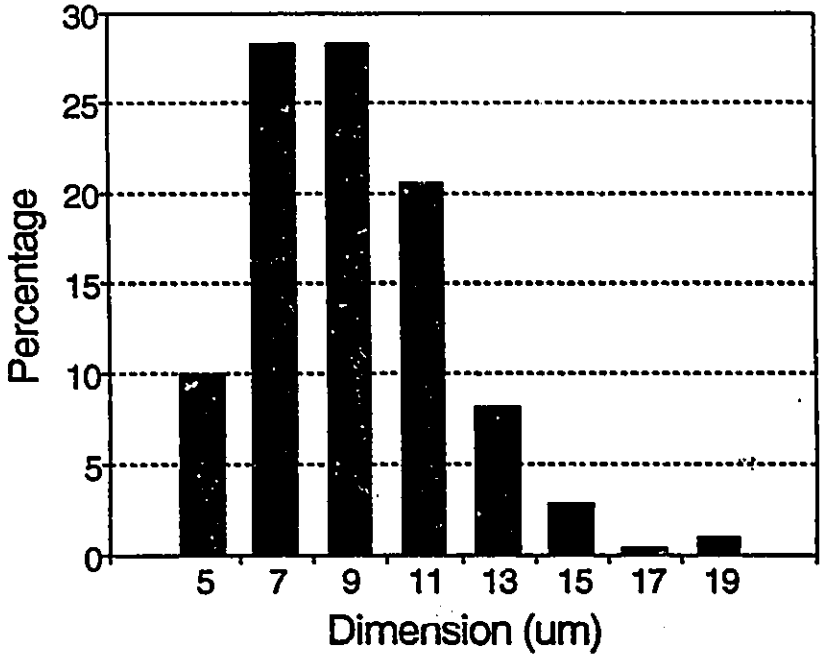

(b)

Figure 5.2: Distribution of SiC particle size a) maximum dimension and b) minimum dimension

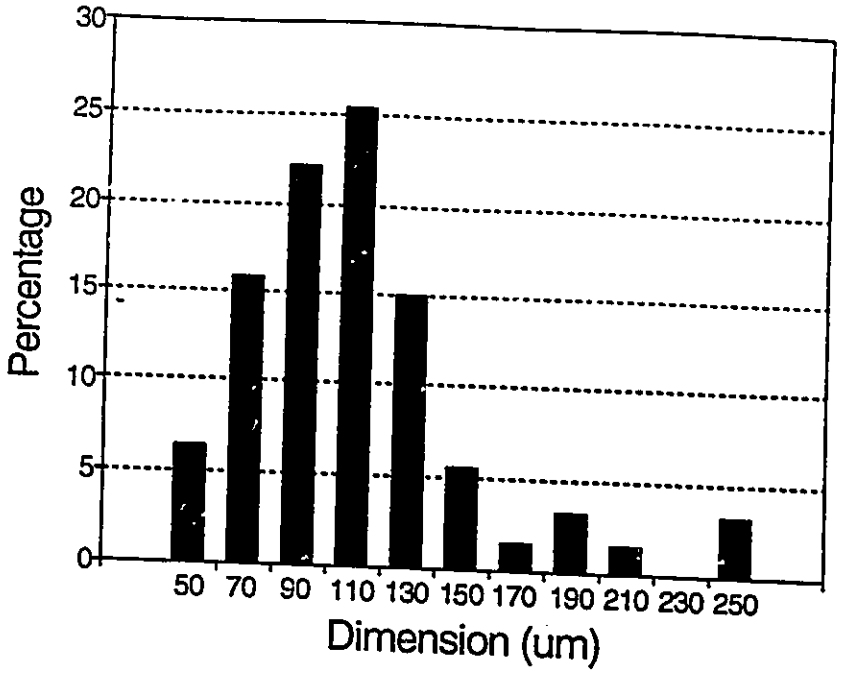

(a)

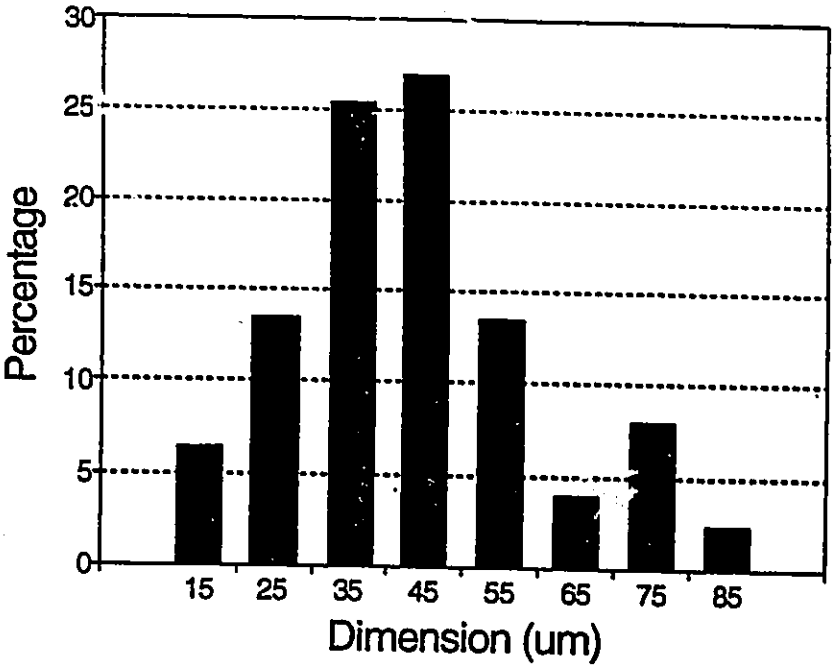

(b)

Figure 5.3: Distribution of graphite particle size a) maximum dimension and b) minimum dimension

In the case of the 10% Gr composite a small graphite peak was detected (Figure 5.4). Nickel containing species were not identified by X-Ray diffraction. Therefore the major constituents are aluminum, silicon, SiC and graphite. The hardness values of these constituents are listed in Table 5.1.

In summary, the hybrid composites consist of 20 vol% SiC particulate and either 3 vol% or 10 vol% nickel coated graphite particles. XRD did not detect the presence of interface reaction products such as Al_4C_3 or Al_3Ni. The presence of both the SiC and the graphite will be shown to have a positive effect on the wear of these composites.

5.2: Wear Rates

The dry sliding wear rates as a function of load are depicted in Figure 5.5. Unlike the carbon fibre composites of chapter 4, these composites do not demonstrate regions of mild and severe wear rates. There appears to be a single relationship between wear rate and load on the log-log plot. An equation of the form:

$$W_d = C\ L^n \qquad (5.1.1)$$

where W_d is the wear rate (mm^3/m), L is the applied load (N) and n and C are

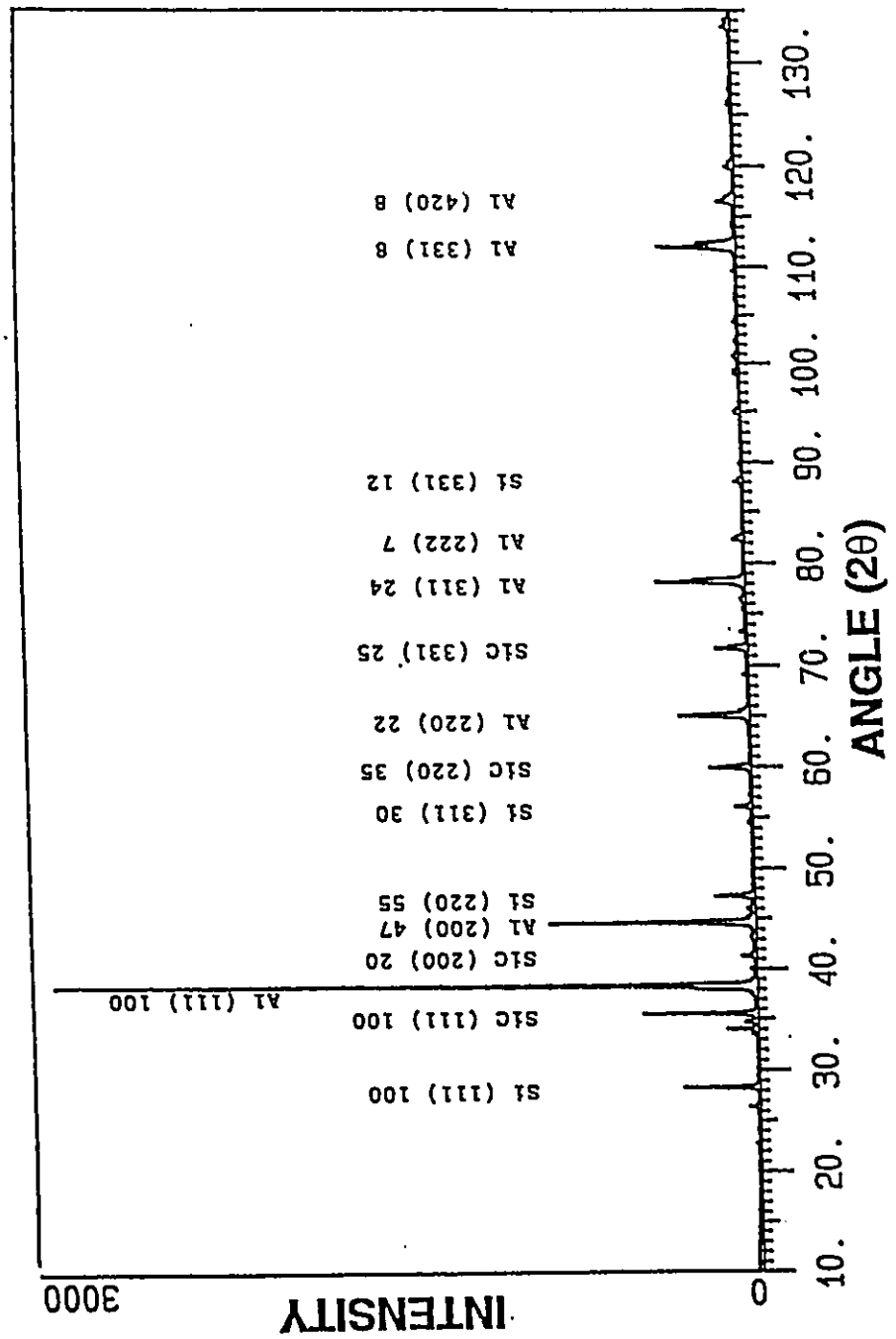

Figure 5.4 a: XRD of the A356-3%Gr-20%SiC composite

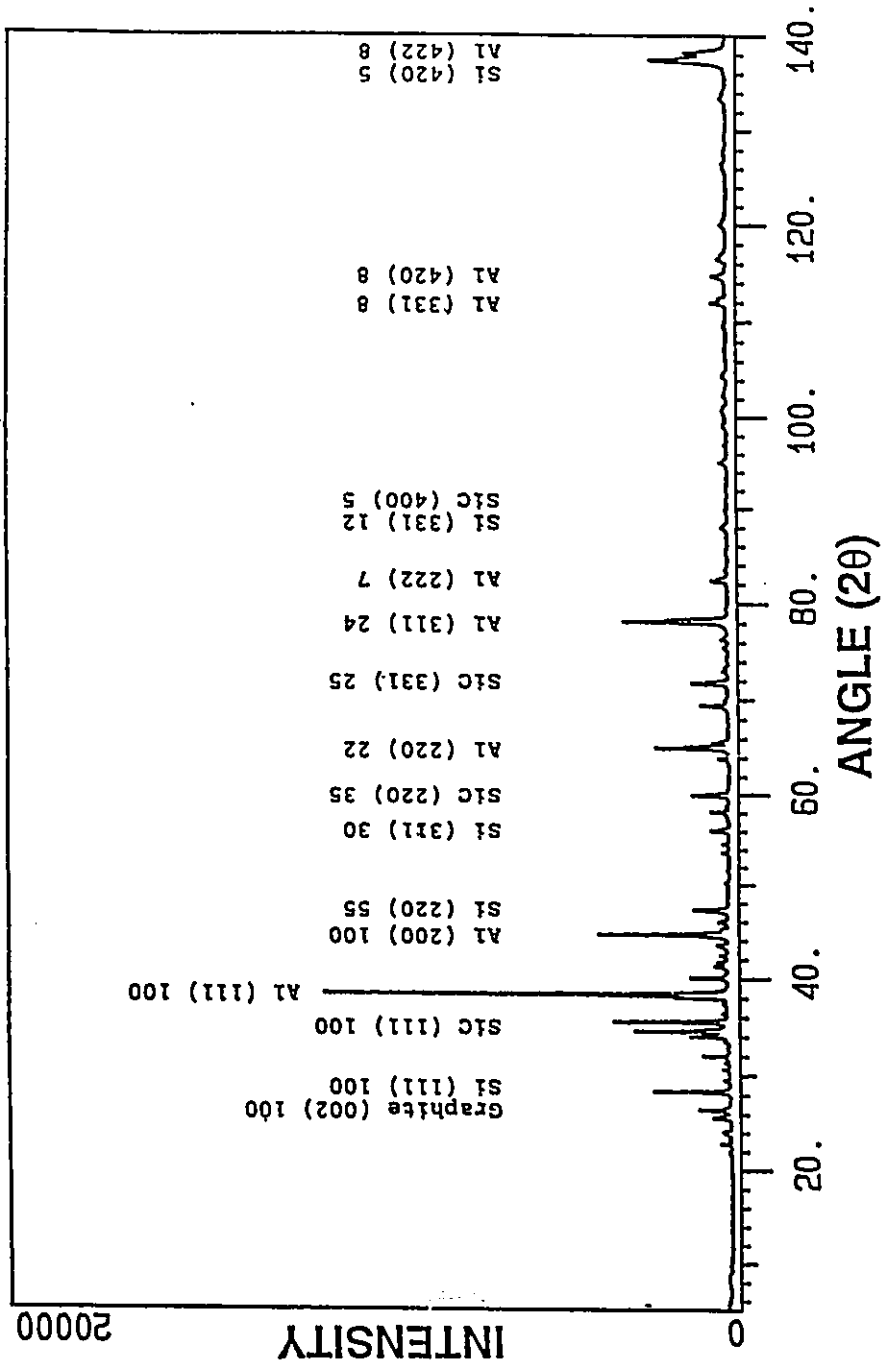

Figure 5.4 b: XRD of the A356-10%Gr-20%SiC composite

Table 5.1: Hardness values of the hybrid composites and their constituents.

	A356-3%Gr-20%SiC	A356-10%Gr-20%SiC
Bulk Hardness	88.5 VHN (1 kg_f) (47.1±3.4, 30-T)	87.0 VHN (1 kg_f) (45.3±5.6, 30-T)
A356	66.8±7.2 VHN	66.8±7.2 VHN
SiC + Matrix	97±8 VHN (100 g_f)	103±13 VHN (100 g_f)
Graphite	61±14 VHN (25 g_f)	61±14 VHN (25 g_f)

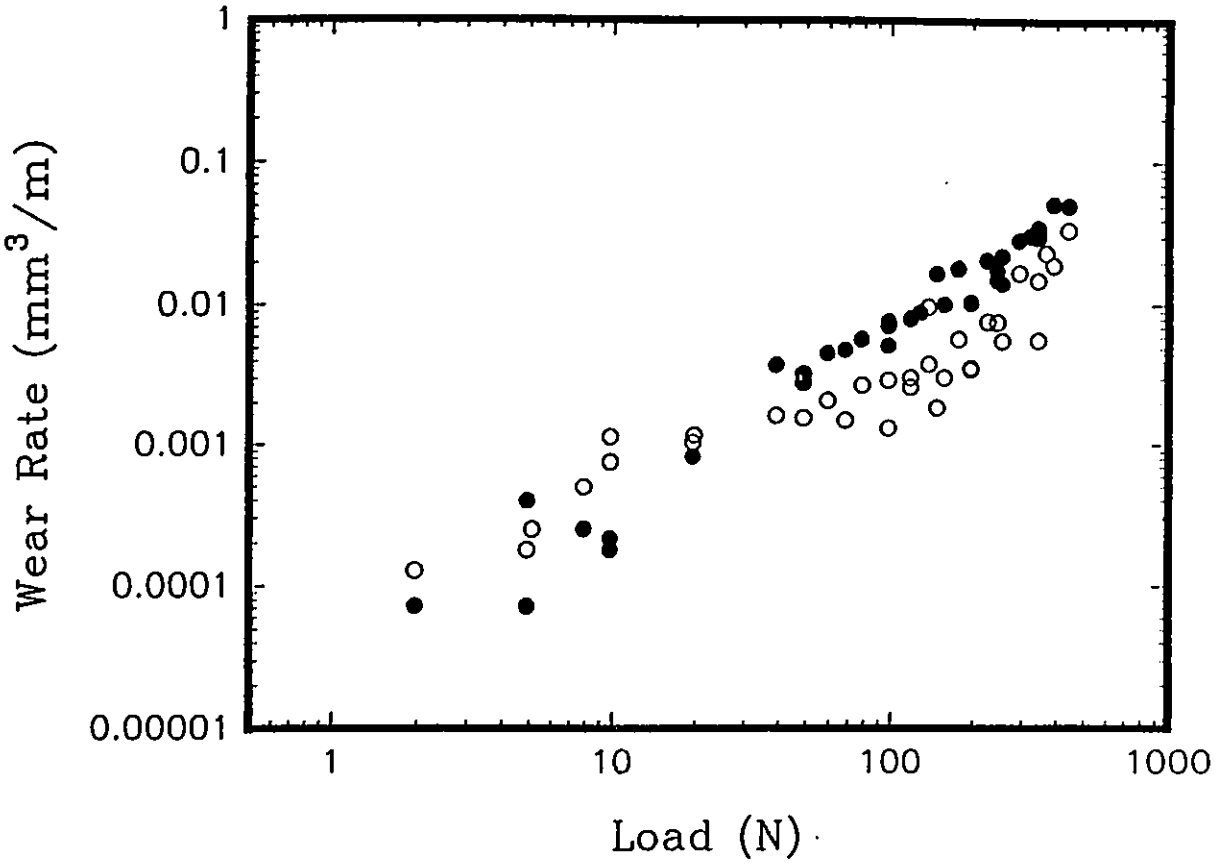

5.5: Wear rate as a function of load for the hybrid composites with (∘) 3% graphite and (•) 10% graphite

constants, describes this relationship. The constants n and C, and the correlation coefficient, are listed in Table 5.2. The single relationship between force and wear rate suggests that there is only one dominant wear mechanism that operates throughout the load range tested. However, it will be shown that the wear behaviour changes as load varies.

At a load of 8 N the composites demonstrated typical wear rates of 2×10^{-4} mm^3/m. At higher loads the A356-3%Gr-20%SiC composites displayed wear rates (1.5×10^{-3} mm^3/m at 70 N) two to three times lower than the composite with 10% graphite (6.0×10^{-3} mm^3/m at 70 N). At extreme loads, both composites exhibited similar wear rates of the order of 5×10^{-2} mm^3/m. The 3% graphite composite may have been somewhat superior at these high applied loads. Most significant, however, is the absence of a substantial increase in the wear rate which would have signified the onset of severe wear. The absence of severe wear separates these materials from other aluminum matrix composites.

Composite systems which involve the addition of hard ceramic reinforcements often show an increase in counterface wear. At loads below 125 N the A356-Gr-SiC composites wore the counterface at similar rates regardless of graphite content (Figure 5.6). At higher loads, wear of the A356-10%Gr-20%SiC composite resulted in less counterface wear compared to the composite with only 3% graphite. Therefore, it appears that the addition of graphite has a beneficial effect on counterface wear especially at higher applied loads.

Table 5.2: Curve fit parameters n and C, and the correlation coefficient r for the A356-Gr-SiC composites.

	A356-3%Gr-20%SiC	A356-10%Gr-20%SiC
n	0.91±0.1	1.25±0.1
C	$5.3 \times 10^{-5} \pm 3 \times 10^{-5}$	$2.1 \times 10^{-5} \pm 6 \times 10^{-6}$
r	0.93	0.98

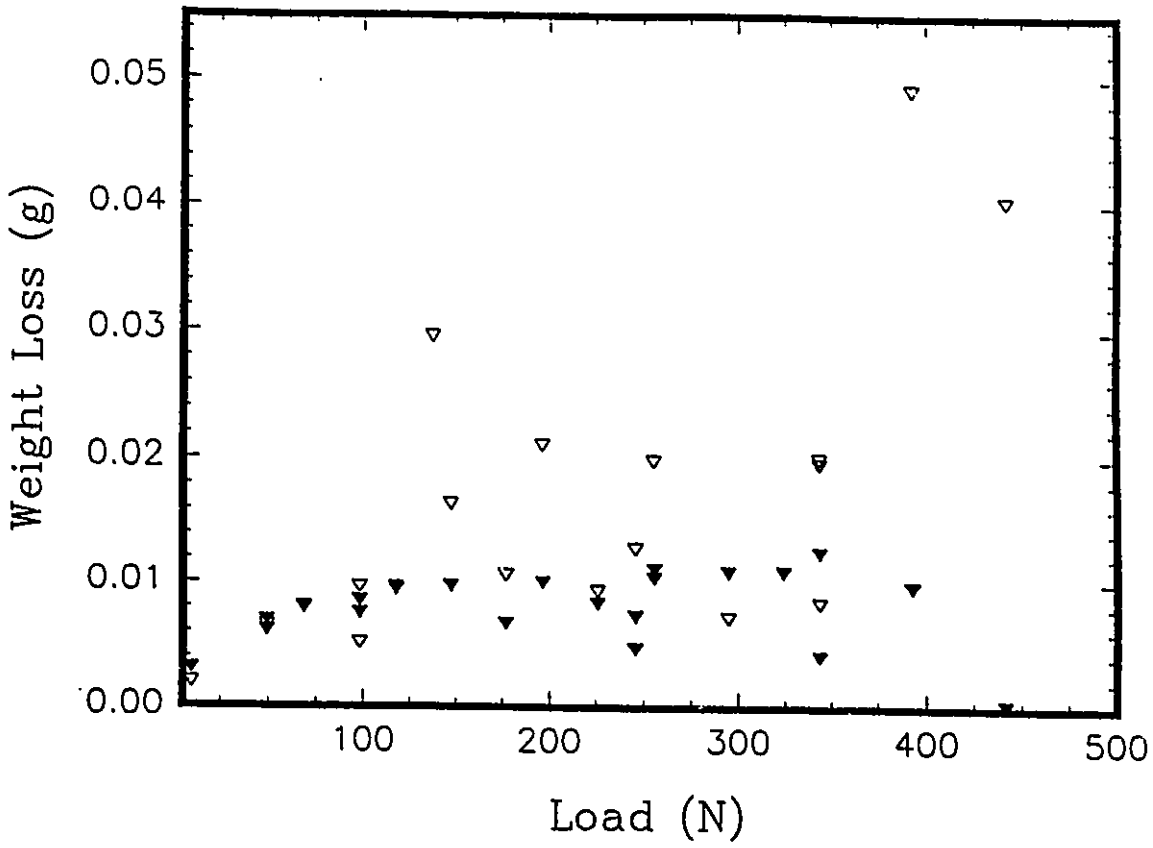

5.6: Counterface wear as a function of load when slid against composites with (▽) 3% graphite and (▼) 10% graphite

Under high loading conditions the A356-3%Gr-20%SiC composite exhibited unusual wear and counterface wear behaviour as a function of sliding distance (Figure 5.7). Initially the sample lost weight at a much higher rate compared to the steel counterface. However, after sliding 700 m the A356-3%Gr-20%SiC sample gained weight. This gain in weight corresponded to a rapid loss of counterface weight. It was observed that the counterface took on a purple-blue-orange appearance indicating oxidation and suggesting that the frictional temperature must be considered.

5.3: Temperature Rise During Sliding

Figure 5.8 shows the contact surface temperature of the sample during sliding at loads of 343 N. The surface temperature of the A356-3%Gr-20%SiC composite increased rapidly during the first ten minutes of sliding. The temperature then increased at a much slower rate, levelling off at approximately 490 K. The composite containing 10% graphite behaved similarly but, the surface temperature was substantially lower (only 445 K after 2000 m of sliding. Therefore sliding of the composite with a higher graphite content resulted in a lower interface temperature at a given load.

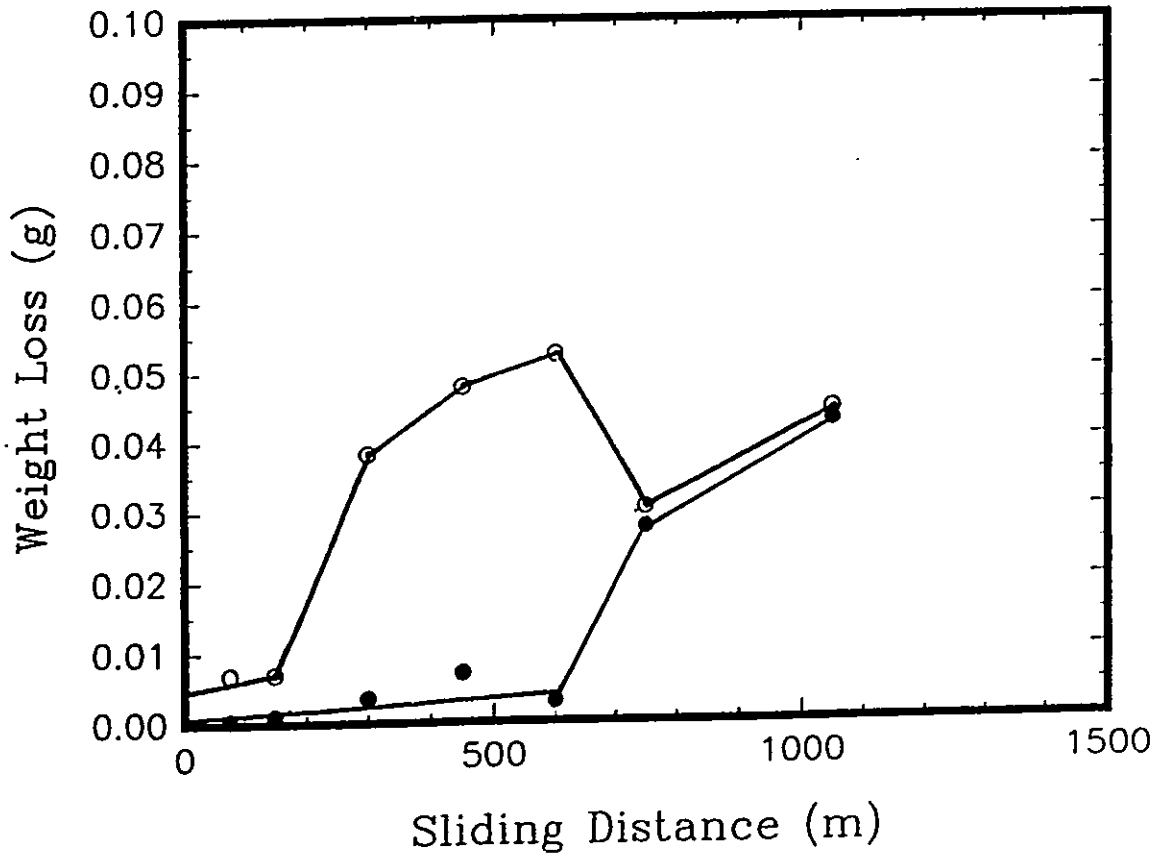

Figure 5.7: Volume loss of an A356-3%Gr-20%SiC composite (∘) and the counterface (•) slid at 427 N as a function of sliding distance

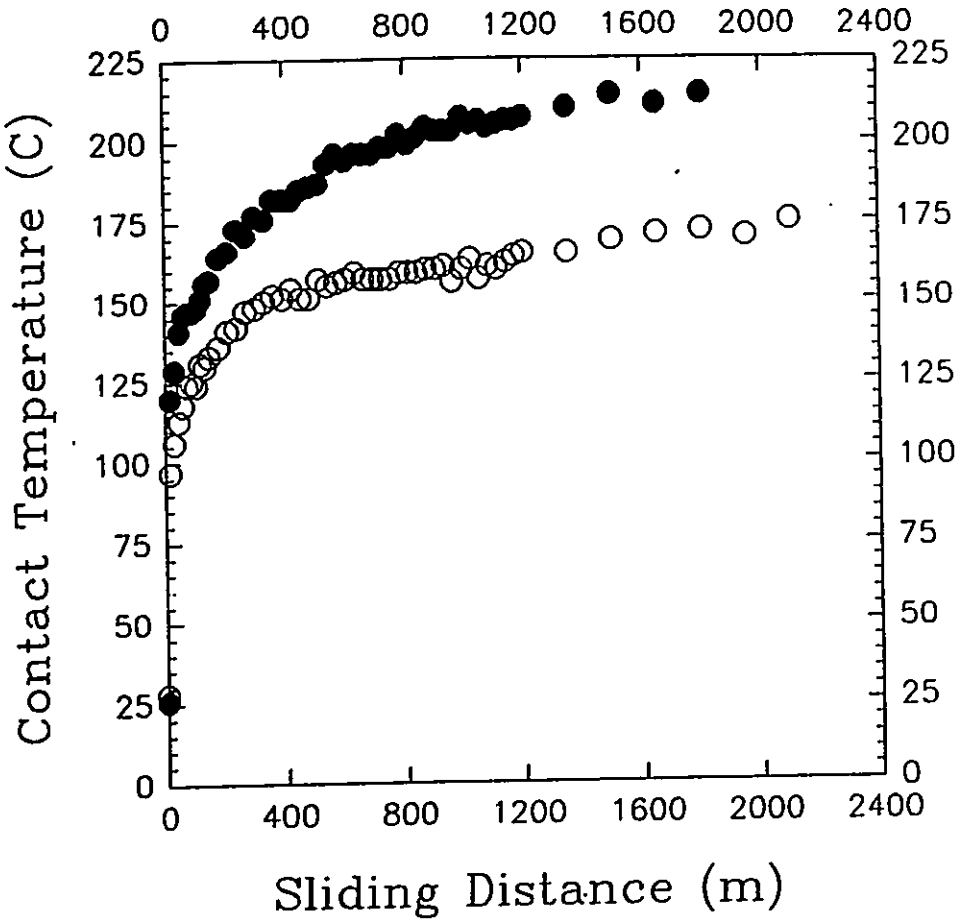

Figure 5.8: The variation of surface temperature with sliding distance for hybrid composites with (•) 3% graphite and (○) 10% graphite slid at 343 N

5.4: Effect of Velocity

The effect of velocity at a constant load of 9.81 N was investigated. Figure 5.9 compares the volume loss of the A356-Gr-SiC composites at sliding speeds of 0.1 m/s and 1 m/s. In both cases the volume loss increased linearly with sliding distance. The amount of volume loss at any given sliding distance was greater at the higher velocity of 1 m/s. An increase in the velocity from 0.1 m/s to 1 m/s resulted in an increase in the wear rate from 2.1×10^{-7} mm^3/m to 1.5×10^{-6} mm^3/m, in the case of the composite with 3% graphite, and 3.6×10^{-8} mm^3/m to 4.7×10^{-7} mm^3/m in the composite with 10% graphite. From these values it should be apparent that the A356-10%Gr-20%SiC composite demonstrated superior wear rates at a load of 9.81 N when tested at either velocity.

5.5: Effect of Solutionizing and Artificial Aging

The consequence of a solutionizing (four hours at 813 K) and aging treatment (nine hours at 428 K) on the wear rate may be observed in Figure 5.10. At the load of 9.81 N, the heat treatment had no effect on the wear rate of the A356-10%Gr-20%SiC composite at either velocity. At a velocity of 1 m/s the wear of the 3% graphite containing composite also remained unaffected by the heat treatment. However, at the lower sliding speed of 0.1 m/s the heat treated A356-3%Gr-20%SiC composite often demonstrated an increase in weight even though a wear scar was

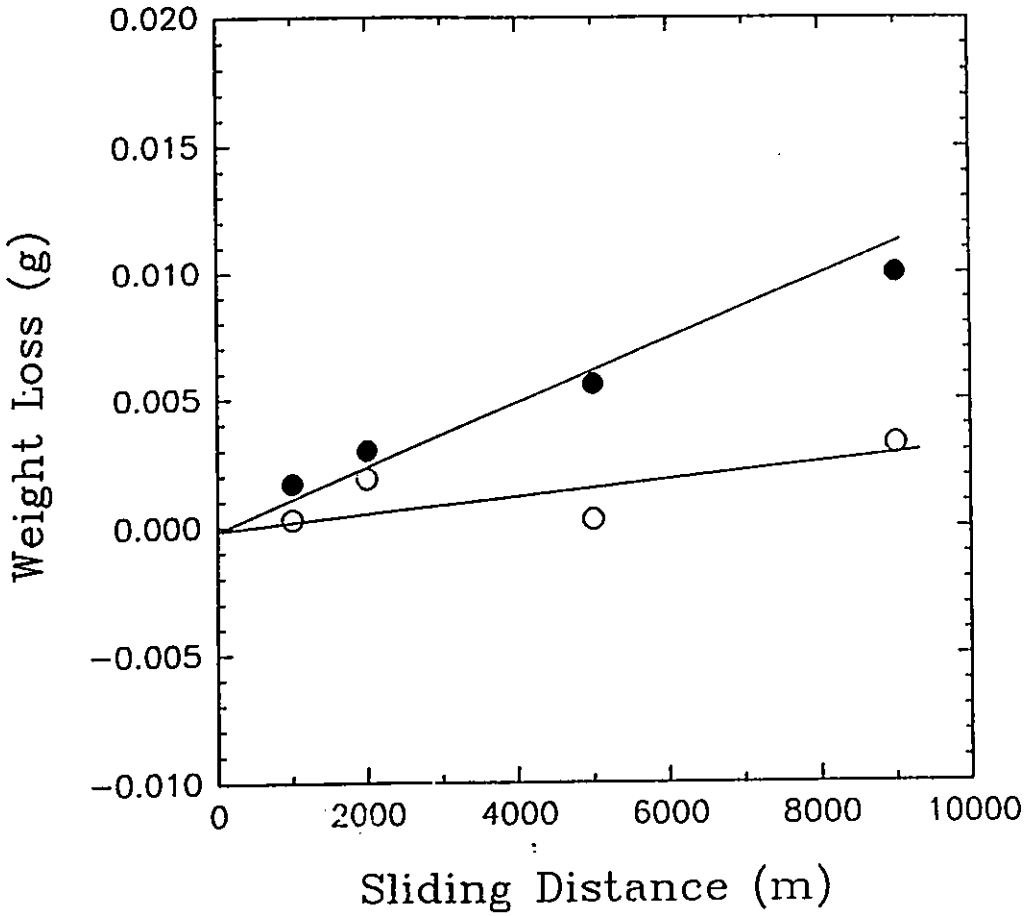

Figure 5.9 a: Effect of velocity on the wear of the A356-3%Gr-20%SiC composite at (∘) 0.1 m/s and (•) 1 m/s

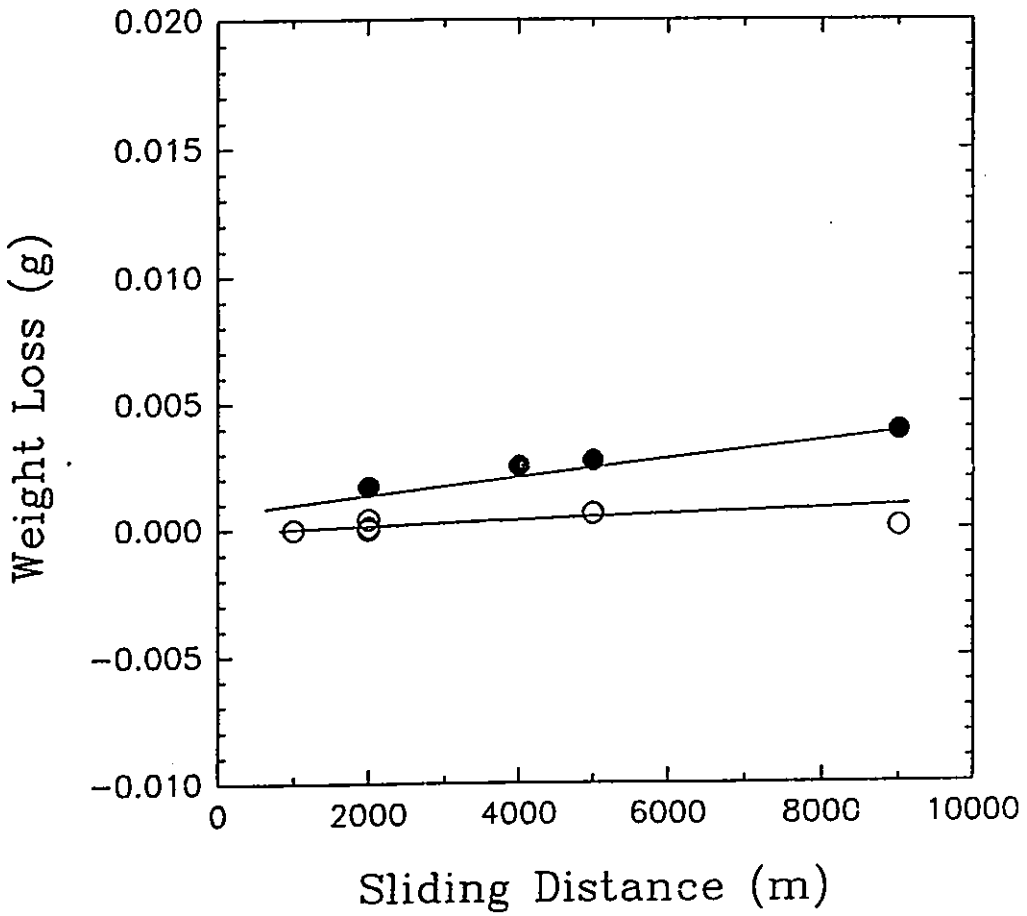

Figure 5.9 b: Effect of velocity on the wear of the A356-10%Gr-20%SiC composite at (∘) 0.1 m/s and (•) 1 m/s

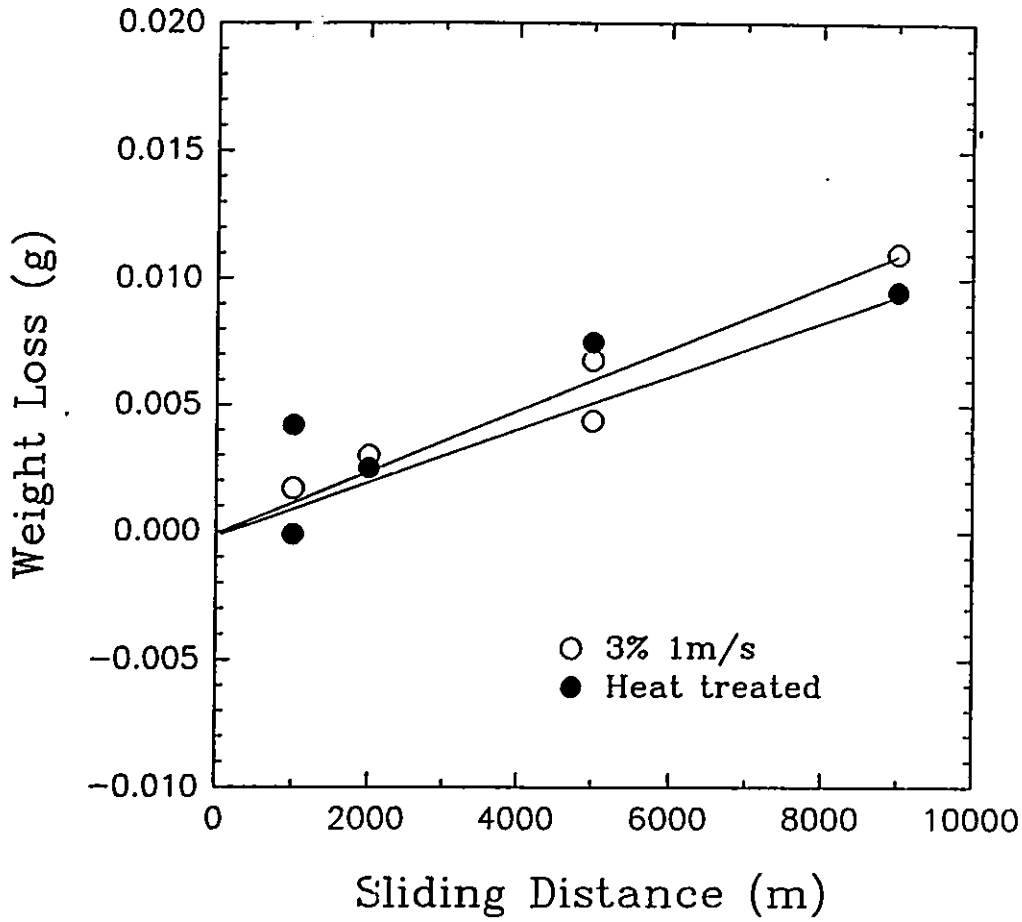

Figure 5.10 a: Effect of solutionizing and aging on the wear of the A356-3%Gr-20%SiC composite at 1 m/s

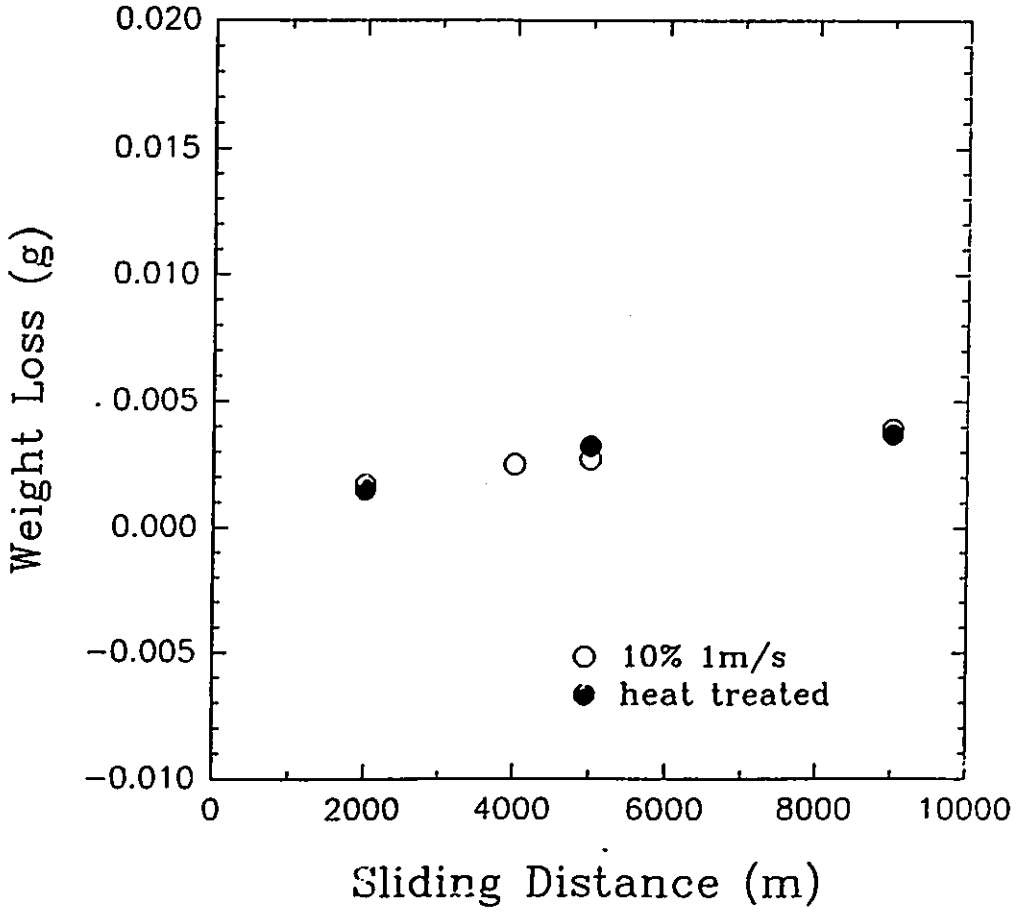

Figure 5.10 b: Effect of solutionizing and aging on the wear of the A356-10%Gr-20%SiC composite at 1 m/s

readily observable. This increase in weight was due to the transfer of steel from the counterface. Therefore, a solutionizing and peak aging treatment appears to increase the abrasive ability of the composites particularly when the graphite concentration is small.

5.6: Characterization of the Worn Surface

As load increased the appearance of the worn surface progressed through a series of steps. At low loads the worn surfaces of the composites appeared to be black or, in the case of the heat treated A356-3%Gr-20%SiC composite, reddish brown. The surface contained many fine particles 1 to 5 μm in size (Figure 5.11). As load increased, the proportion of the area covered with particles decreased and grooved areas with lapps were formed by the hard asperities of the counterface and debris particles (Figure 5.12). These plateaus were surrounded by particulate material (Figure 5.13). The counterface displayed signs of abrasive wear including the formation of an abundance of particles in the wear scar (Figure 5.14). At extreme loads the worn surface became relatively smooth and glossy in appearance with few particulate containing areas (Figure 5.15). Figure 5.16 contrasts the particles formed on the wear surface at high and low loads. The particles formed at low loads and the particles formed at high loads appear to have the same morphology. However, at extreme loads the worn surface was almost completely devoid of these particles.

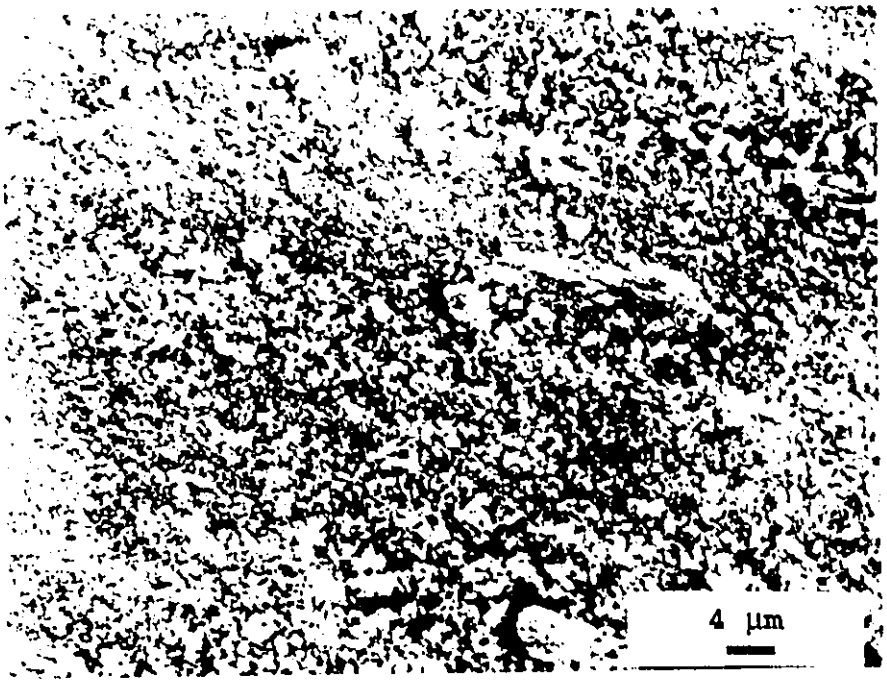

Figure 5.11: Worn surface of an A356-3%Gr-20%SiC composite after sliding 1000 m at a load of 4.9 N (sliding direction left to right)

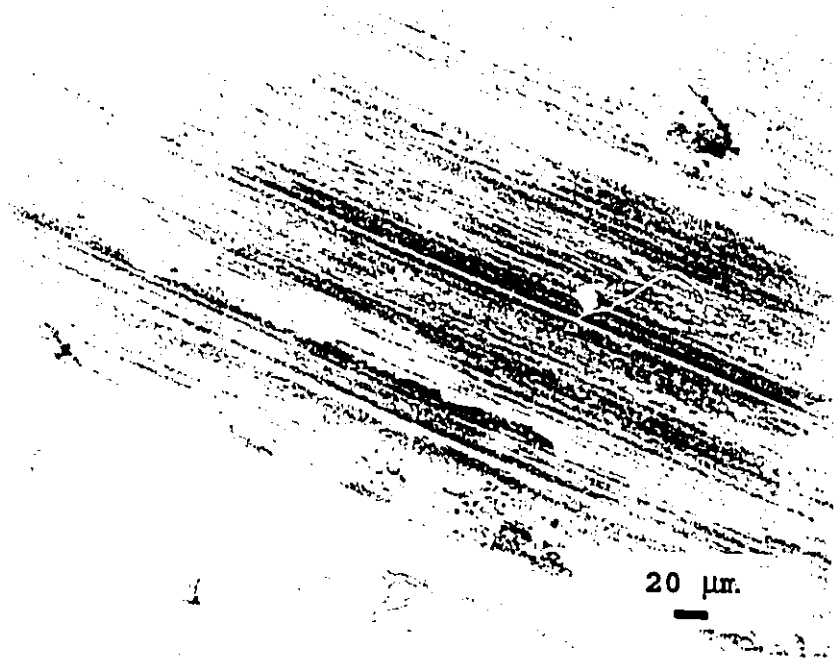

Figure 5.12: Worn surface of an A356-10%Gr-20%SiC composite after sliding at a load of 69 N (sliding direction left to right)

Figure 5.13: Worn surface of an A356-10%Gr-20%SiC composite after sliding at a load of 10 N (sliding direction right to left)

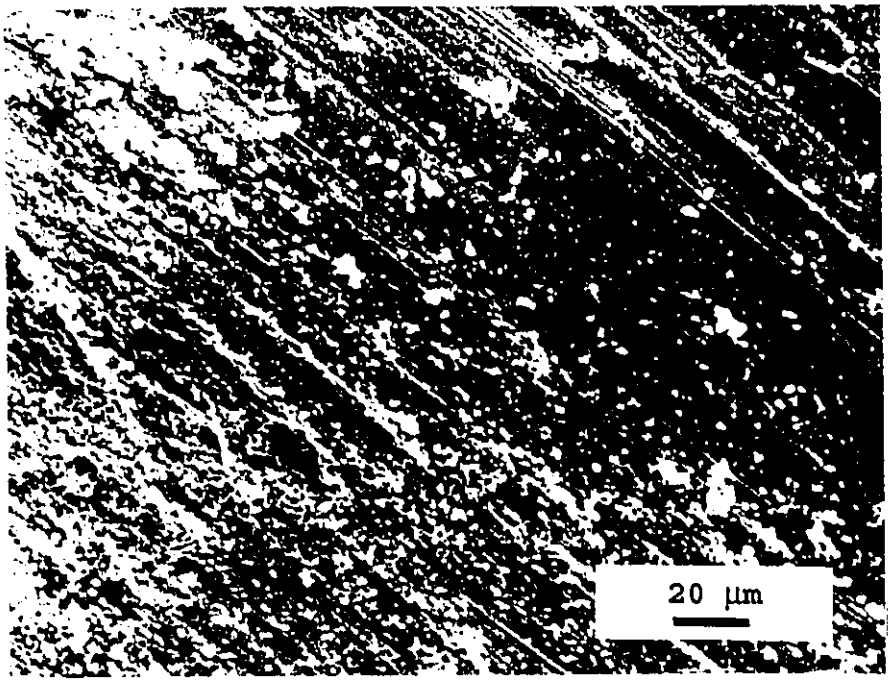

Figure 5.14: Surface of the steel counterface after sliding against an A356-3%Gr-20%SiC composite at a load of 343 N.

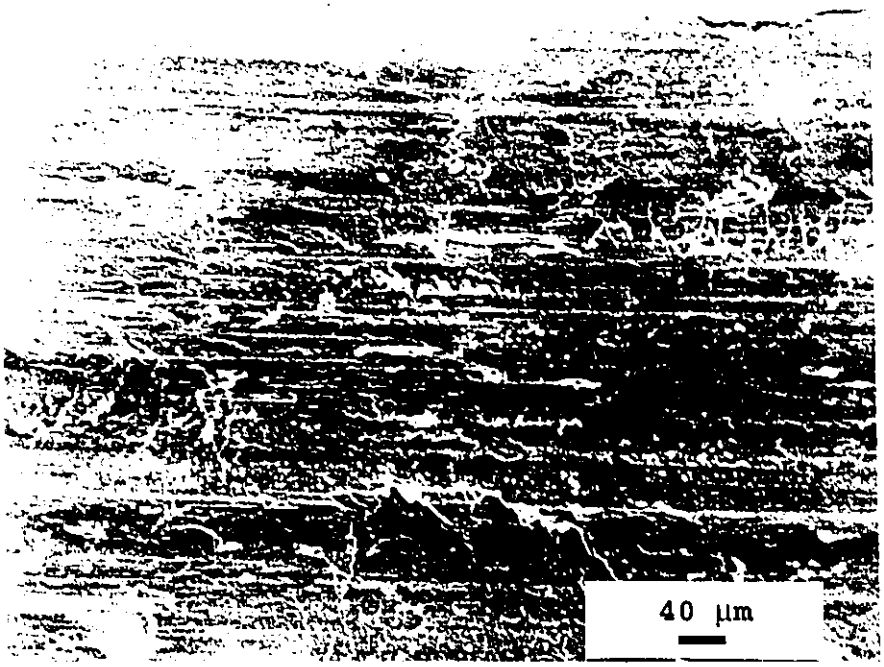

(a)

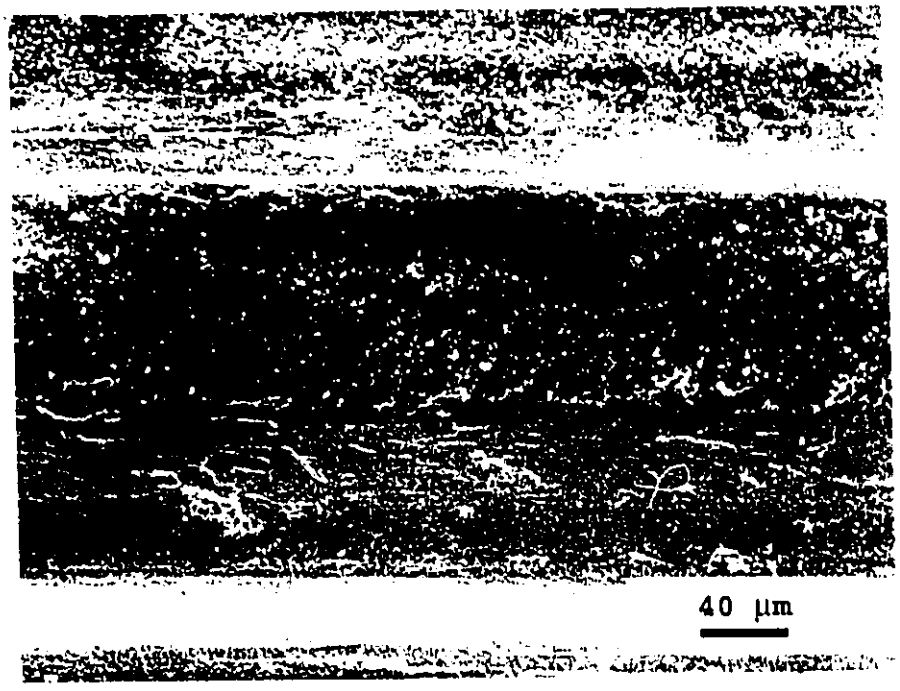

(b)

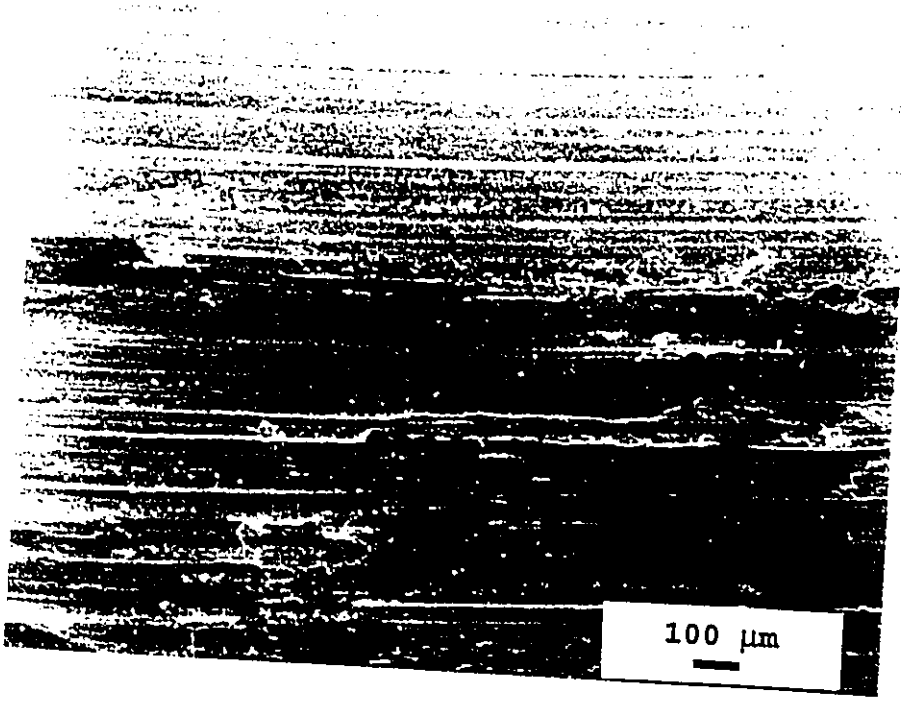

(c)

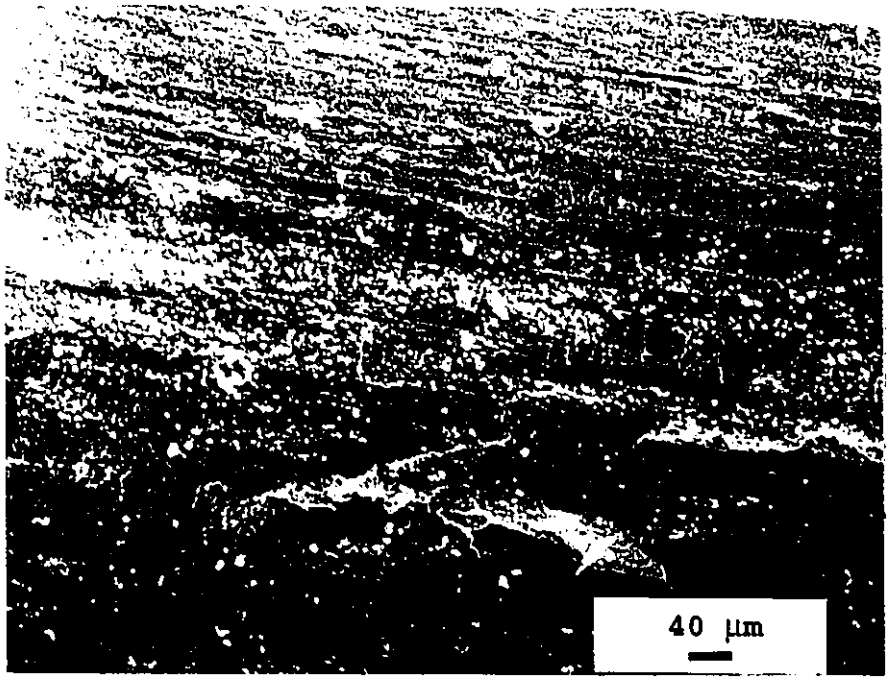

(d)

Figure 5.15: High load worn surfaces a) A356-3%Gr-20%SiC, 294 N; b) A356-3%Gr-20%SiC, 441 N; c) A356-3%Gr-20%SiC, 226 N; d) A356-10%Gr-20%SiC, 343 N (sliding left to right)

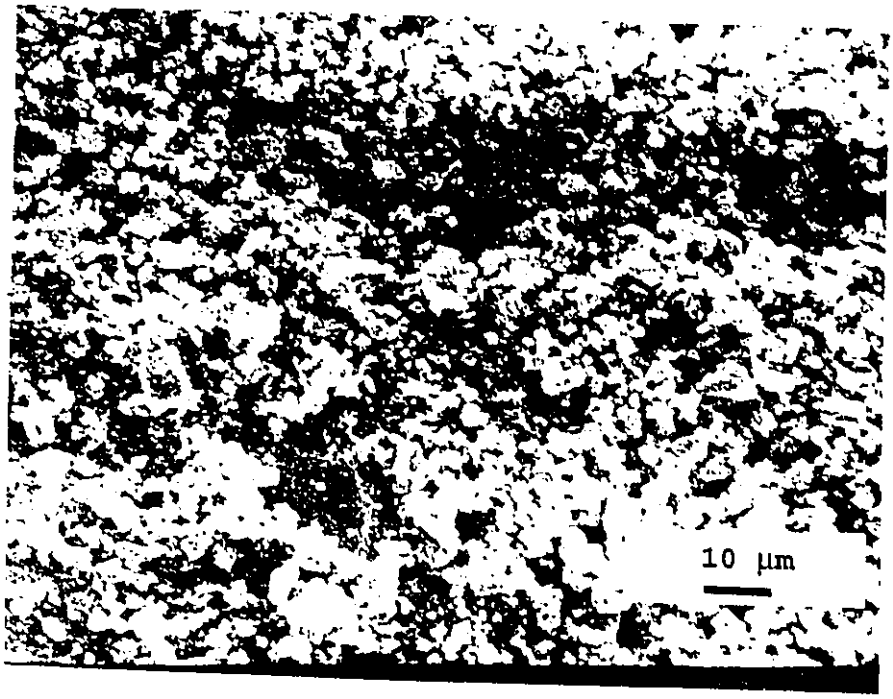

(a)

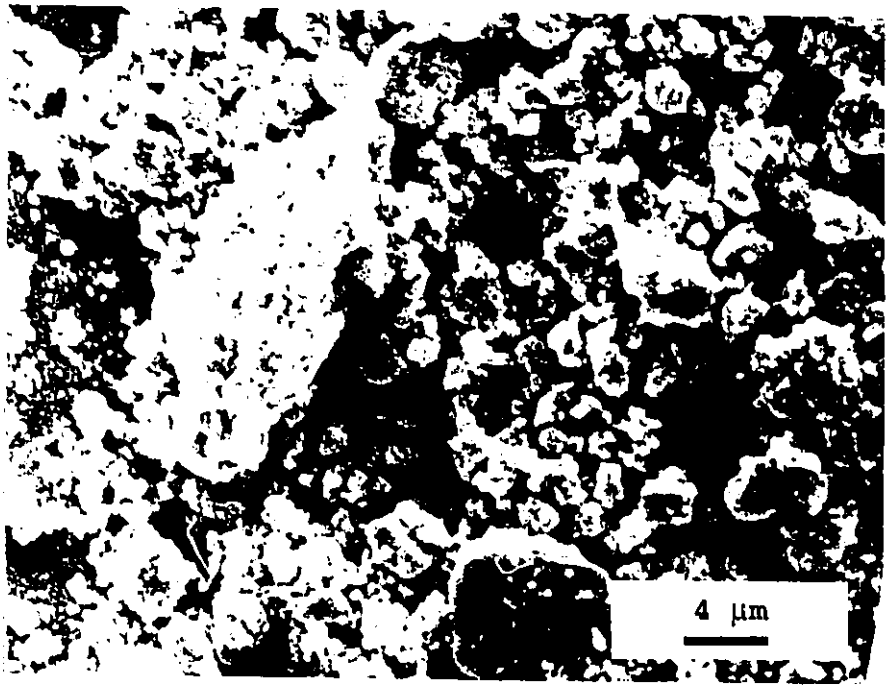

(b)

Figure 5.16: Particles on the worn surface of hybrid composites a) 10 N, 10% Gr, b) 441 N, 3%Gr

Samples tested under extreme loading conditions exhibited other features on the worn surface such as cracks (Figure 5.17 and Figure 5.18). Depressions (Figure 5.19) and blisters (Figure 5.20) suggested the formation of a surface layer. Evidence that a surface layer had formed was found at lower loads also (Figure 5.21 and 5.22).

The composition of the surface layer was investigated to help interpret the influence of the surface on the wear rate. Figure 5.23 documents the relative amounts of iron (from the counterface), aluminum and silicon (from the sample) found on the worn surface at different loads determined using EDS. Two very different behaviours may be observed. The composite with 10% graphite had a large concentration of iron (42 at%) on the worn surface at a load of 4.9 N. As load increased the concentration of iron decreased and remained at approximately 2 at% to 10 at%. The A356-3%Gr-20%SiC composite had a somewhat higher concentration of iron (53 at%) at 4.9 N. The iron level decreased at intermediate loads (98 N to 343 N) but remained greater in the 3% graphite composites compared to the 10% graphite composites. At extreme loads the iron content increased to 75 at% to 85 at% indicating that transfer from the ring to the sample was occurring at a much greater rate. This was not observed in the composite with a 10% graphite. Therefore the graphite content of the composite influenced the composition of the surface layer formed.

Carbon, or graphite, could not be detected using the EDS system at our

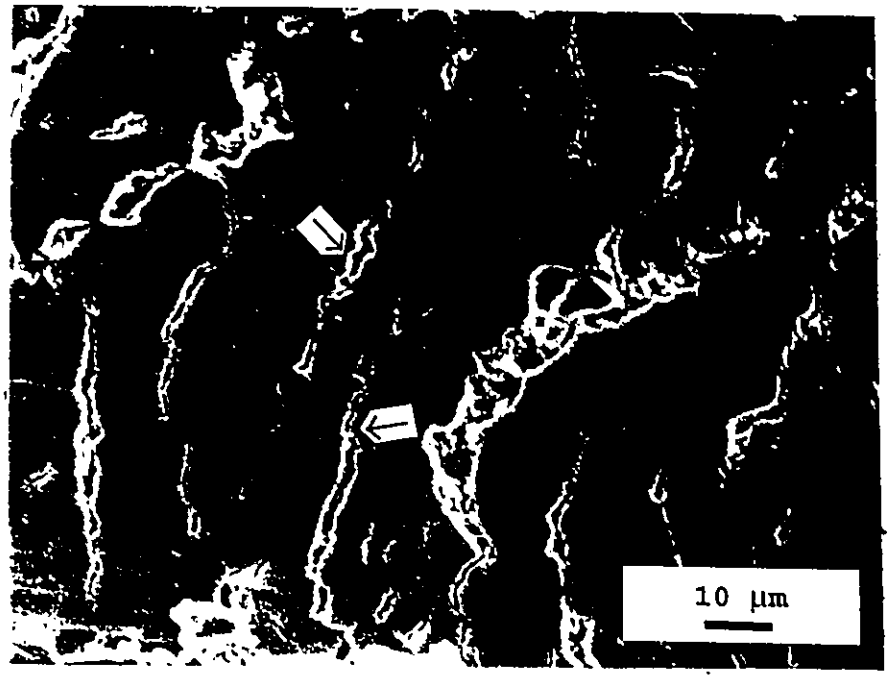

Figure 5.17: Cracks on the worn surface of an A356-3%Gr-20%SiC composite tested at 441 N (sliding left to right)

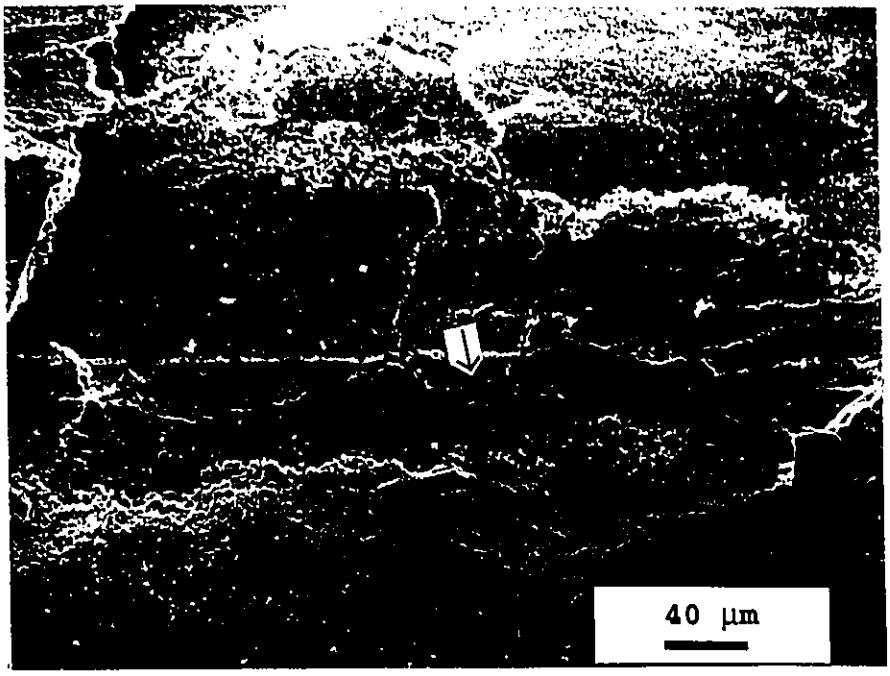

Figure 5.18: Cracks in the worn surface of an A356-3%Gr-20%SiC composite tested at 441 N (sliding direction left to right)

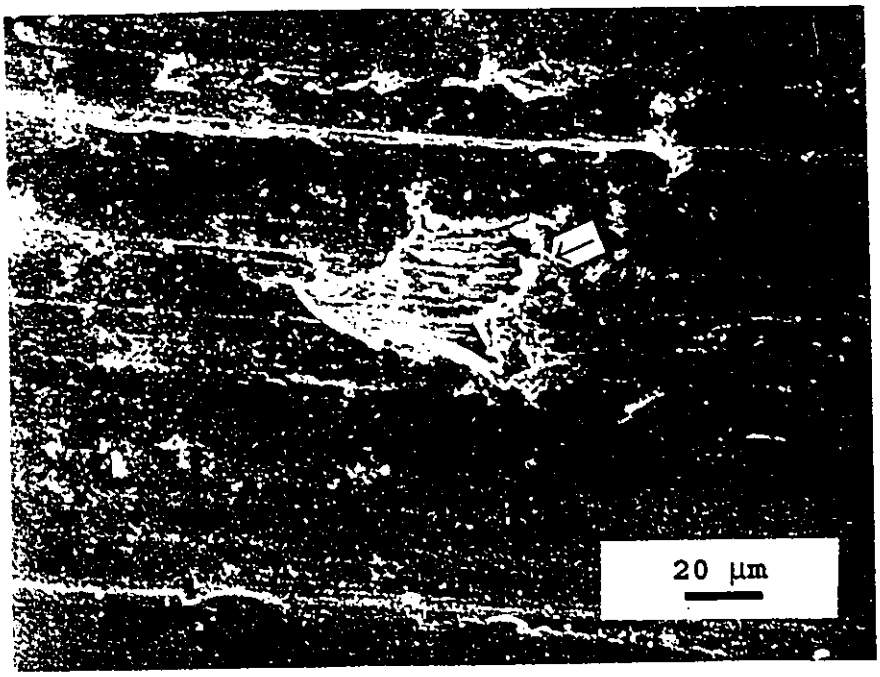

Figure 5.19: Cavity in the worn surface of an A356-3%Gr-20%SiC composite tested at 441 N (sliding left to right)

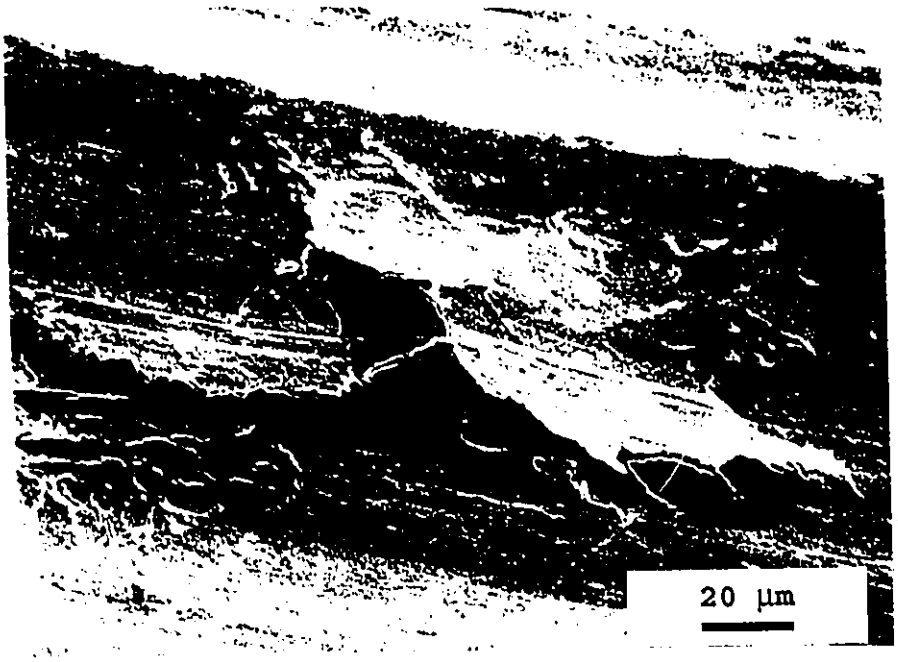

Figure 5.20: Blister on the worn surface of an A356-3%Gr-20%SiC composite tested at 441 N (sliding left to right)

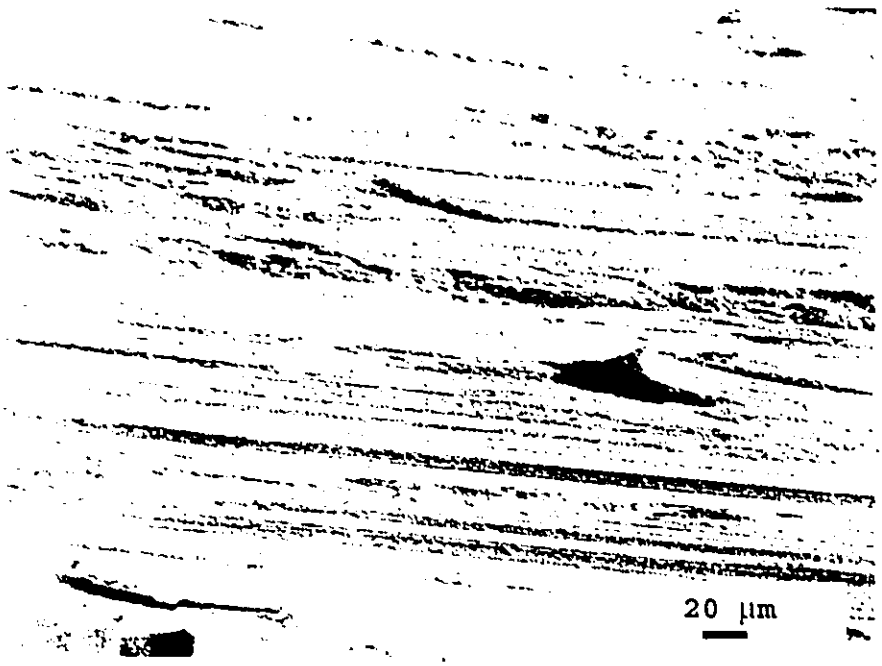

Figure 5.21: Worn surface of an A356-10%Gr-20%SiC composite at a load of 69 N (sliding left to right)

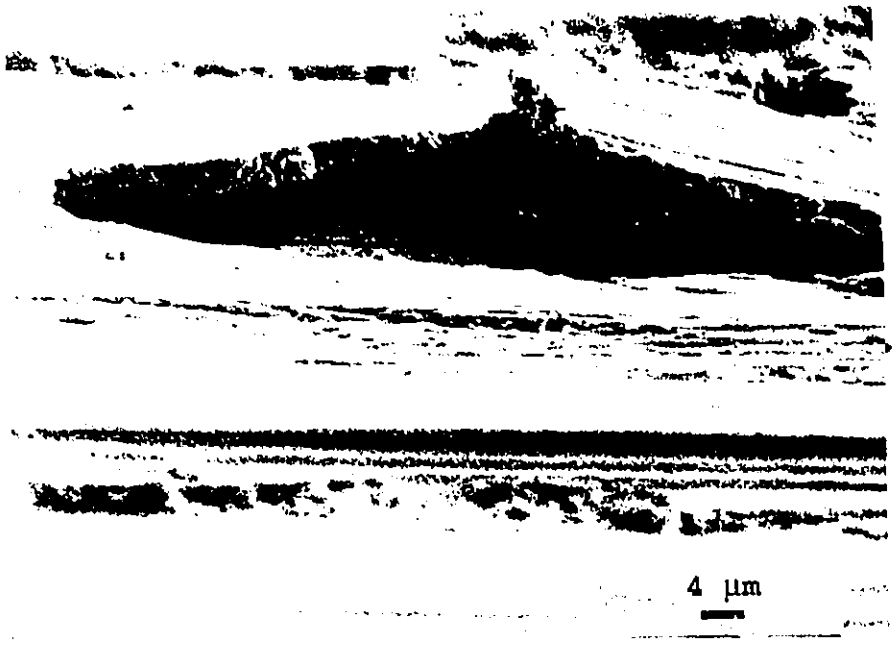

Figure 5.22: Worn surface of an A356-10%Gr-20%SiC composite tested at a load of 69 N (sliding left to right)

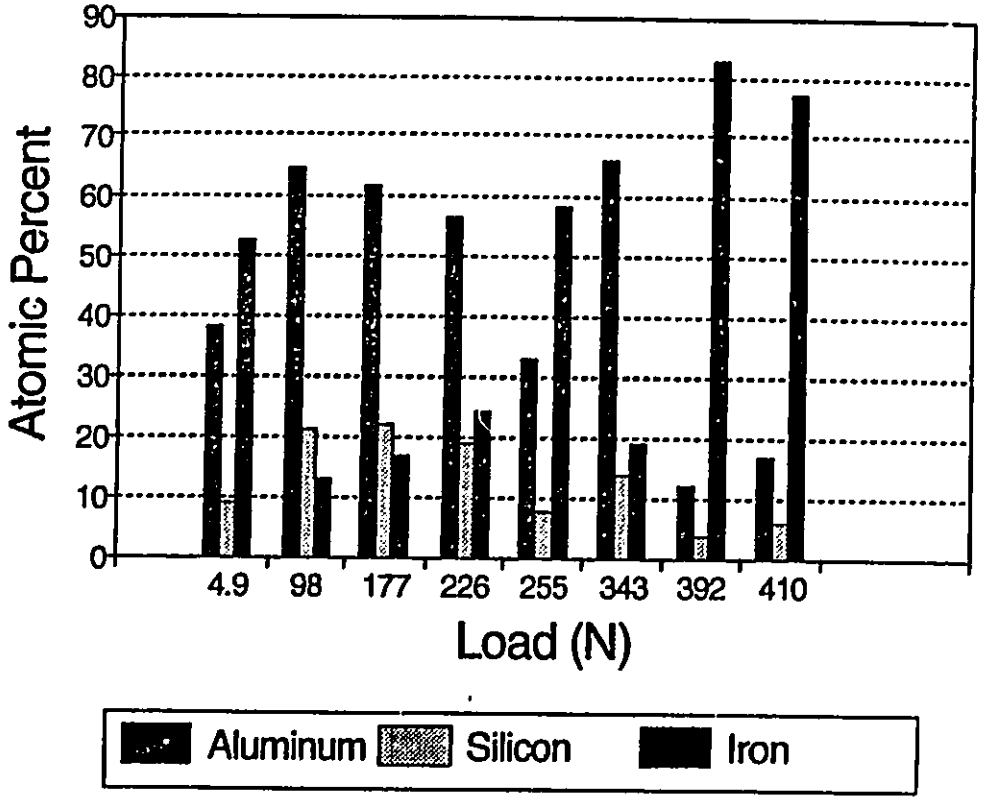

Figure 5.23 a: Composition of the worn surface as a function of load for the A356-3%Gr-20%SiC composite

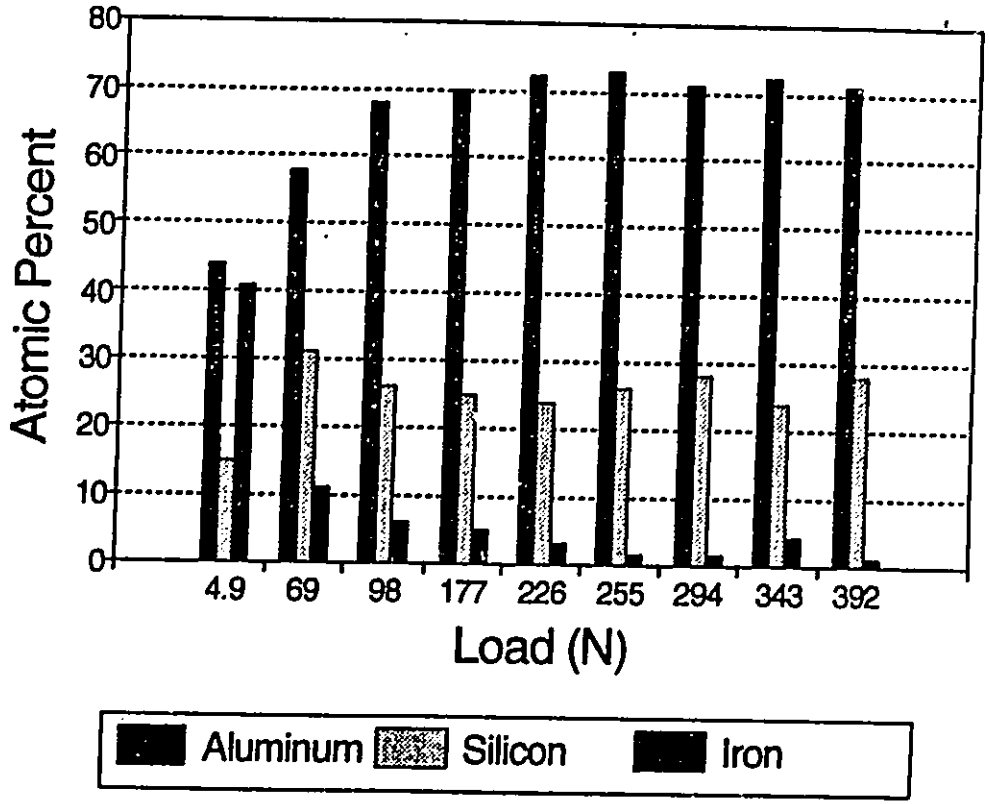

Figure 5.23 b: Composition of the worn surface as a function of load for the A356-10%Gr-20%SiC composite

disposal. Auger electron spectroscopy was used to identify the presence of graphite on the worn surface. A typical AES survey is displayed in Figure 5.24. Carbon atoms were found on all samples examined. The ratios of iron:oxygen:carbon are displayed in Table 5.3. Since carbon, most likely graphite, was found on the worn surface, the possibility of solid lubrication existed at all loads.

5.7: Characterization of the Subsurface Microstructure

Examination of polished cross sections revealed the extent of damage as depth below the worn surface increased. This damage may be as simple as strain deformed grains or be as severe as subsurface cracks and particle fracture. The subsurface damage is an indication of the wear mechanism operating at that load.

At low loads (4.9 N) the worn surface was covered with iron containing species. Inspection of the subsurface (Figure 5.25) reveals that the SiC particles have remained intact. Fracture of the particles has not occurred indicating that the particles maintain their reinforcing capability. In fact, subsurface strain appears to be limited to the very near surface.

With increasing load the composition of the worn surface decreased in iron

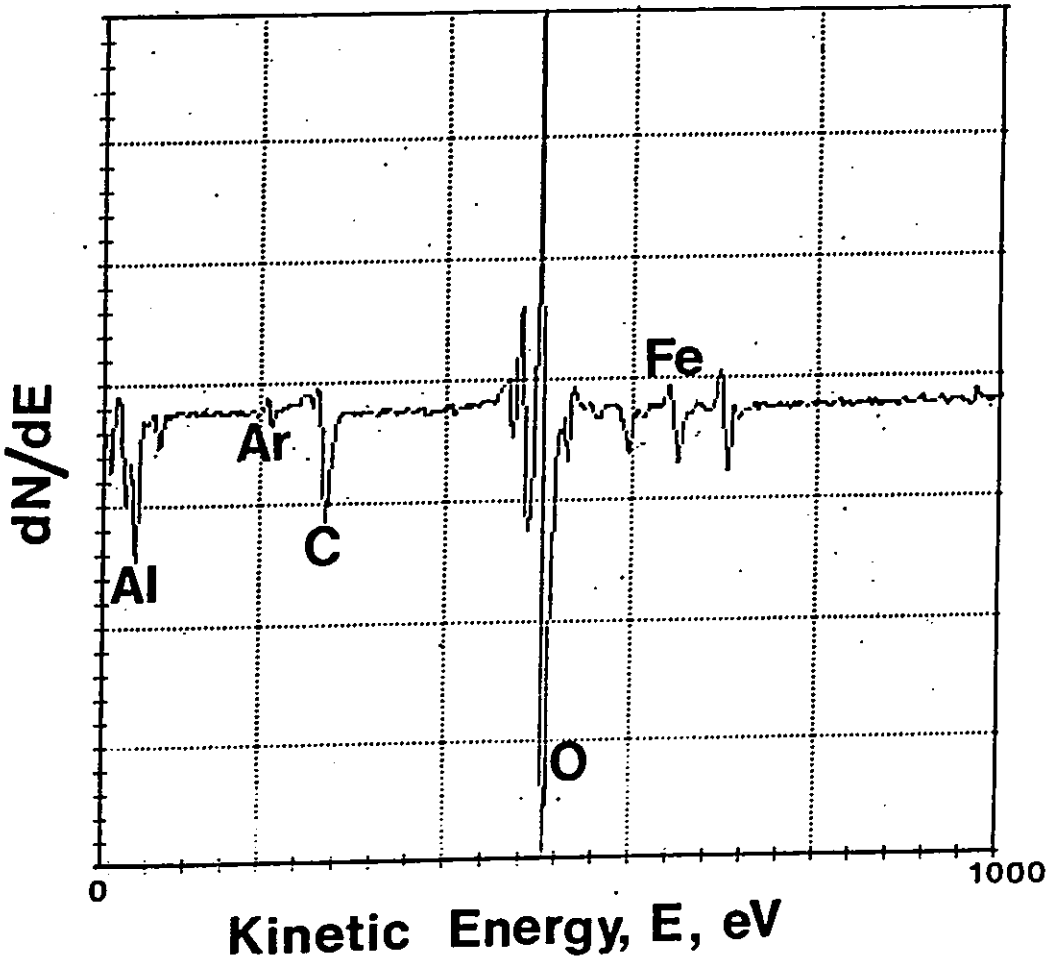

Figure 5.24: AES survey of the worn surface of an A356-10%Gr-20%SiC composite worn at a load of 10 N

Table 5.3: AES results indicating the presence of carbon on the worn surface.

Load	C	Fe	O
9.8 N	7.8	33.4	58.7
137 N	11.0	30.5	58.5
441 N	12.1	29.5	58.2

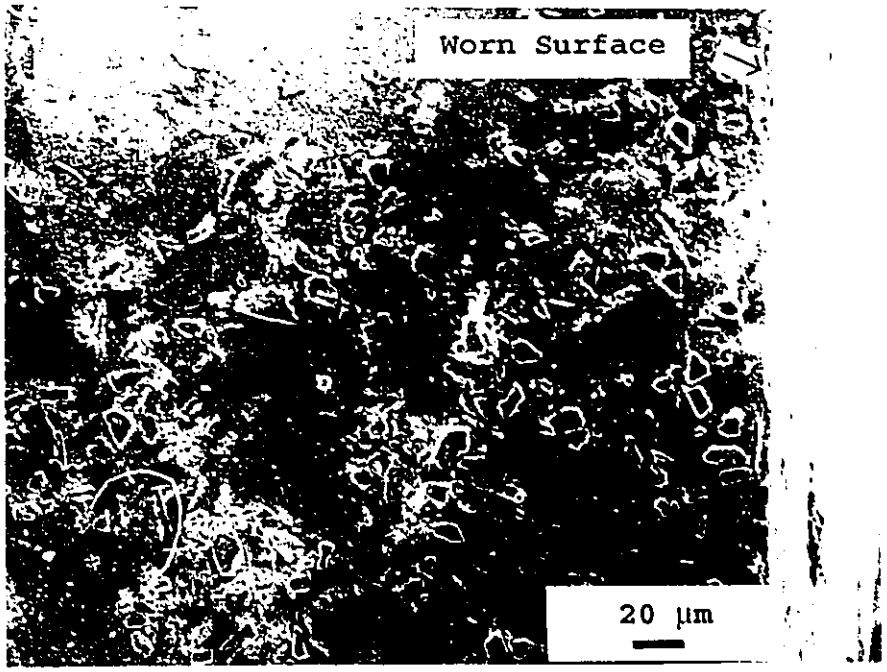

Figure 5.25: Section of a sample, with 10% graphite, tested at 4.9 N (sliding direction top to bottom)

content. Examination of the subsurface indicated that a tribolayer had formed on the worn surface (Figure 5.26). This tribolayer was approximately 10 μm thick at a load of 49 N and appeared to consist of intimately mixed materials (Figure 5.27). The SiC particles below this layer were not fractured. In actuality, the grains below the tribolayer appear to remain equiaxed indicating that the damage in the subsurface is limited to the tribolayer.

Tribolayers continued to form as the load increased (Figure 5.28). The thickness of the tribolayers was observed to increase with increasing load; sometimes exceeding 30 μm. The tribolayer was determined to consist of broken silicon and SiC particles mixed with aluminum and iron containing compounds (Figure 5.29). Strain in the subsurface was not sufficient to cause fracture of the SiC particles below the tribolayer, however, sublayer damage was realized. Cracks appeared to form at discontinuities such as SiC particle clusters (Figure 5.30) and porosity (Figure 5.31). This crack propagation may have increased the wear rate to a degree dependant on the ease of crack formation and propagation.

5.8: Examination of the Debris

The morphology and composition of the debris provided evidence for wear mechanism determination. At low loads the debris was particulate. At higher loads both the morphology and the composition of the debris changed depending on the

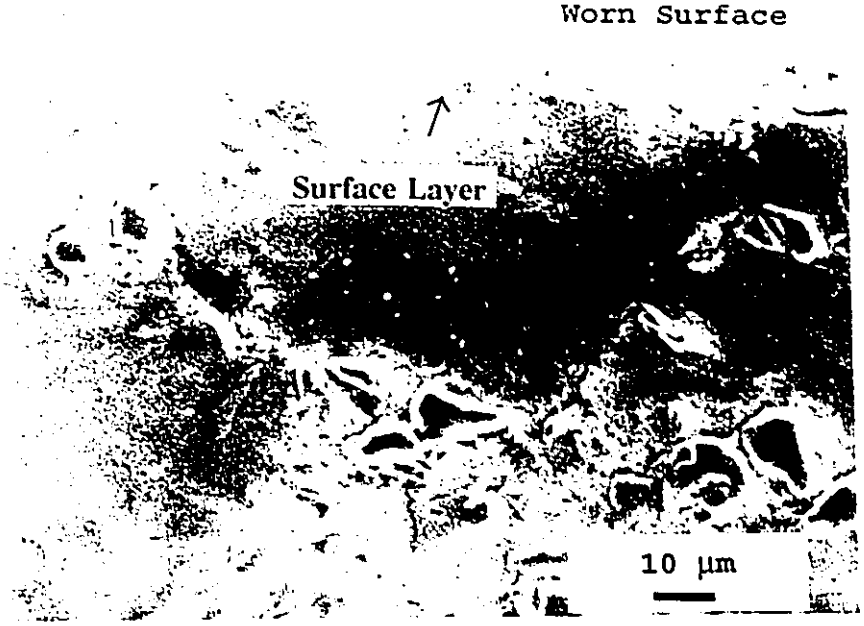

Figure 5.26: Section of a sample with 3% graphite tested at 49 N (sliding left to right)

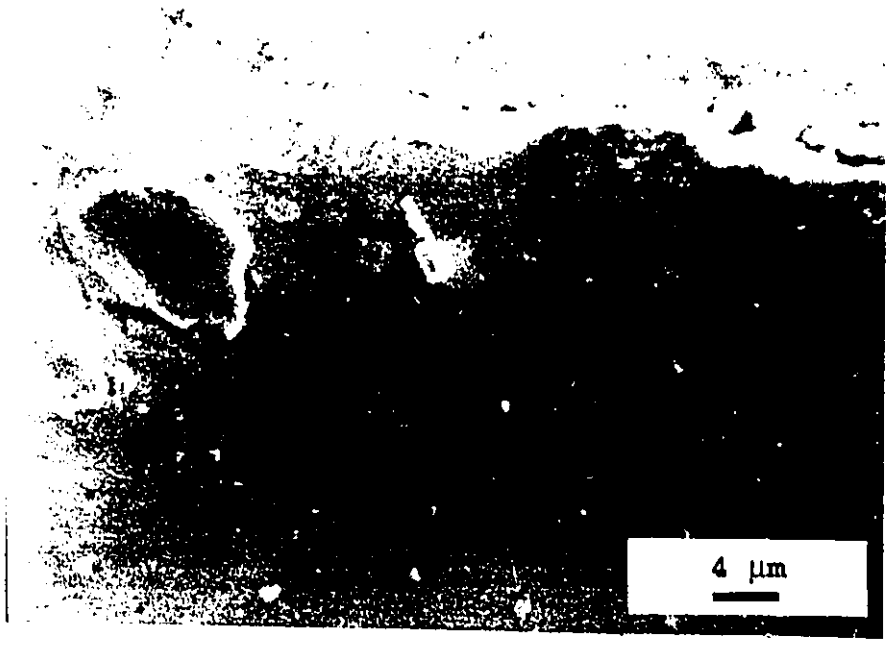

Figure 5.27: Section of a sample with 3% graphite tested at 49 N (sliding left to right)

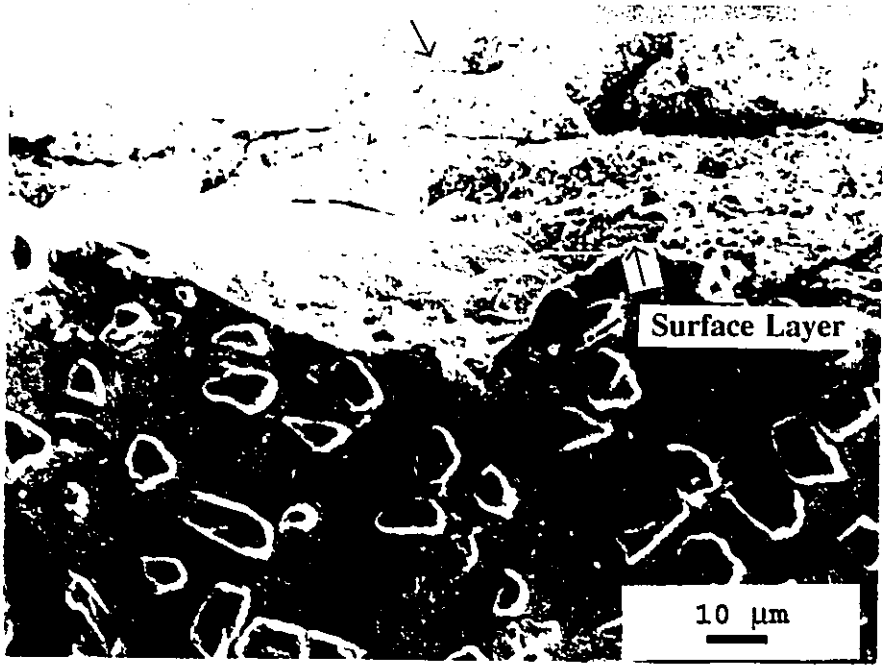

Figure 5.28: Surface layers on an A356-3%Gr-20%SiC sample tested at 343 N (sliding left to right)

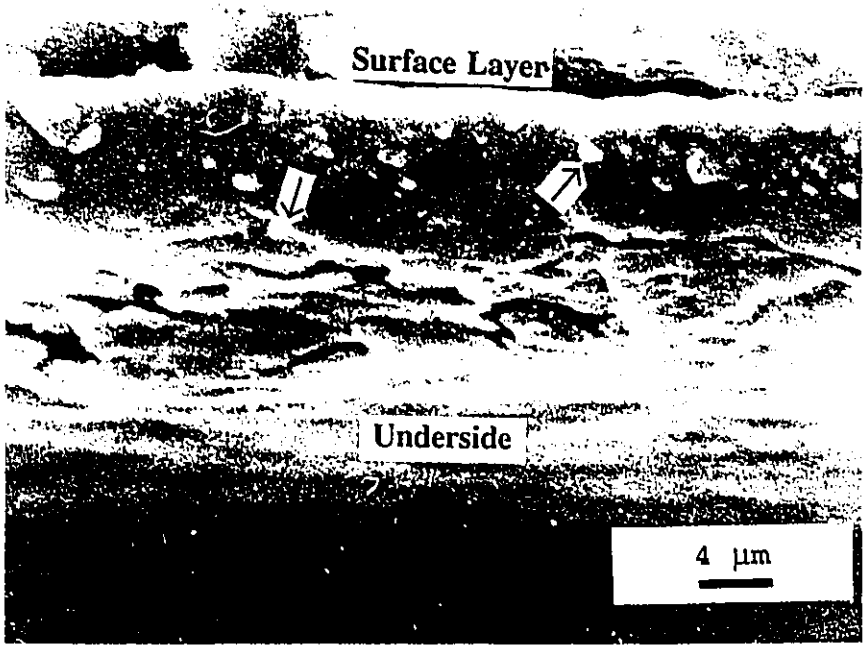

Figure 5.29: Fractured SiC particles in the surface layer

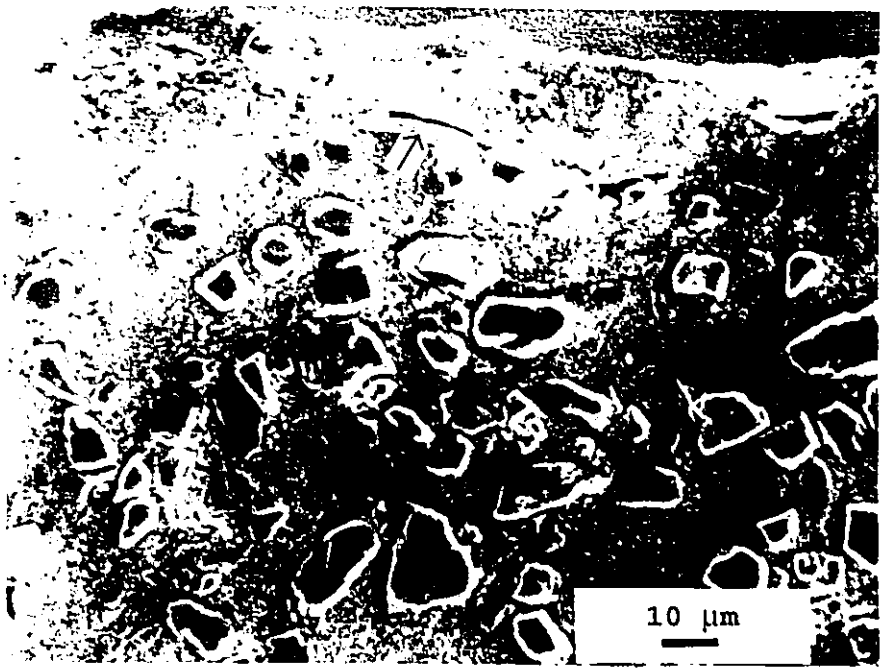

Figure 5.30: Crack growing from a particle cluster

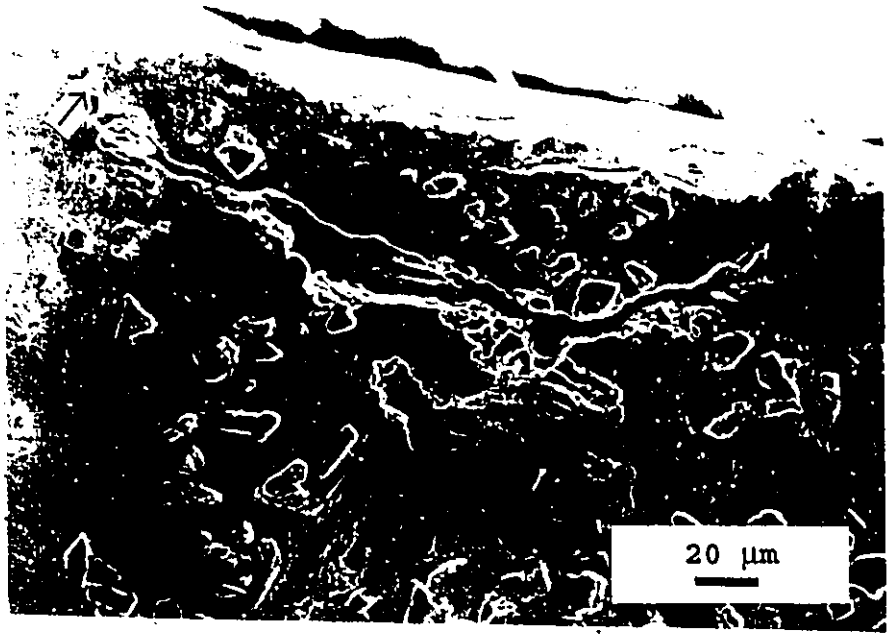

Figure 5.31: Porosity perpetuating a subsurface crack

applied load and the graphite content.

Particulate debris was observed on the worn surface at low loads. X-ray Diffraction (XRD) studies indicated that the debris consisted of native iron and aluminum with silicon, SiC and the possibility of amorphous or non-stoichiometric oxide compounds (Figure 5.32). When heat treated A356-3%Gr-20%SiC samples were tested at low loads the debris appeared reddish brown and likely contained Fe_2O_3 similar to a SiC composite without graphite [73,74].

At intermediate loads (50 N to 110 N) the XRD pattern (Figure 5.33) denoted aluminum and iron, silicon and SiC similar to the pattern at lower loads. Macroscopically the debris was a black powder. This observation indicated that the debris did not change greatly between low and intermediate loads.

At extreme loads the composition of the debris, generated from composites with 10% graphite, continued to be made up of aluminum, iron, silicon and SiC (Figure 5.34). However, the A356-3%Gr-20%SiC composite generated debris with a large concentration of iron oxides (Figure 5.35). This agrees with the observation that the counterface experienced severe oxidation at high loads. The oxide product was worn from the surface of the steel ring, deposited on the sample surface and released into the debris.

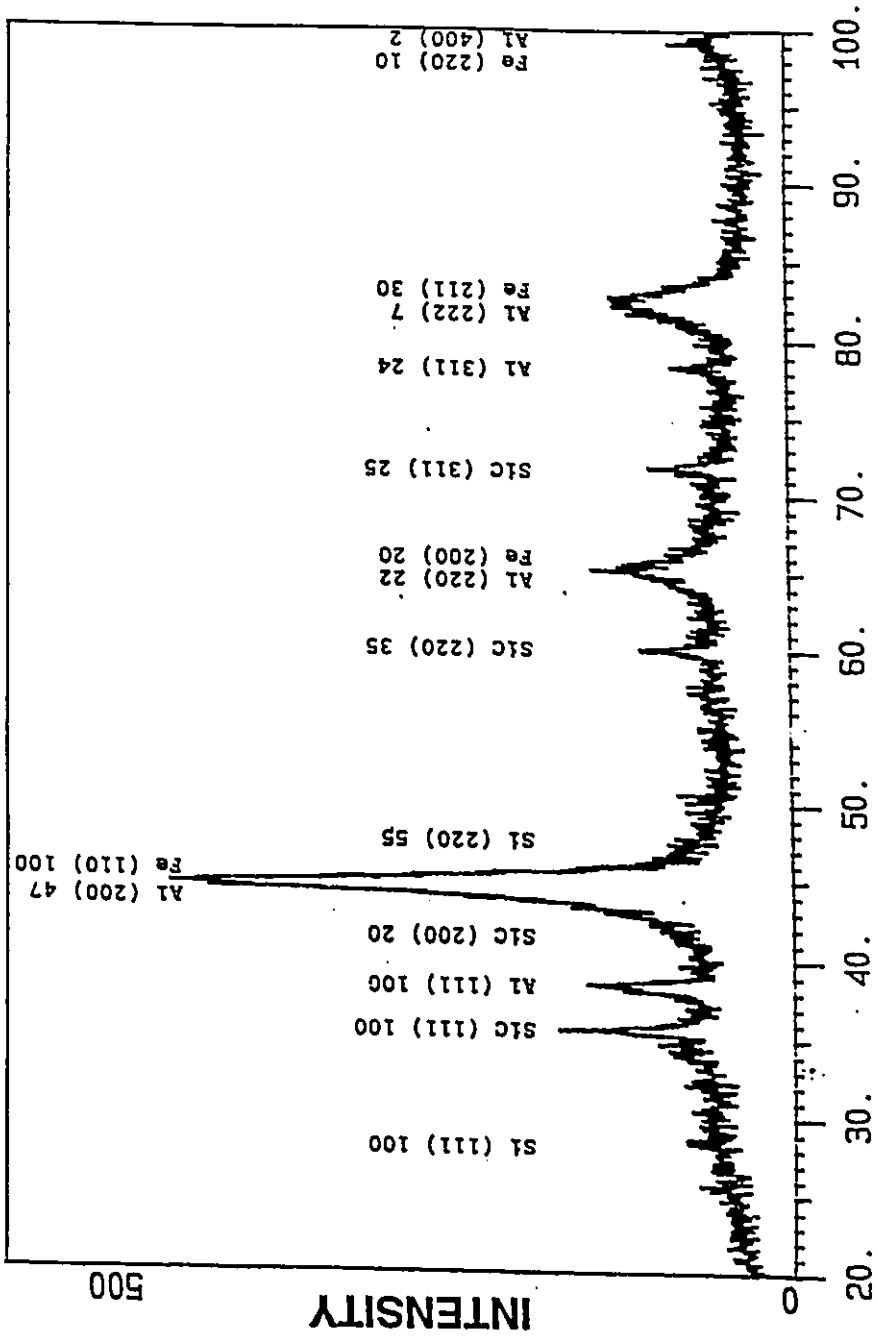

Figure 5.32: XRD of the debris from a test at 10 N

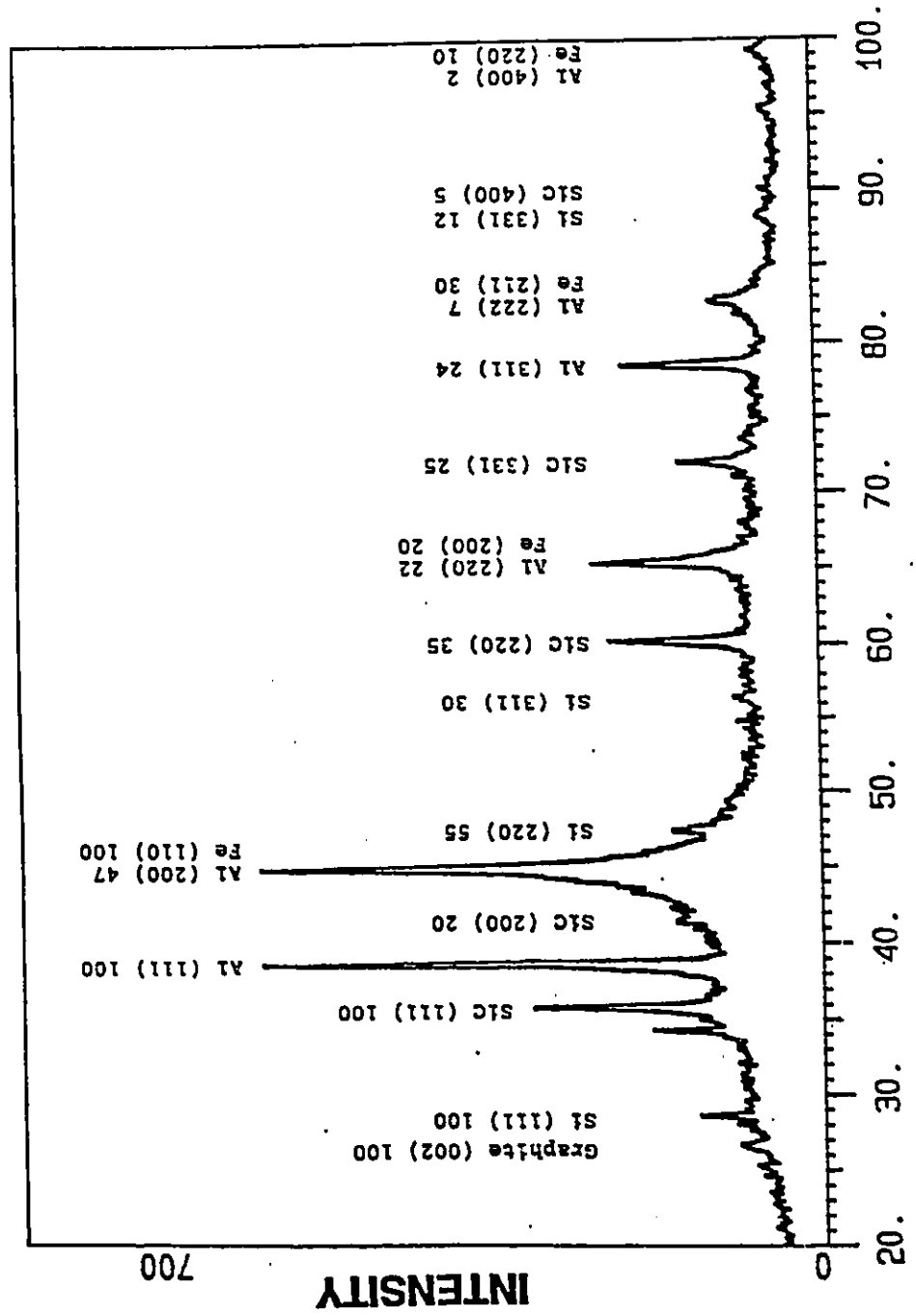

Figure 5.33: XRD of the debris from tests at intermediate loads

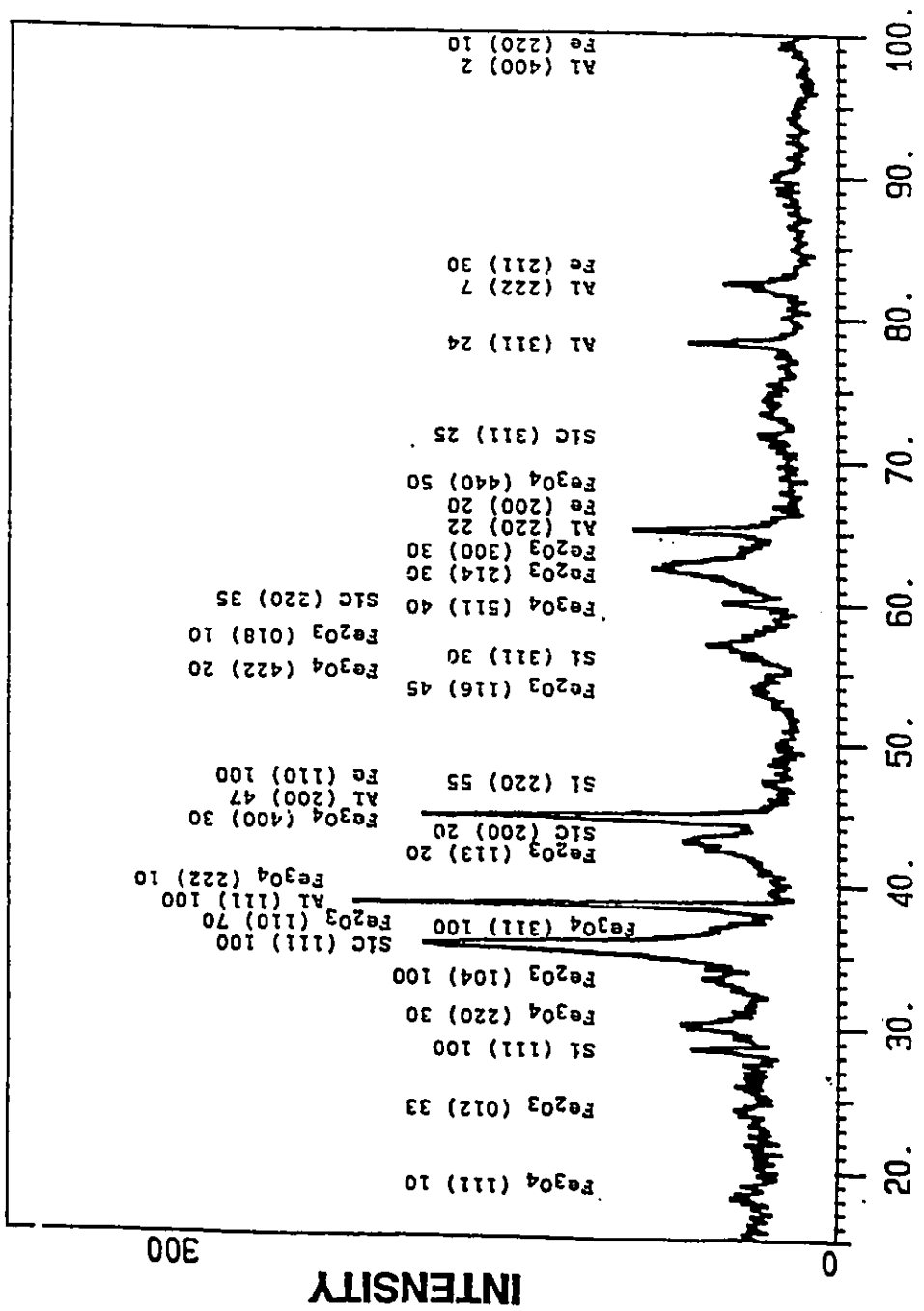

Figure 5.34: XRD of the debris generated from an A356-10%Gr-20%SiC composite at a load of 441 N

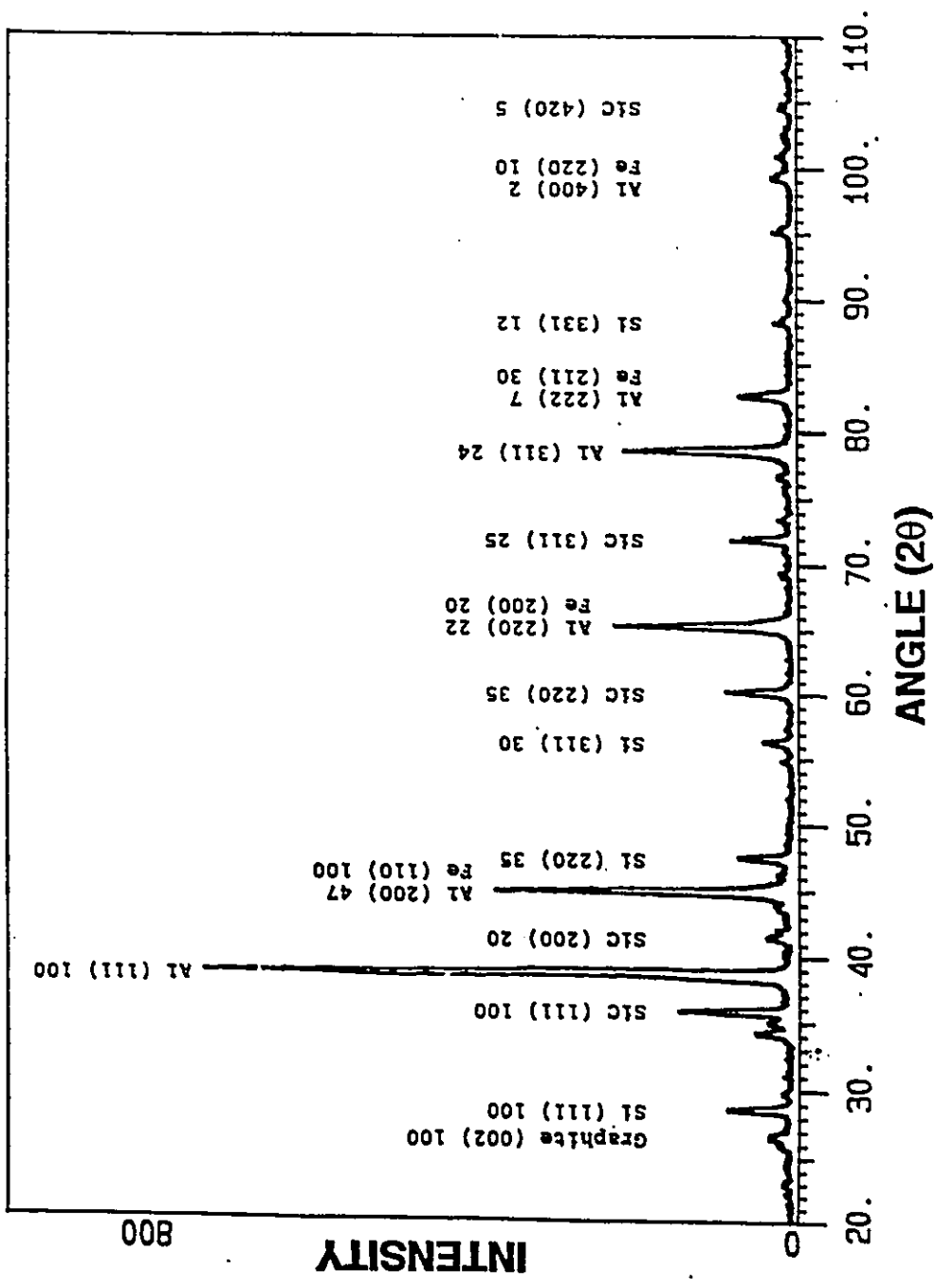

Figure 5.35: XRD of the debris generated from an A356-3%Gr-20%SiC composite at a load of 441 N

The morphology of the debris also changed at high loads. Plates of compacted material were observed amongst smaller particulate debris (Figure 5.36). This suggested that regions of the tribolayer spalled off leaving a depression on the worn surface.

5.9: Summary of Observations

The A356-Gr-SiC composites did not show the characteristics of severe wear. A tribolayer was formed on the worn surface of the samples whose composition changed as load increased and was shown to consist of an intimate mixture of materials from the sample and the counterface. At extreme loads the concentration of graphite in the sample dramatically affected the composition of the surface with lower graphite content leading to more abrasive wear of the counterface and greater iron content on the sample's worn surface.

At intermediate loads the A356-3%Gr-20%SiC composite demonstrated wear rates 1 to 3 times lower than the composite with 10% graphite. At higher loads the wear rates of either composite were similar. The A356-10%Gr-20%SiC composite demonstrated slightly lower wear rates at a low load of 9.81 N.

An increase in sliding speed from 0.1 m/s to 1 m/s, at 10 N load, increased the wear rate. A solutionizing and peak aging treatment (Section 3.3) did not influence

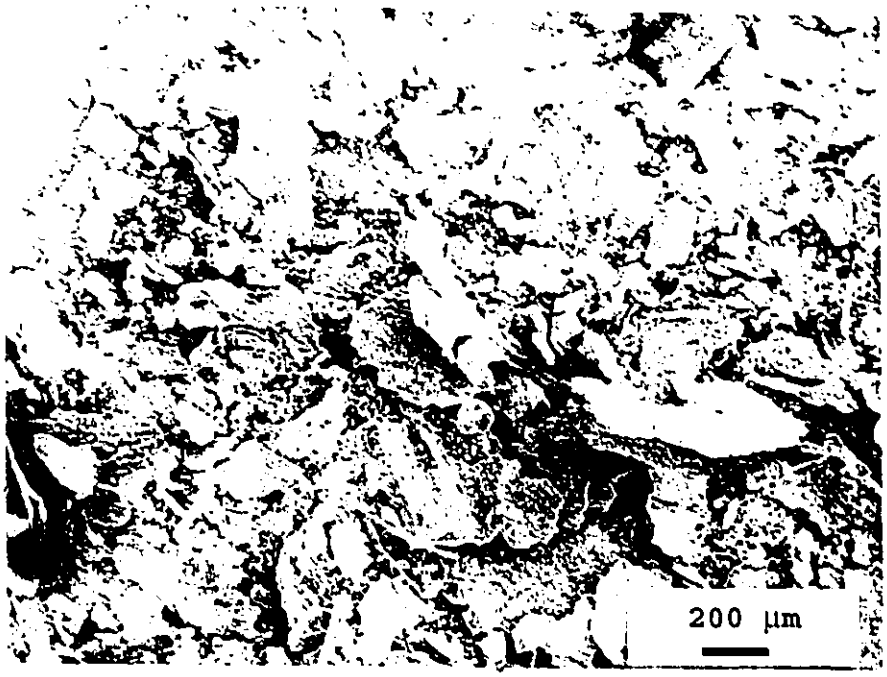

Figure 5.36: Debris from an A356-3%G-20%SiC composite sample slid at a load of 343 N

the wear rate, at low loads, with the exception of the 3% graphite composite. The A356-3%Gr-20%SiC heat treated composite often increased in weight when tested at a load of 9.81 N and a speed of 0.1 m/s.

Part B: Discussion

5.10: Wear Mechanisms

Examination of the worn surface and the debris indicated that material transfer is important at low loads. Iron and iron oxides were transferred due to the abrasive action of the SiC particles. The hard ceramic particles machined the counterface releasing iron from the steel surface. Some of the transferred iron was oxidized resulting in a layer of lubricating iron oxides on the worn surface which reduced the damage to the underlying material. The 10% graphite composite demonstrated marginally lower wear rates at low loads due to the higher concentration of graphite in the surface which also reduced the surface and subsurface damage.

The subsurface SiC particles did not fracture indicating that they were able to act as load bearing elements and support the load reducing or preventing intimate contact between the aluminum matrix and the steel counterface.

As the load increased the tribolayer incorporated more aluminum from the composites. The sublayer SiC particles were intact which suggests that the subsurface damage was reduced with respect to the unreinforced alloy. This was likely due to the lubricating properties of the graphite which reduced the subsurface stress resulting in a decrease in strain induced damage.

The capability of the material to cope with the applied stress is important. Since graphite is a soft material, addition of graphite to a metal matrix frequently reduces the mechanical properties. Inclusion of 10% graphite resulted in a greater deterioration of the strength and ductility than the addition of only 3% graphite. Since the A356-10%Gr-20%SiC composites demonstrated higher wear rates at intermediate loads it is reasonable to conclude that the poor mechanical properties of the bulk material decreased the efficiency of the lubricating layer. This effect was likely amplified since iron oxides were not prevalent on the worn surface at intermediate loads. Therefore the variation of the wear rate with graphite content was due to the degradation of the mechanical properties induced by the addition of the soft graphite.

Wear occurred through the spalling of the surface layer. Flake type debris was observed as well as delaminating layers on the worn surface. The tribolayer was then regenerated with material from the sample resulting in a progressive loss of material from the sample surface. Subsurface damage processes, such as cracking,

may have increased the wear rate.

5.11: Prevention of Severe Wear

At extreme loads, high wear rates and the characteristics of severe wear were not observed. The addition of graphite reduced subsurface damage allowing mild type wear to occur at high loads. However, two very different behaviours were observed depending on the graphite content.

In the case of the 10% graphite composite the graphite concentration in the tribolayer was sufficient to prevent the severe damage and adhesion characteristic of severe wear. In the composites with only 3% graphite, lubrication by graphite allowed the composite to display mild wear at high loads. However, the lower concentration of graphite was not as effective at decreasing the coefficient of friction. This resulted in greater surface temperatures. Rapid counterface oxidation took place at this elevated temperature. The oxidation of iron follows an exponential relationship with temperature [17]:

$$\Delta m^2 = A_p t \exp(-Q/RT) \qquad (5.10.1)$$

where Δm is the oxygen uptake of the metal surface per unit area, A_p is the parabolic rate constant, t is time, Q is the activation energy, T is the absolute temperature and R is the universal gas constant. Due to the exponential relation, a small increase in temperature results in a significant increase in the oxidation rate.

The iron oxides were transferred to the sample surface and incorporated into the tribolayer. Since iron oxides have been shown to possess lubricating tendencies [123] the oxidation of the steel ring supplied additional lubricant for the composite. The incorporation of the iron oxides increased the hardness of the tribolayer from 175 ± 65 VHN (A356-10%Gr-20%SiC composite with no oxidation) to 800 ± 200 VHN when counterface oxidation occurred. The combined effects of improved lubrication and higher hardness allowed mild wear to continue to higher loads.

In the unreinforced alloy and a composite consisting of SiC alone, the onset of severe wear occurs at a specific transition temperature. This temperature is 418 K and 435 K respectively [80,81]. Since the heat generated is proportional to the velocity (v), load (P) and coefficient of friction (ie. $q=\mu \cdot v \cdot P$) a decrease in any of these factors will reduce the surface temperature. An expression for the surface temperature of the composite is:

$$T_i = \mu \cdot a \frac{P \cdot v \cdot \Delta x}{K \cdot A} + T_s \qquad (5.10.2)$$

where T_i is the interface temperature, T_s is the sink temperature a distance Δx away, a is the heat distribution coefficient and is equal to 0.5 during steady state [124], v is the velocity, P is the load, K is the thermal conductivity and A is the area of contact. Therefore, due to the lower coefficient of friction, a higher load or velocity is required in order to achieve any arbitrary surface temperature in the graphite

containing composites. Since the transition to severe wear is believed to occur at a specific transition temperature the reduction in the coefficient of friction would necessitated more severe loading conditions to reach the transition temperature. Hence, the onset of severe wear is pushed to higher loads.

The lubricating ability of the tribolayers not only increased the load required to reach the transition temperature but increased the transition temperature also. The A356-3%Gr-20%SiC composite reached a surface temperature of 494 K at a load of 345 N without experiencing severe wear even though the transition temperature for the composite with 0% graphite was exceeded by 59 K. Therefore the addition of graphite particles to a composite with 20% SiC particles increased the transition temperature and the transition load effectively preventing severe wear from occurring in this investigation.

5.12: Comparison With the Unreinforced Alloy and a Composite With SiC Reinforcement Only.

Figure 5.37 contrasts the wear rates of the A356-Gr-SiC composites, the unreinforced alloy and an A356-20%SiC composite without graphite. The unreinforced material demonstrated two wear regimes, mild and severe, while the SiC composite displayed a third region at low loads.

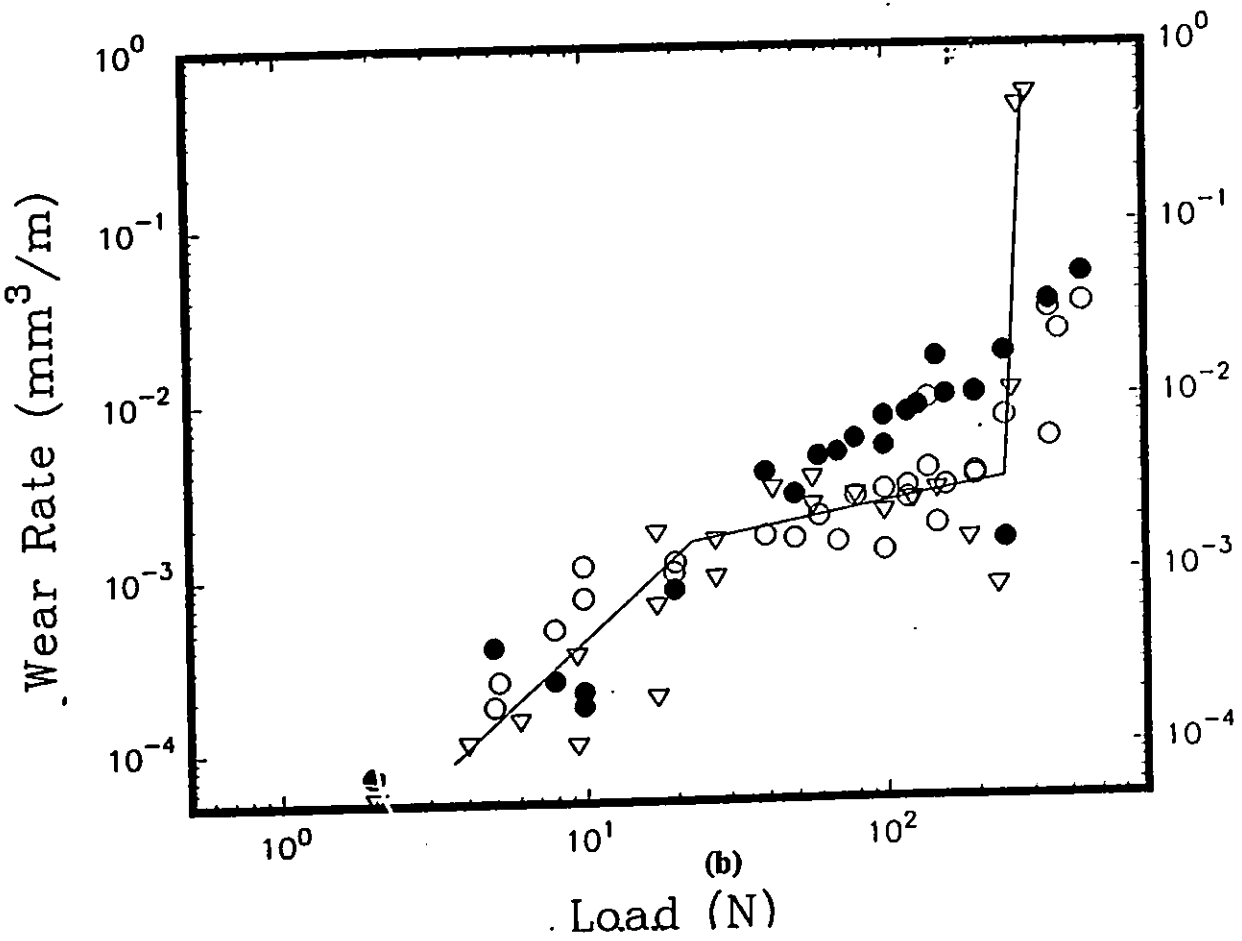

Figure 5.37: Wear rate comparison of the a) unreinforced alloy (▽) and b) A356-20% SiC (▽) and the hybrid composites with (○) 3% graphite and (•) 10% graphite

At loads less than 10 N the composites demonstrated wear rates up to ten times lower (2×10^{-4} mm^3/m at 8 N) than the unreinforced alloy (1.2×10^{-3} mm^3/m at 8 N). This was due to the load supporting effect granted by the hard SiC particles. These particles reduced contact between the steel counterface and the matrix. A lubricating film formed on these composites consisting of iron oxides (A356-20%SiC) and, graphite and iron oxides (A356-Gr-SiC composites) which further improved the wear properties.

In the load range 10 to 80 N, the A356-3%Gr-20%SiC composite had a marginally lower wear rate (1.5×10^{-3} mm^3/m at 70 N) with respect to the unreinforced alloy (2.9×10^{-3} mm^3/m at 70 N). The SiC composite, without graphite, demonstrated wear rates comparable to the 3% graphite composite. However, 10% graphite addition increased the wear rate two to three times (6×10^{-3} mm^3/m at 70 N).

Severe wear materialized at loads of 80 N and 245 N, for the A356 alloy and the SiC reinforced composite respectively, and was followed by seizure. Severe wear was not observed in the graphite containing materials. This represented a substantial improvement in the tribological properties at high loads.

5.13: Comparison of the A356-Gr-SiC Composites With the A356-CF Composites

The wear rate data for the A356-Gr-SiC composites is compared with that of the A356-CF composites in Figure 5.38. All of the composites demonstrated mild wear at low loads. The hybrid composite with 10% graphite demonstrated wear rates 2 to 3 times lower than any of the other composites. At intermediate loads the 10% graphite composite wore at rates nearly five times greater than the A356-CF composites. At high loads, greater than 250 N, the A356-Gr-SiC composites demonstrated superior wear rates compared to the A356-CF composites. The hybrid composites were able to sustain the higher loads with little damage compared to the A356-CF composites which displayed severe wear.

In summary it would appear that the loading conditions are paramount. At extremely low loads the graphite and SiC combine to give effective lubrication and reinforcement resulting in low wear. As the load increases the delamination wear mechanism is believed to become dominant. The A356-Gr-SiC composites must have poor resistance to this mechanism; possibly due to the increased number of sights for crack nucleation and easier crack propagation. The A356-CF composites were less susceptible to this type of damage which led to lower wear rates. At extremely high loads, the A356-Gr-SiC composites were superior due to the absence of severe wear. Severe wear was observed in the A356-CF composites giving very high wear rates.

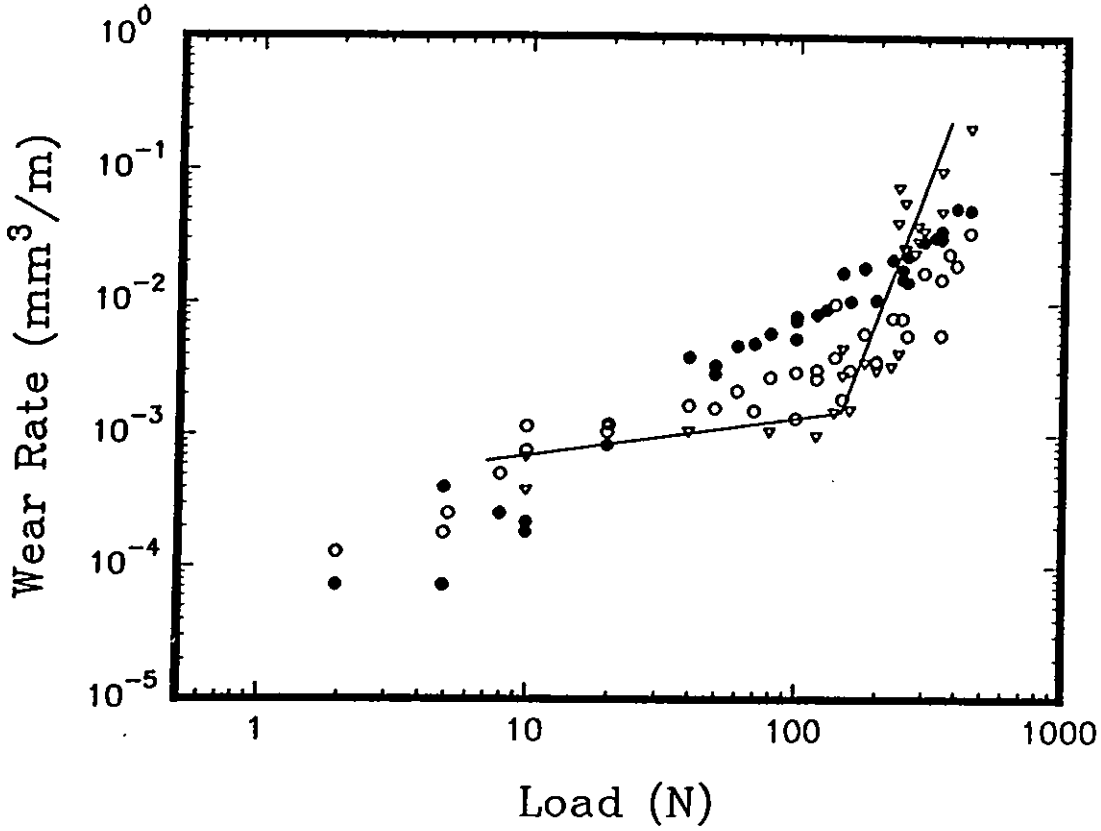

Figure 5.38: Wear Rate Comparison of the A356-3%Gr-20%SiC (∘) and A356-10%Gr-20%SiC (•) composites with the A356-CF (▽) composites with normal fibres

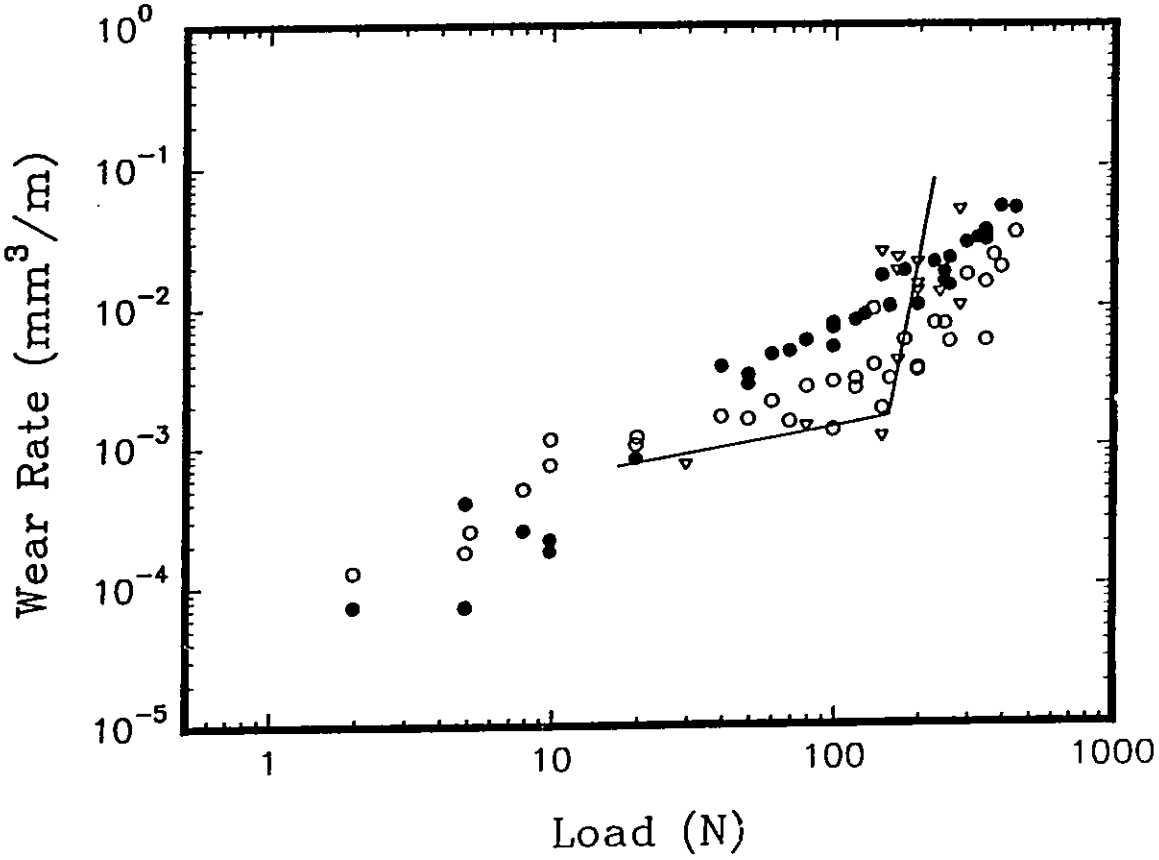

Figure 5.39: Wear Rate Comparison of the A356-3%Gr-20%SiC (○) and A356-10%Gr-20%SiC (●) composites with the A356-CF (▽) composites with parallel fibres

5.14: Comparison with Other Al Based MMCs

Figure 5.40 compares the wear rates of the A356-Gr-SiC composites with other metal matrix composites with hard ceramic reinforcement. All of the data, taken from the literature, was obtained using pin on disk type testing machines. Each investigation used a different composite with differing matrices. The sliding velocities varied from 0.5 m/s to 2.68 m/s and the sliding distances from 300 m to 500 m. Therefore, due to the differences in testing conditions and the material an absolute comparison is not valid, however, insight may be obtained from the figure.

At intermediate loads the A356-Gr-SiC composites demonstrated wear rates similar to the other composites. However, each of these composites demonstrated a transition to severe wear and/or seizure. The hybrid composites were able to sustain much higher loads with relatively low wear rates. This indicates that the useful range at which these materials may be used has been extended.

Alternative strategies for tribological component materials include the addition of graphite alone. Figure 5.41 compares the wear rates of the A356-Gr-SiC composites with composites containing 2 or 3 wt% graphite in an aluminum based matrix. Again the reader must be cautioned to regard this comparison with discretion. The composites with graphite alone appear to have somewhat superior wear properties at low to intermediate loads. However these materials have been

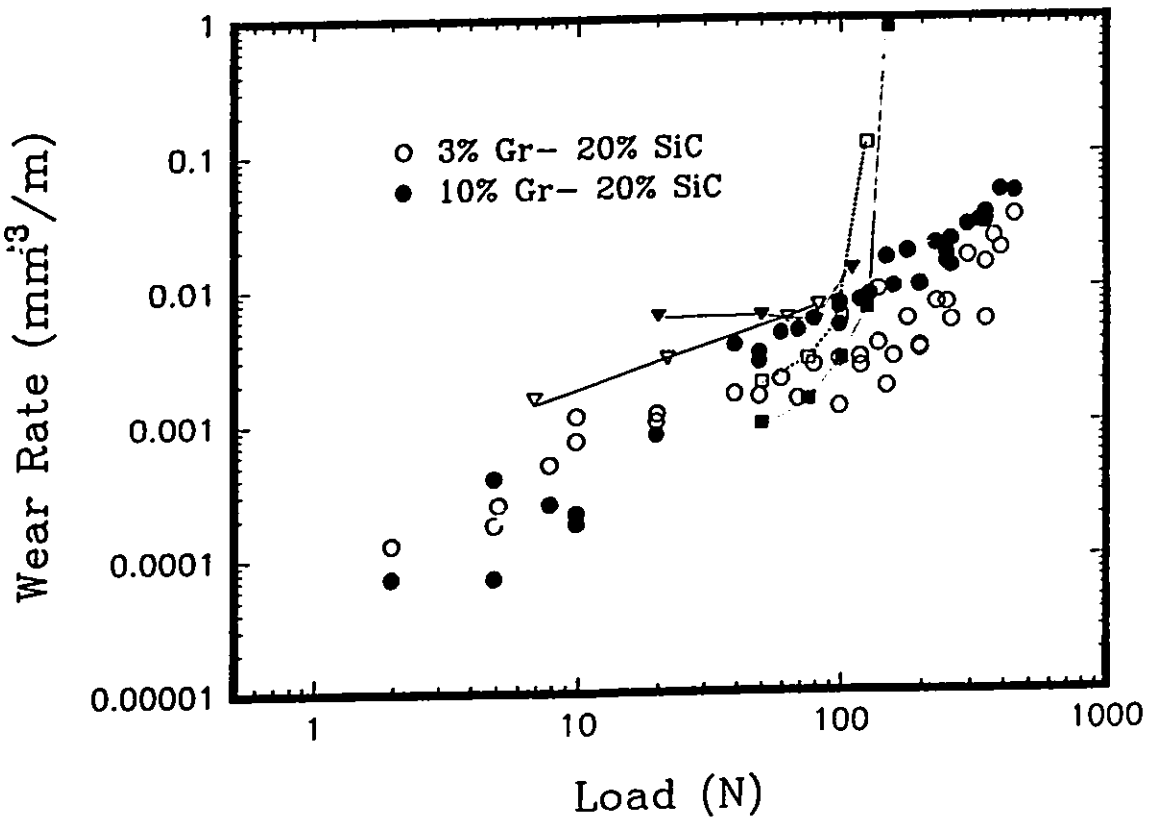

Figure 5.40: Wear rate comparison of composites with hard particle reinforcement, (▾) 6061-20% SiC_w, 1.5 m/s, 300 m, against WC-8%Co [98]; (▿) A356-15% SiC_p, 0.5 m/s, 450 m, against steel [85]; (■) Al-4.5Cu-0.12Fe-SiC_p, 0.5 m/s, 500 m, 2.68 m/s [82]; (□) Al-4.5Cu-0.12Fe-SiC_w, 2.68 m/s, 500 m [82] and the hybrid composites

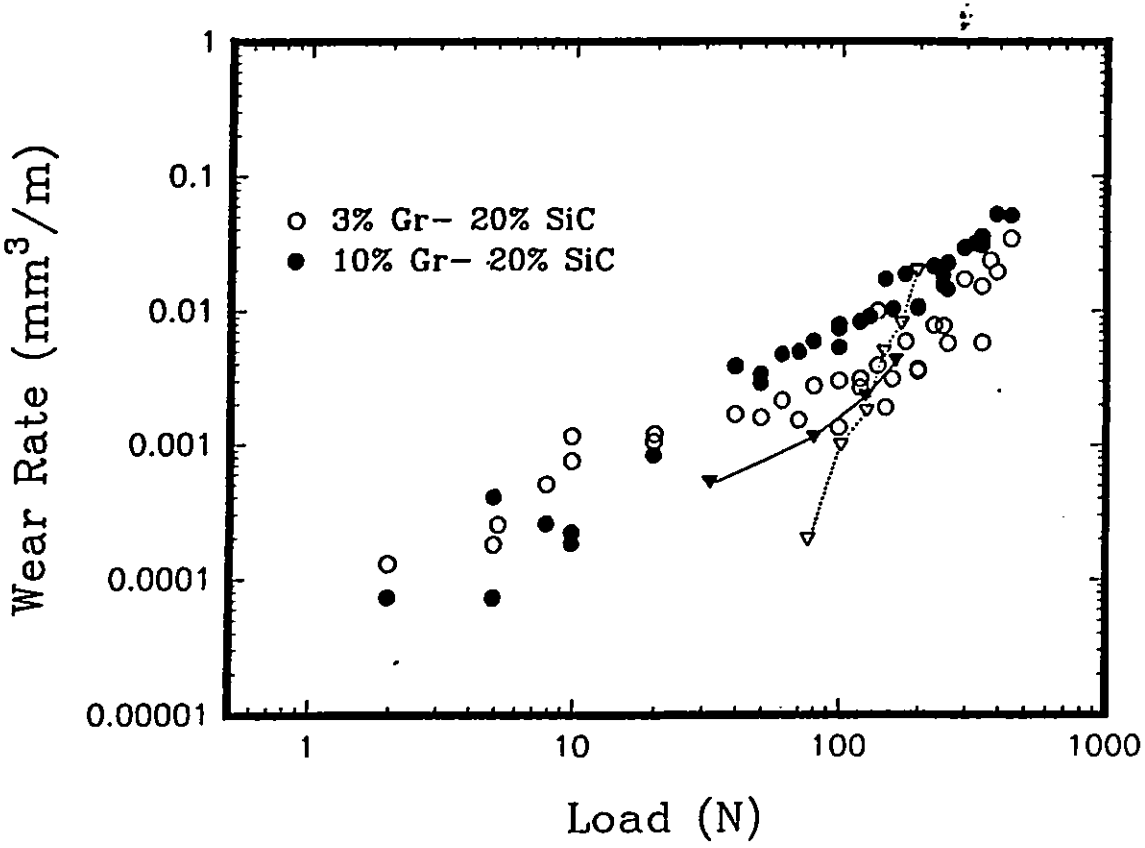

Figure 5.41: Wear rate comparison of MMCs with graphite particle lubrication; (▽) Al-4.5Cu-0.12Fe-3% Gr, 2.68 m/s, 500 m, against steel [122]; (▾) Al-12% Si-2% Gr, 1 m/s, 1800 m, against steel [117]

observed to seize [98] indicating that the A356-Gr-SiC composites possess superior wear properties at extreme loads.

From this discussion it may be concluded that the concept of hybrid reinforcement of aluminum alloys is technologically important and deserves more investigation. The tribological behaviour is just beginning to be investigated. Even though it would appear that composites containing graphite alone may have superior wear resistance, the beneficial effect of hard particle reinforcement on the mechanical properties of the hybrid composite may prove substantial. Therefore, further research in to hybrid composites may yield a material with the appropriate tribological and mechanical properties.

Chapter 6: Conclusions and Future Work

6.1: Conclusions

The main conclusions which may be drawn from this work are:

1) The A356-CF composites demonstrated superior wear resistance with respect to the unreinforced material over the entire load range tested. Both of the carbon fibre composites demonstrated two wear regimes identified by a change in debris morphology. Mild wear was observed at low loads while, at higher loads, severe wear followed by seizure was witnessed. The load at which the transition occurred varied from 150 to 200 N. The unreinforced alloy displayed a transition to severe wear at 80 N.

2) Mild wear was characterized by low wear rates, surface grooves, plastic deformation and particulate and flake type debris. The subsurface carbon fibres remained largely intact reinforcing the matrix. The nickel aluminide intermetallic was, likely, responsible for significantly increasing the load carrying capability.

3) Evidence of abrasive wear of the sample and counterface was observed during mild wear. Subsurface crack nucleation and growth likely occurred resulting in the removal of a flake of surface material. The reinforcing effects of the carbon fibres

and intermetallic additions were more substantial than the proposed increase in subsurface crack nucleation.

4) Evidence of solid lubrication was not found. The carbon fibres were found to be fracture on the wear surface with fibre fragments in the debris. This showed that the fibres were not smeared on to the worn surface forming a lubricating film.

5) Severe wear rates were improved due to particle hardening of the surface by broken silicon particles. The transition to severe wear occurred in the load range of 150 to 200 N in the case of the A356-CF composites. The composite with normally orientated fibres may have been more effective at delaying the transition to severe wear to a higher load.

6) The A356-Gr-SiC composites exhibited a linear increase in the wear rate with increasing load. No evidence of seizure was observed over the entire load range tested.

7) The hybrid composites display superior wear resistance compared to the unreinforced alloy at loads below 10 N. At intermediate loads graphite addition resulted in a decrease , up to three times, in wear resistance compared to the unreinforced alloy and an A356-20%SiC composite without graphite. The wear rate of the composite with 10% graphite was one to two times higher than the composite

with only 3% graphite. However, graphite addition decreased the counterface wear.

8) An increase in velocity from 0.1 m/s to 1 m/s increased the wear of the hybrid composites four times at a load of 9.81 N. A solutionizing and peak aging treatment increased to the abrasiveness of the composites but, in general, did not significantly affect the wear rates at speeds greater than 0.1 m/s.

9) At high loads graphite addition decreased the frictional heating at the contact surfaces. Tribolayers that consisted of carbon, iron oxides, aluminum and other matrix materials were formed on the surfaces of the A356-Gr-SiC composites. The lower contact temperatures and the formation of protective layers increased the critical temperature required for the transition to severe wear.

10) In comparing the A356-CF composites and the A356-Gr-SiC composites it may be concluded that at intermediate loads, where subsurface crack nucleation and growth may dominate, reinforcement with carbon fibres resulted in superior wear resistance. At either low or high loads the hybrid composites displayed greater wear resistance.

6.2: Suggestions for Future Work

The author would suggest that there are two main areas where further study should take place. Firstly, the wear behaviour of the hybrid composites at very low loads should be examined in more detail. The lubricating effect of the graphite and the reinforcing effect of the SiC may be best in this range. Secondly, an investigation in to the subsurface crack nucleation and growth process in the nickel coated carbon fibre composites would be of interests. This type of composite appears to offer a greater resistance to this form of wear than any of the other materials tested.

REFERENCES

1 Ford, T.; New Materials; Aircraft Engineering, March 1992, pgs 2-3

2 Peel, C.J.; B2a-K Metal Matrix Composites for Aerospace Applications; Euromat '91, 1992, pgs 41-51

3 Ford, T.; Advanced Aerospace Composites; Aircraft Engineering, Sept 1991, pgs 23-25

4 Prasad, S.V., P.K. Rohatgi; Tribological Properties of Al Alloy Particle Composites; JOM, 1987, pgs 22-26

5 Lee, C.S., Y.H. Kim, K.S. Han, T. Lim; Wear Behaviour of Aluminum Matrix Composite Materials; Journal of Materials Science, 27, Feb. 1, 1992, pgs 793-800

6 Lampman, S.R.; Tuning Up the Metals in Auto Engines; Advanced Materials and Processes, May 1991, pgs 17-20

7 Chowdiah, M.P., K. Nagesha Rao, S. Ranganath; Wear Mechanisms of Spheroidal Graphite Irons; Proceedings of the IX National Conference on Industrial Tribology, 1991, pgs M125-M137

8 Eyre, T.S.; Friction and Wear of Cast Irons; in ASM Handbook, vol. 18, Friction, Lubrication and Wear Technology, 1992, pgs 695-701

9 Krishnan, B.P., N. Ranan, K. Narayanaswamy, P.K. Rohatgi; Performance of an Al-Si-Graphite Particles Composite Piston in a Diesel Engine; Wear, 60, 1980, pgs 205-215

10 Ebisawa, M., T. Hara, T. Hayashi, H. Ushio; Production Process of Metal Matrix Composite (MMC) Engine Block; Presented at SAE International Conference and Exposition, Detroit, MI, 1991, SAE Technical Paper 910835

11 Yust, C.S.; Tribology and Wear; International Metal Reviews, 1985, vol 30, No 3, pgs 141-154

12 ASME Research Committee on Lubrication; Strategy for Energy Conservation; American Society of Mechanical Engineers, New York, 1981

13 Klaus, E.E.; Energy Conservation in Road Transportation Through Lubricant Technology; Lubrication Engineering, 1978, 34, No. 11, pgs 611-617

14 Standard Terminology Relating to Erosion and Wear; G40, Annual Book of ASTM Standards, ASTM

15 Vingsbo, O.; Fundamentals of Friction and Wear; in Engineering Materials for Advanced Friction and Wear Applications, ASM, 1988, pgs 1-10

16 Ludema, K.C.; Sliding and Abrasive Wear; in ASM Handbook, vol. 18, Friction and Wear Applications, ASM, 1992, pgs 236-241

17 Quinn, T.F.J.; Review of Oxidational Wear Part 1: The Origins of Oxidational Wear; Tribology International, Oct. 1983, Vol 16, 5, pgs 257-271

18 Quinn, T.F.J.; Review of Oxidational Wear Part 2: Recent Developments and Future Trends in Oxidational Wear Research; Tribology International, Dec 1983, Vol 16, No. 6, pgs 305-315

19 Finkin, E.F.; Adhesive Wear: A General Review of the Experimental Knowledge and Theory; Materials in Engineering Applications, Vol 1, April 1979, pgs 154-161

20 Archard, J.F.; Single Contacts and Multiple Encounters; Journal of Applied Physics, 32, 1961, pgs 1420-1425

21 Archard, J.F.; Contact and Rubbing of Flat Surfaces; Journal of Applied Physics, 24, 1953, pgs 981-988

22 Archard, J.F., W. Hirst; The Wear of Metals Under Unlubricated Conditions; Proceedings of the Royal Society of London, 236A, 1956, pgs 397-410

23 Rigney, D.A.; Sliding Wear of Metals; Annual Reviews of Materials Science, 1988, 18, pgs 141-163

24 Suh, N.P.; The Delamination Theory of Wear; Wear, 25, 1973, pgs 111

25 Suh, N.P.; An Overview of the Delamination Theory of Wear; Wear 44, 1977, pgs 1-16

26 Suh, N.P.; An Update on the Delamination Theory of Wear; in Fundamentals of Friction and Wear of Materials, ASM, 1981, pgs 43-71

27 Suh, N.P.; The Delamination Theory of Wear; Elsevier Sequoia, 1977

28 Heilmann, P., W.A.T. Clark, D.A. Rigney; Orientation Determination of Subsurface Cells Generated By Sliding; Acta Metalurgica, vol 31, 1983,

pgs 1293-1305

29 Fleming, J.R., N.P. Suh; Mechanics of Crack Propagation in Delamination Wear; Wear, 44, 1977, pgs 39-56

30 Kimura, Y.; The Role of Fatigue in Sliding Wear; in Fundamentals of Friction and Wear of Materials, D.A. Rigney ed., ASM, 1981, pgs 187-221

31 Ritchie, R.O.; On the Relationship Between Delamination Wear and the Initiation and Growth of Fatigue Cracks in Ultra-High Strength Steels; in Fundamentals of Tribology, N.P. Suh & N. Saka eds., MIT, 1978, pgs 127-134

32 Hearle, A.D., K.L. Johnson; Mode II Stress Intensity Factors for a Crack Parallel to the Surface of an Elastic Half-Space Subjected to a Moving Point Load; Journal of the Mechanics and Physics of Solids, Vol. 33, No. 1, 1985, pgs 61-81

33 Hills, D.A., D.W. Ashelby; On the Determination of Stress Intensification Factors for a Wearing Half-Space; Engineering Fracture Mechanics, Vol. 13, 1980, pgs 69-78

34 Rosenfield, A.R.; Elastic Plastic Fracture Mechanics and Wear; Wear, 72, 1981, pgs 245-254

35 Alpas, A.T., J.D. Embury; The Role of Subsurface Deformation and Strain Localization on the Sliding Wear Behaviour of Laminated Composites; Wear, 146, 1991, pgs 285-300

36 Rosenfield, A.R.; A Shear Instability Model of Sliding Wear; Wear, 116, 1987, pgs 317-328

37 Zhang,J., A.T. Alpas; Delamination Wear in Ductile Materials Containing Containing Second Phase Particles; Materials Science and Engineering A, A160, 1993, pgs 25-35

38 Rice, J.R., D.M. Tracy; On the Ductile Enlargement of Voids in Triaxial Stress Fields; Journal of the Mechanics and Physics of Solids, 17, 1969, pgs 201-217

39 Zum Gahr, K.H.; Microstructure and Wear of Materials; Elsevier, New York, 1987

40 Lim, S.C., M.F. Ashby; Wear Mechanism Maps; Acta Metallurgica, Vol 35, No 1, 1987, pgs 1-24

41 Tabor, D.;Future Directions of Research in Adhesion and Friction: Status of Understanding; Proceeding of the International Conference on Tribology in the 80's, NASA Lewis Research Center, Cleveland, OH, NASA, 1983, pgs 119-142

42 Akagaki, T., D.A. Rigney; Sliding Wear of Metals in Vacuum; Wear of Materials, ASME, 1991

43 Lancaster, J.K.; A Review of the Influence of Environmental Humidity and Water on Friction, Lubrication and Wear; Tribology International, Dec. 1990, vol 23, no 6, pgs 371-389

44 Kasak, A., T.A. Nuemeyer; Observations of Wear on High Hardness Steels; Wear, 14, 1969, pgs 445-454

45 Proskuryakov, Y.G., I.V. Pozdnyakova; Increasing the Wear Resistance of Surfaces by Work Hardening; Russian Engineering Journal, 43, 9, 1963, pgs 35-38

46 Rabinowicz, E.; Friction, Wear and Lubrication: Study Guide; MIT, Cambridge, 1977

47 Montgomery, R.S.; The Sliding Behaviours of Copper Alloys; in Wear of Materials 1983, K.C. Ludema ed., ASME, NY NY, 1983, pgs 465-470

48 Montgomery, R.S.; Hardness as a Guide to the Wear Characteristics of Tin Containing Nodular Cast Iron; Wear, 24, 1973 pgs 247-248

49 Xue, Q.J., K.C. Ludema; Plastic Failure Effects in Scuffing of Soft Metals; in Wear of Materials 1983, K.C. Ludema ed., ASME, 1983, pgs 499-506

50 Scott, D., A.I. Smith, J.Tait, G.R. Tremain; Materials and Metallurgical Aspects of Piston Ring Scuffing - A Literature Review; Wear, 33, 1975, pgs 293-315

51 Ruff, A.W.; Comparison of Standard Testing Methods for Non-Lubricated Sliding Wear; Wear of Materials, ASME, 1989, pgs 717-721

52 Glaeser, W.A.; Wear Experiments in the Scanning Electron Microscope; Wear, 73, 1981, pgs 371-386

53 Moore, M.A., R.M. Douthwaite; Plastic Deformation Below Worn Surfaces; Metallurgical Transactions A, Vol 7A, Dec 1976, pgs 1833-1839

54 Rainforth, W.M., R. Stevens, J. Nutting; Deformation Structures Induced by Sliding Contact; Philosophical Magazine A, Vol 66, No 4, 1992, pgs 621-541

55 Chiu, C., J.D. Embury, T. Castillo; Metallography of Adhesive Wear in Aluminum Alloys; Metallography, Vol 20, 1987, pgs 99-112

56 Kuo, S.M., D.A. Rigney; Sliding Behaviour of Aluminum; Materials Science and Engineering, A157, 1992, pgs 131-143

57 Fischer, T.E.; Modelling Tribochemistry; in Approaches to Modelling Friction and Wear, F.F. Ling & C.H.I. Pan eds., pgs 67-72, Springer-Verlog, NY, 1986

58 Ganapathi, S.K., D.A. Rigney; An HREM Study of the Nanocrystalline Materials Produced By Sliding Processes; Scripta Metallurgica et Materialia, Vol 24, 1990, pgs 1675-1678

59 Ives, L.K.; Microstructural Changes in Copper Due to Abrasive, Dry and Lubricated Wear; Wear of Materials, 1979, ASME, pgs 246-256

60 Dautzenberg, J.H.; The Role of Dynamic Recrystallization in Dry Sliding Wear; Wear, 60, 1980, pgs 401-411

61 Heilman, P., J. Don, T.C. Sun, W.A. Glaeser, D.A. Rigney; Sliding Wear and Transfer; Wear of Materials, 1983, ASME, pgs 414-425

62 Clarke, J., A.D. Sarkar; The Role of Transfer and Back Transfer of Metals in the Wear of Binary Al-Si Alloys; Wear, 82, 1982, pgs 179-195

63 Clarke, J., A.D. Sarkar; Wear Characteristics of As-Cast Binary Aluminum-Silicon Alloys, Wear, 54, 1979, pgs 7-16

64 Jasim, K.M., E.S. Dwarakadasa; Wear in Al-Si Alloys Under Dry Sliding Conditions; Wear, 119, 1987, pgs 119-130

65 Jasim, K.M., E.S. Dwarakadasa; Effect of Sliding Speed on the Adhesive Wear of Binary Al-Si Alloys; Journal of Material Science Letters, 12, 1993, pgs 650-653

66 Shivanath, R., P.K. Sengupta, T.S. Eyre; Wear of Aluminum-Silicon Alloys; The British Foundryman, Vol 70, 12, Dec. 1977, pgs 349-356

67 Pramila Bai, B.N., S.K. Biswas; Characterization of Dry Sliding Wear of Al-Si Alloys; Wear, 120, 1987, pgs 61-74

68 Pramila Bai, B.N., S.K. Biswas; Mechanisms of Wear in Dry Sliding of a Hypoeutectic Aluminum Alloy; Journal of the ASLE, Vol 43,1, Jan 1987, pgs 57-61

69 Pramila Bai, B.N., S.K. Biswas; Effect of Load on Dry Sliding Wear of Al-Si Alloys; ASLE Transactions, Vol 29,1, pgs 116-120

70 Pramila Bai, B.N., E.S. Dwarakadasa, S.K. Biswas; Subsurface Damage in Dry Wear of Al-Si Alloys; Wear, 71,1981, pgs 381-384

71 Antoniou, R., D.W. Borland; Mild Wear of Al-Si Binary Alloys During Unlubricated Sliding; Materials Science and Engineering, 93, 1987, pgs 57-72

72 Pramila Bai, B.N., H.S. Shamasunder, S.K. Biswas; Debris Analysis in Dry Sliding Wear of Al-Si Alloys; Materials Science and Engineering, A104, 1988, pgs L11-L14

73 Subramanian, C.; On Mechanical Mixing During Dry Sliding of Aluminum 12.3 wt% Silicon Alloy Against Copper; Wear, 161, 1993, pgs 53-60

74 Somi Reddy, A., B.N. Pramila Bai, K.S.S. Murthy, S.K. Biswas; Wear and Seizure of Binary Al-Si Alloys; Wear, 1994, pgs 115-127

75 Torabian, H., J.P. Pathak, S.N. Tiwari; Wear Characteristics of Al-Si Alloys; Wear, 172, 1994, pgs 49-58

76 Subramanian, C.; Effects of Sliding Speed on the Unlubricated Wear Behaviour of Al-12.3 wt% Si Alloy; Wear, 151, 1991, pgs 97-110

77 Subramanian, C.; Wear of Al-12.3 wt% Si Alloy Slid Against Various Counterface Materials; Scripta Metallurgica et Materialia, Vol 25, 1991, pgs 1369-1374

78 Wilson, S., A. Ball; Wear Resistance of an Aluminum Matrix Composite; in Tribology of Composite Materials, ASM International, Materials Park, OH, 1991, pgs 123-131

79 Rauta, V., M. Saynatjoki; Tribological Properties of SiC Particulate Reinforced Cast Aluminum Matrix Composites; Tribologia, Vol 10, No.4, 1991, pgs 48-68

80 Alpas, A.T., J.Zhang; Effect of SiC Particulate Reinforcement on the Dry Sliding Wear of Aluminum- Silicon Alloys (A356); Wear, 155, 1992, pgs 83-104

81 Alpas, A.T., J.Zhang; Wear Rate Transitions in Cast Aluminum Silicon Alloys Reinforced With SiC Particles; Scripta Metallurgica et Materialia, Vol 26, 1992, pgs 505-509

82 Modi, O.P., B.K. Prasad, A.H. Yegneswaran, M.L. Vaidya; Dry Sliding Wear Behaviour of Squeeze Cast Aluminum Alloy-Silicon Carbide Composites; Materials Science and Engineering, A151, 1992, pgs 235-245

83 Martinez, M.A., A. Martin, J. Llorca; Wear of Al-Si Alloys and Al-Si/SiC Composites at Ambient and Elevated Temperatures; Scripta Metallurgica et Materialia, Vol 28, 1993, pgs 207-212

84 Wang, A., H.J. Rack; Transition Wear Behaviour of SiC Particulate and SiC Whisker Reinforced 7091 Al Metal Matrix Composites; Material Science and Engineering, A147, 1991, pgs 211-224

85 Pramila Bai, B.N., B.S. Ramasesh, M.K. Surappa; Dry Sliding Wear of A356-Al-SiC_p Composites; Wear, 157, 1992, pgs 295-304

86 Skolianos, S., T.Z. Kattamis; Tribological Properties of SiC_p Reinforced Al-4.5% Cu- 1.5% Mg Alloy Composites; Materials Science and Engineering, A163, 1993, pgs 107-113

87 Surappa, M.K., S.V. Prasad, P.K. Rohatgi; Wear and Abrasion of Cast Al-Alumina Particle Composites; Wear, 77, 1982, pgs 295-302

88 Hosking, F.M., F.F. Portillo, R. Wunderlin, R. Mehrabian; Composites of Aluminum Alloys: Fabrication and Wear Behaviour; Journal of Materials Science, 17, 1982, pgs 477-498

89 Zhang, J., A.T. Alpas ; Wear Regimes and Transitions in Al_2O_3 Particle Reinforced Aluminum Alloys; Materials Science and Engineering, A161, 1993, pgs 273-284

90 Chiao, Y.S., F.M. Pan, C.A. Lin, J.L. Horng, S.J. Lin; Studies of Al_2O_3(p)-6061 Al Composites Under Dry Sliding Conditions Using Scanning Electron Microscopy, Energy Dispersive Spectrometry and X-Ray Diffractometry; Wear, 161, 1993, pgs 155-160

91 Nesarikar, A.R., S.N. Tewari, E.E. Graham; Room Temperature Wear Characteristics of Al_2O_3 - Particle Reinforced Aluminum Alloy Composites; Materials Science and Engineering, A147, 1991, pgs 191-199

92 Saka, N., D.P. Karalekas; Friction and Wear of Particle Reinforced Metal-

Ceramic Composites; in Wear of Materials 1985, ASME, 1985, pgs 784-793

93 Brechet, Y., J. Newell, S. Tao, J.D. Embury; A Note on Particle Comminution at Large Plastic Strains in Al-SiC Composites; Scripta Metallurgica et Materialia, Vol 28, 1993, pgs 47-51

94 Alahelisten, A., F. Bergman, M. Olsson, S. Hogmark; On the Wear of Aluminum and Magnesium Metal Matrix Composites; Wear, 165, 1993, pgs 221-226

95 Park, H.C.; Wear Behaviour of Hybrid Metal Matrix Composites; Scripta Metallurgica et Materialia, Vol 27, 1992, pgs 465-470

96 Lee, C.S., Y.H. Kim, K.S. Han, T. Lim; Wear Behaviour of Aluminum Matrix Composite Materials; Journal of Materials Science, 27, 1992, pgs 793-800

97 Prasad, S.V., K.R. Mecklenburg; Friction Behaviour of Ceramic Fibre Reinforced Aluminum Metal Matrix Composites Against a 440C Steel Counterface; Wear, 162-164, 1993, pgs 47-56

98 Cao, L., Y. Wang, C.K. Yao; The Wear Properties of an SiC-Whisker-Reinforced Aluminum Composite; Wear, 140, 1990, pgs 273-277

99 Arikan, R., S. Murphy; Anisotropic Wear of Planar Random Metal Matrix Composites With Zinc Alloy Matrix; Wear, 143, 1991, pgs 149-157

100 Nayeb-Hashemi, H., J.T. Blucher, J. Mirageas; Friction and Wear Behaviour of Aluminum-Graphite Composites as a Function of Interface and Fibre Direction; Wear, 150, 1991, pgs 21-39

101 Eliezer, Z., V.D. Khanna, M.F. Amateau; On the Effect of Fibre Orientation on the Wear of Composite Materials; Wear, 153, 1979, pgs 387-389

102 Amateau, M.F., R.H. Flowers, Z. Eliezer; Tribological Behaviour of Metal Matrix Composites; Wear, 54, 1979, pgs 175-185

103 Saka, N., N.K. Szeto, T. Ertyrk; Friction and Wear of Fibre Reinforced Metal Matrix Composites; Wear 157, 1992, pgs 339-357

104 Pearsall, K.J., Z. Eliezer, M.F. Amateau; The Effect of Sliding Time and Speed on the Wear of Composite Materials; Wear, 63, 1980, pgs 121-130

105 Delmonte, J.; Technology of Carbon and Graphite Fibre Composites; Van Nostrand Reinhold Co., Toronto, 1981, pgs 41-46

106 Islam, M.U., W. Wallace; Carbon Fibre Reinforced Aluminum Matrix Composites, A Critical Review; Division of Mechanical Engineering Report, National Research Council of Canada, NRC No. 23498, 1984/6

107 Personal Communication; Ashland Petroleum Company, Ashland, Kentucky, USA, 1992

108 Ciby, S., B.C. Pai, K.G. Satyanarayana, V.K. Vaidyan, P.K. Rohatgi; Structure Formation During Processing Short Carbon Fibre - Reinforced Aluminum Alloy Matrix Composites; Journal of Materials Engineering and Performance, Vol 2, (3), 1993, pgs 353-358

109 Abraham, S., B.C. Pai, K.G. Satyanarayana, V.K. Vaidyan; Copper Coating on Carbon Fibres and Their Composites With Aluminum Matrix; Journal of Materials Science, 27, 13, 1992, pgs 3479-3486

110 Stephenson, T.F., J.A.E. Bell; Nickel Coated Carbon Fibre Paper : A Low Cost Alternative to Particulate Reinforced Metal Matrix Composites; Proc. Int. Sym. on Advances in Production and Fabrication of Light Metals and Metal Matrix Composites, Edmonton Alberta, Canada, Aug. 1992, The Metallurgical Society of CIM, pgs 511-519

111 Rohatgi, P.K., Y. Liu, T.L. Barr; Tribological Behaviour and Surface Analysis of Tribodeformed Al Alloy - 50% Graphite Particle Composites; Metallurgical Transactions, A22, 1991, pgs 1435-1441

112 Das, S., S.V. Prasad, T.R Ramanchandran; Tribology of Al-Si Alloy - Graphite Composites : Triboinduced Graphite Films and the Role of Silicon Morphology; Materials Science and Engineering, A138, 1991, pgs 123-132

113 Liu, Y.B., S.C. Lim, S. Ray, P.K. Rohatgi; Friction and Wear of Aluminum - Graphite Composites : The Smearing Process of Graphite During Sliding; Wear, 159, 1992, pgs 201-205

114 Rohatgi, P.K., S. Ray, Y. Liu; Tribological Properties of Metal Matrix - Graphite Particle Composites; International Materials Reviews, Vol 37, 1992, No 3, pgs 129-150

115 Rohatgi, P.K., Y. Liu, T.L. Barr; Modelling and Characteristics of the Lubricating Film Formed During Sliding Wear of Al/Graphite Composites; in Tribology of Composite Materials, ASM, 1991, pgs 113-121

116 Chen, L.H., D.A. Rigney; Transfer During Unlubricated Sliding Wear of Selected Metal Systems; Wear, 105, 1985, pgs 47-61

117 Gibson, P.R., A.J. Clegg, A.A. Das; Production and Evaluation of Squeeze Cast Graphitic Al-Si Alloys; Materials Science and Technology, Vol 1, 1985, pgs 559-567

118 Jha, A.K., S.V. Prasad, G.S. Upadhyaya; Sintered 6061 Aluminum Alloy - Solid Lubricant Particle Composites : Sliding Wear and Mechanisms of Lubrication; Wear, 133, 1989, pgs 163-172

119 Rohatgi, P.K., N.B. Dahotre, Y. Liu, T.L. Barr; Wear Behaviour of Flake Graphite and Microcrystalline Carbon Dispersed Al Matrix Composites ; in Engineering Materials For Advanced Friction and Wear Applications, F.A. Schmidt and P.J. Blau eds., ASM, 1988, pgs 85-92

120 Petty, E.R.; Hot Hardness and Other Properties of Some Binary Intermetallic Compounds of Aluminum; Journal of the Institute of Metals, Vol 89, 1961, pgs 343-349

121 ASM Committee on Aluminum and Aluminum Alloys; Properties of Cast Aluminum; Metals Handbook, 9th ed., Vol 2, ASM International, Materials Park, OH, 1979, pgs 164-167

122 Das, S., S.V. Prasad, T.R. Ramachandran; Microstructure and Wear of Cast (Al-Si Alloy)-Graphite Composites; Wear, 133, 1989, pgs 173-187

123 Krageliskii, I.V.; Friction and Wear; Butterworths, London, 1965, pgs 92-93

124 Ashby, M.F., J. Abulawi, H.S. Kong; Temperature Maps for Frictional Heating in Dry Sliding; Tribology Transactions, 34, 1991, pgs 557-587

Vita Auctoris

Name:	**William Ames**
Place of Birth:	**Windsor, Ontario, Canada**
Year of Birth:	**1967**
Education:	**Vincent Massey Secondary School, Windsor 1982-1987**
	University of Windsor, Windsor, Ontario 1987-1991 B.A.Sc.
	University of Windsor, Windsor, Ontario 1992-1994 M.A.Sc.